Technical Report Documentation Page

1. Report No.	2. Government Accession No.	3. Recipient's Catalog No.
FHWA/TX-10/0-5270-1		

4. Title and Subtitle	5. Report Date
SEAL COAT DAMAGE EVALUATION DUE TO SUPERHEAVY LOAD MOVES BASED ON A MECHANISTIC-EMPIRICAL APPROACH	December 2009 Published: March 2010
	6. Performing Organization Code

7. Author(s)	8. Performing Organization Report No.
Jeong Ho Oh and Andrew J. Wimsatt	Report 0-5270-1

9. Performing Organization Name and Address	10. Work Unit No. (TRAIS)
Texas Transportation Institute The Texas A&M University System College Station, Texas 77843-3135	11. Contract or Grant No. Project 0-5270

12. Sponsoring Agency Name and Address	13. Type of Report and Period Covered
Texas Department of Transportation Research and Technology Implementation Office P.O. Box 5080 Austin, Texas 78763-5080	Technical Report: September 2007–August 2009
	14. Sponsoring Agency Code

15. Supplementary Notes

Project performed in cooperation with the Texas Department of Transportation and the Federal Highway Administration.
Project Title: A Logical Guideline for Superheavy Load Review Policy
URL: http://tti.tamu.edu/documents/0-5270-1.pdf

16. Abstract

The number of superheavy load (SHL) moves has increased drastically within the past 5 years in Texas. Along with the increasing SHL moves, the Texas Department of Transportation (TxDOT) has become increasingly aware of the rising concerns associated with fresh seal coat damage caused from SHL moves. Concerned about the effects of SHL moves on seal coat placed routes, TxDOT sponsored a research project with the Texas Transportation Institute to characterize critical factors related to the failure mechanism of seal coat, propose a mechanistic approach to evaluate failure potential, and develop a guideline for regulating SHL moves to mitigate further seal coat damages.

This report describes research efforts and findings to propose a mechanistic approach to evaluate seal coat damage potential via charactering material properties playing a vital role in controlling seal coat behavior subject to SHL moves and validating the proposed mechanistic approach based on pilot field tests conducted in the Bryan and San Antonio Districts taking into account different levels of critical factors identified from this study. Moreover, the efforts were extended to establish a database on SHL routing information gathered from the TxDOT Construction Division from the pavement reviews conducted over the past 5 years in order to review the current guideline for SHLs. The project offered the first opportunity to provide a guideline for regulating SHL moves in order to preserve routes with fresh seal coats by delivering a tool that can be used to evaluate the route in a timely fashion before SHL moves occur.

17. Key Words	18. Distribution Statement
Superheavy Load, Seal Coat, Tensile Strength, Surface Energy, Pavement Surface Temperature, Slope, Curing Period, Wheel Force	No restrictions. This document is available to the public through NTIS: National Technical Information Service Springfield, Virginia 22161 http://www.ntis.gov

19. Security Classif.(of this report)	20. Security Classif.(of this page)	21. No. of Pages	22. Price
Unclassified	Unclassified	120	

Form DOT F 1700.7 (8-72) **Reproduction of completed page authorized**

SEAL COAT DAMAGE EVALUATION DUE TO SUPERHEAVY LOAD MOVES BASED ON A MECHANISTIC-EMPIRICAL APPROACH

by

Jeong Ho Oh
Assistant Research Engineer
Texas Transportation Institute

and

Andrew J. Wimsatt
Materials and Pavements Division Head
Texas Transportation Institute

Report 0-5270-1
Project 0-5270
Project Title: A Logical Guideline for Superheavy Load Review Policy

Performed in cooperation with the
Texas Department of Transportation
and the
Federal Highway Administration

December 2009
Published: March 2010

TEXAS TRANSPORTATION INSTITUTE
The Texas A&M University System
College Station, Texas 77843-3135

DISCLAIMER

The contents of this report reflect the views of the authors, who are responsible for the facts and the accuracy of the data presented herein. The contents do not necessarily reflect the official view or policies of the Federal Highway Administration (FHWA) or the Texas Department of Transportation (TxDOT). This report does not constitute a standard, specification, or regulation. Its contents are not intended for construction, bidding, or permit purposes. The use of names of specific products or manufacturers listed herein does not imply endorsement of those products or manufacturers. The engineer in charge of the project was Dr. Jeong Ho Oh, Texas P.E., #100318.

ACKNOWLEDGMENTS

This project documented herein was conducted as a part of a research project sponsored by the Texas Department of Transportation and the Federal Highway Administration. The authors gratefully wish to express gratitude for the support and guidance of the project director, Dr. Dar Hao Chen, of the Material and Pavement Section of TxDOT's Construction Division. In addition, the authors thank Dr. German Claros and the project advisory committee for their valuable comments during this project. The authors also acknowledge for the support provided by the Bryan, Lubbock, and San Antonio Districts in the evaluation of seal coat damage to develop guidelines for regulating superheavy load moves. In particular, the authors acknowledge the contributions made by the following TxDOT engineers and support staff:

- Darlene Goehl, Karl Nelson, Terry Paholek, and James Kreamer of the Bryan District;
- Stacey Young of the Lubbock District;
- John Bohuslav, Johnny Martinez, Eddie Reyes, Emil Noll, Anne Strick, and Carl Friesenhahn of the San Antonio District; and
- Ray Hutchinson, Trinea Moreno, Ron Johnson, and Robert Hood of the Motor Carrier Division.

A special note of thanks should be given to Dr. Robert Lytton for providing his expert theoretical background to develop a mechanistic approach in this project, Dr. Emmanuel Fernando for assisting in preparation of the proposal, and Mrs. Cindy Estakhri for coordinating to obtain seal coat binder materials to perform laboratory tests. In addition, the authors extend thanks to former graduate research assistants Mr. Das Gautam, Dr. Sang Ick Lee, and Dr. Chi Hun Lee for performing laboratory testing and establishing extensive superheavy load database demanding in this study.

Finally, the authors also acknowledge the technical support provided by Mr. Gerry Harrison and Mr. Jason Huddleston in installing a wheel force transducer onto the test truck and operating the test truck to collect data for validating the mechanistic approach developed in this project.

TABLE OF CONTENTS

Page

List of Figures ix

List of Tables xii

CHAPTER I INTRODUCTION 1

CHAPTER II REVIEW OF LITERATURES 5

SHL Regulation and Analysis 5

Overview of Seal Coat in Texas 7

Evaluation of Seal Coat Performance 10

CHAPTER III DAMAGES AND COSTS ASSOCIATED WITH SHL MOVES 11

Damages Associated with SHL Moves 11

Cost Assoicated to Repair Damage 19

CHAPTER IV DEVELOPMENT OF A MECHANISTIC APPROACH 23

Seal Coat Failure Mechanism 23

Material Characterization 25

Crack Density Function 25

Film Thickness 25

Surface Energy 27

Relaxation Modulus Properties (E_1, m, t_1/aT) 32

Consideration of Aging Effect 38

CHAPTER V FIELD TESTING AND VALIDATION 45

Field Test during FY08 45

Field Test during FY09 59

Further Validations Based on Case Studies 70

SH 43 – Tyler District 70

FM 2210 –Fort Worth District 71

US 285 –Odessa District 72

FM 109 –Yoakum District 73

SH 56 –Paris District 74

CHAPTER VI ESTABLISHING DATABASE AND GUIDELINE 75
SHL Database 75
Outline of Guideline 80
CHAPTER VII FINDINGS AND RECOMMENDATIONS 83
REFERENCES 89
APPENDIX A DERIVATION OF TENSILE STRENGH 93
APPENDIX B FIELD TEST RESULTS OF FM 97/28 95
APPENDIX C M-E SDEP USER'S MANUAL 103

LIST OF FIGURES

Page

Figure 1. Seal Coat Damage due to SHL Moves. 2
Figure 2. Superheavy Load Evaluation Process *(4).* 6
Figure 3. Normalized FWD Deflection on FM 796 12
Figure 4. SCI and BCI on FM 796. 13
Figure 5. Severe Damage on FM 796. 13
Figure 6. Variation of Expected Soil Moisture Contents across Texas *(18)*. 15
Figure 7. Cumulative Percentile of Deflection W1 16
Figure 8. Seal Coat Damage along with Slope. 18
Figure 9. SH56 and US377 Seal Coat Damaged Sections 21
Figure 10. Free Body Diagram of Seal Coat Damage. 23
Figure 11. Film Thickness versus Tensile Strength (*25*).. 26
Figure 12. Wilhelmy Plate Test Set Up. 28
Figure 13. Universal Sorption Test Set Up. 29
Figure 14. Temperature-Viscosity Relationship of Seal Coat Binders. 34
Figure 15. Plan Sheet Example. 36
Figure 16. Molded Seal Coat Mixture. 36
Figure 17. Shift of Master Curve from Original Condition to Aged Condition. 42
Figure 18. Variation of Tensile Strength with Pavement Surface Temperature. 42
Figure 19. Variation of Tensile Strength with Curing Period. 43
Figure 20. Percent of Increase in Tensile Strength along with Curing Period. 43
Figure 21. Test Routes Layout in Bryan District. 45
Figure 22. Slope Measurement Using a Digital Protractor. 46
Figure 23. Measured Wheel Force and Moment Components. 47
Figure 24. Comparison of Wheel Force Transducer with Static Scale. 48
Figure 25. Loaded Test Truck along the Test Segment. 49
Figure 26. Measured Wheel Force and Moment from Normal Driving. 50
Figure 27. Measured Wheel Force and Moment from Brake Applied Driving. 50
Figure 28. Low Level of Damage. 51
Figure 29. High Level of Damage. 51

Figure 30. Relationship between Deflections and Temperature from FWD Tests. 52
Figure 31. Seal Coat Damage (a) Normal Drive (b) Brake-Applied Drive. 53
Figure 32. Sand Patch Test Conducted. 54
Figure 33. Texture Depth Measured in FY08 Testing. 55
Figure 34. Relationship between Failure Ratio (F/T) and Damage Rate. 59
Figure 35. Test Truck for Bryan District Tests. 61
Figure 36. Test Truck for San Antonio District Tests. 61
Figure 37. Measured Wheel Forces (a) Bryan District (b) San Antonio District. 62
Figure 38. Comparison of Segment Before and After Test. 63
Figure 39. Severe Damage of Surface Treatments. 64
Figure 40. Failure Ratio versus Damage Rate from FY09 Field Tests. 69
Figure 41. Relationship between Vertical and Longitudinal Wheel Forces. 69
Figure 42. Snapshot of SHL Database. 77
Figure 43. Cumulative Percentile of GVW 77
Figure 44. Cumulative Percentile of Maximum Tire Load 78
Figure 45. Percentage of Routes including Seal Coat 78
Figure 46. Percentage of Travel Distance. 79
Figure 47. Percentage of SHL with Push Truck. 79
Figure 48. Percentage of Major City Traveling SHL Moves 80
Figure 49. Proposed Guideline of SHL Moves on Seal Coat Routes. 81
Figure 50. Maximum Tire Load versus GVW. 81
Figure B1. Shipping of Wind Turbine. 95
Figure B2. FM 97 Location 1 on Milepost 336. (a) July 11th; (b) December 6th. 97
Figure B3. Comparison of Transverse Profile of FM 97 Location 1 97
Figure B4. FM 97 Location 2 on Milepost 336+60. (a) July 11th;
(b) December 6th. 98
Figure B5. Comparison of Transverse Profile of FM 97 Location 2 98
Figure B6. FM 97 Location 3 on Milepost 336-2040'. (a) July 11th;
(b) December 6th. 99
Figure B7. Comparison of Transverse Profile of FM 97 Location 3 99

Figure B8. FM 28 Location 1 on Milepost 186+900' (a) July 11th;
(b) December 6th. 100
Figure B9. Comparison of Transverse Profile of FM 28 Location 1..... 100
Figure B10. FM 28 Location 2 on Milepost 182+2100' (a) July 11th;
(b) December 6th. 101
Figure B11. Comparison of Transverse Profile of FM 28 Location 2..... 101
Figure B12. FM 28 Location 3 on Milepost 182+5400' (a) July 11th;
(b) December 6th. 102
Figure B13. Comparison of Transverse Profile of FM 28 Location 3..... 102
Figure C1. Snapshot of Input Screen on "Calculate Failure Ratio" Worksheet. 103
Figure C2. Select Binder Type for A-VTS Coefficient Calculation and MAAT. 104
Figure C3. Select Aggregate Grade and Mixture Type. 105
Figure C4. Select Aggregate Gradation. 106
Figure C5. Select Aggregate Sources for Surface Energy Calculation. 107
Figure C6. Run Analysis to Calculate Failure Ratio..... 108

LIST OF TABLES

Page

Table 1. Typical Binder Materials Used for Seal Coats in Texas. 8
Table 2. Aggregate Gradation for Lightweight Aggregate. 9
Table 3. Aggregate Gradation for Limestone, Gravel, and Sandstone Aggregate. 9
Table 4. Results of *LoadGage* Analysis. 17
Table 5. Results of AI Equations Used Analysis. 18
Table 6. Statewide Maintenance Activities during FY09. 20
Table 7. Measured Surface Energy Components. 30
Table 8. Calculated Total Surface Energy of Seal Coat Mixtures. 31
Table 9. DSR Test Results of Seal Coat Binders. 34
Table 10. Air Voids Measured. 37
Table 11. Inputs Used to Estimate Tensile Strength. 40
Table 12. Description of Test Locations in FY08 47
Table 13. Field Validation Results of FY08 Tests 56
Table 14. Calibrated Coefficient from Field Validation in FY08. 58
Table 15. Description of Test Locations in FY09 60
Table 16. Texture Depth Measured in FY09 Testing. 65
Table 17. Calibrated Coefficients from FY09 Tests. 66
Table 18. Field Validation Results of FY09 Tests 66
Table 19. Pavement Surface Temperature Range versus Time. 70

CHAPTER I INTRODUCTION

Recent years have seen a significant increase in requests for superheavy load (SHL) moves in Texas. The source provided by the Motor Carrier Division of the Texas Department of Transportation (TxDOT) indicated that the number of SHL increased exponentially during past 5 years. The number of permitted SHL moves were slightly over 100 in Fiscal Year (FY) 2004 but rapidly increased close to 1800 in FY09. TxDOT has been required to regulate for SHL moves to accommodate increasing the gross vehicle weight (GVW) leading to higher wheel loads that are directly associated with pavement damage. In current practice, TxDOT performs a pavement review of the SHL route in the event of the GVW is over 500 kips or the tire load exceeds 5 kips. The pavement review process typically takes about 4–6 weeks. It has been often observed that movers made an attempt to reduce the GVW by reducing the number of axles to meet the 500 kips criterion to expedite their transport by avoiding the review process. The side effect of reducing the number of axles directly leads to a significant increase in tire load, which in turn has a major impact on pavement performance.

Field monitoring on SHL moves in the past 5 years revealed that the moves primarily caused damage on fresh seal coat pavements typically less than 5 weeks after seal coated as shown in Figure 1. Structural failure rarely occurred from a weak load bearing capacity of underlying layers induced by a sudden increase of moisture content level from considerable amount of rainfall prior to SHL moves made, unsupported pavement edge conditions, and structurally poor condition. Regulating SHL moves travelling along with fresh seal coat pavements has been a challenging task due to the lack of statewide seal coat scheduling and streamlined procedure to evaluate expecting seal coat damage potential. Considering huge mileage of seal coat placed annually (around 20,000 mile/year) by TxDOT for a pavement preservation means, it is imperative to establish an effective guideline to regulate and route SHL moves to mitigate further seal coat damages resulting in significant reducing the cost to repair deteriorated routes. Tentatively, TxDOT adopted a criterion that reroute SHL moves to 5 weeks or older pavements based on the limited field monitoring *(1)*.

Figure 1. Seal Coat Damage due to SHL Moves.

However, the field observations also indicated that the cause of seal coat damage is not only tied to the curing period but also to the environmental and geometric conditions such as pavement surface temperature and pavement grades at the time of SHL moves. Interacting forces between tire and seal coat surface are related to the material properties of seal coat materials and components of wheel forces. Therefore it should be crucial to examine seal coat behaviors under various environmental and geometric conditions in assessment of evaluating seal coat damage potential and developing a logical guideline for SHL moves in the near future.

Additionally, establishing a routing system that considers seal coat scheduling is also important for TxDOT engineers along with a tool for evaluating seal coat damage potential to process pavement review and routing in a timely fashion. An effort to develop an advanced routing system called Texas Permit Routing Optimization System (TxPROS) by the Motor Carrier Division (MCD) is underway to include features that will optimize candidate routes accounting for the factors such as vertical clearance, lane width, structure height, load rating, turn restrictions, and bridge/construction/pavement data *(2)*.

To accomplish the project objectives, the researchers carried out a comprehensive work plan that covered the following tasks:

- reviewed current TxDOT and other state's practice on overweight/superheavy load regulation, TxDOT seal coat specification, and previous literatures dealing with damage evaluations due to SHLs;
- proposed a preliminary mechanistic approach to evaluate seal coat damage along with identification of critical parameters and material characterization;
- conducted pilot field tests to validate the proposed mechanistic approach;
- calibrated/revised a preliminary mechanistic approach and developed a tool based in Microsoft Excel® spreadsheet format; and
- established a single electronic source of SHLs database collected by TxDOT during the past 5 years for the pavement review to overview the current SHL procedure.

The following chapters of this report document each of the tasks conducted in this project.

CHAPTER II REVIEW OF LITERATURES

The researchers conducted a comprehensive search of the literature and found relevant reports or papers pertaining to the practice of SHL regulation and analysis, case studies on SHL moves, seal coat specification, and seal coat material characterization. This chapter presents the findings from the review conducted by researchers to outline items to be considered in this study.

SHL Regulation and Analysis

An emphasis was primarily placed on reviewing the current practice of TxDOT in order to accomplish objectives of this project. The loaded trucks exceeding 254,300 lb of GVW with less than 95 ft of axle spacing is defined as SHL by TxDOT. All loads of this magnitude should be permitted through the MCD. Among permitted loads, in case of GVW over 500,000 lb or trailer tire load exceeding 5000 lb, the MCD requests the construction division, materials and pavements section (CST-M&P) to conduct pavement analysis to check if structurally inadequate route exists and to provide information on movement dates, routes, and load configuration diagrams. CST-M&P provides recommendations on proposed routes to MCD if a reroute is necessary as schematized in Figure 2. Recognizing significant concerns on seal coat pavement damages, there needs to be established more detailed guidelines similar to handle pavement structural adequacy through field data collection and determination of pavement life using Asphalt Institute performance prediction equations. In this review, researchers also made an attempt to gather information on SHL moves adopted in other transportation agencies, yet found that sufficient detail information was not relatively available on how to route and analyze pavements with specific criteria unlike the bridge evaluation process that is in effective. Here is brief summary of the review:

- Missouri DOT *(3)*

  The Missouri DOT defines SHL when the GVW is over 160 kips with dimension 16 ft height and width, and 150 ft length. The guideline states that at least 2 weeks should be assured for evaluating the route for SHL moves.

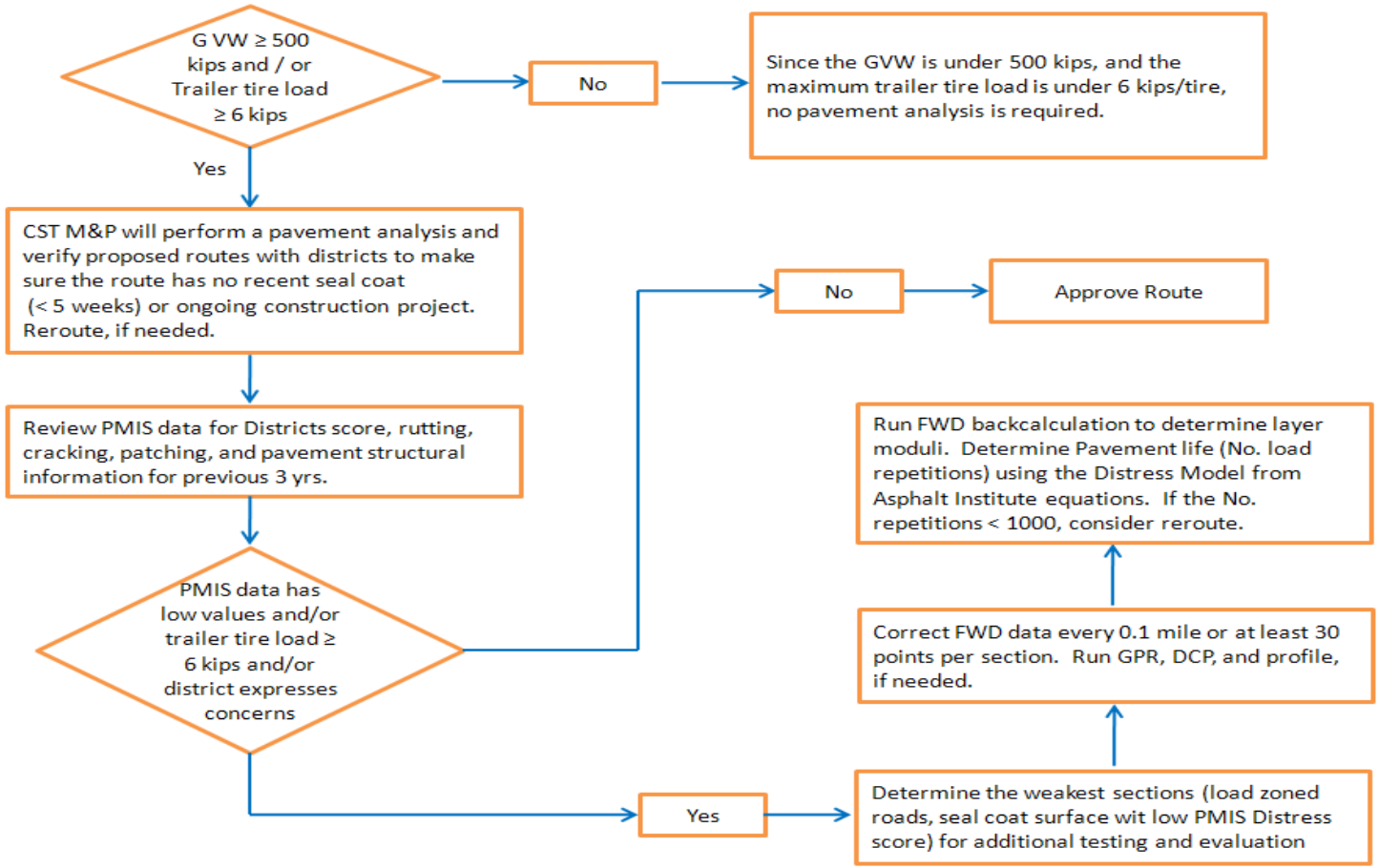

Figure 2. Superheavy Load Evaluation Process *(4)*.

- California DOT *(5)*

  The basic principle of their guideline is to limit overloads under structural load limits on bridge and pavement, which are based on structural analysis, load equivalencies using GVW, number of axles, and axle spacing criteria. The agency also utilizes the weigh-in-motion (WIM) devices with screening programs such as PrePass^{TM} to monitor SHLs to establish database.

- New Zealand (*6*)

  When the permit was applied, the application is processed with the Transit New Zealand overweight permit manual to issue permit in case where the bridges and pavements along the route meet the required structural adequacy. After SHL moves are made, an inspection for damage and pursuit of compensation for identified damage needs to be conducted.

Overview of Seal Coat in Texas

One primary objective of this project in regard to superheavy load moves on seal coat was to identifying seal coat materials used on such routes. Seal coats and surface treatments are simple and cost-effective if adequate care is taken in the planning and execution of the work (*7*). The Texas DOT constructs more than 20,000 miles lanes of seal coats costing approximately $200 million every year in the State for pavement preservation means *(7*). The performance of seal coat depends on (*8*):

- construction techniques used,
- properties of the bituminous binder,
- amounts of aggregate and binder used and the uniformity of application,
- development of good adhesion initially that must be assured through the service life,
- strength of underlying layer,
- amount and type of traffic, and
- environmental condition.

It is desirable in Texas to place seal coats on a 6 to 8 year cycle, but it is not always possible due to funding constraints (*7*). Therefore careful decisions need to be

made in selection of sites and material types taking into account traffic volume, existing surface deficiency type, and so on.

Typical binder materials used for seal coats are categorized (1) asphalt cement, (2) emulsified asphalt, (3) cutbacks (*8*). Table 1 shows typical binders used in the TxDOT district surface treatment program.

Table 1. Typical Binder Materials Used for Seal Coats in Texas.

Binder	Brief Description
AC20-5TR, AC15-5TR, AC10-2TR	Asphalt cement with 2000 (1500 and 1000 for AC15-5TR and AC10-2TR) poises viscosity at 140 °F, modified with 5% (2% for AC10-2TR) tire rubber.
AC-15P	Asphalt cement with 1500 poises viscosity at 140 °F, modified with a polymer.
AC20-XP	Asphalt cement with 2000 poises at 140 °F with no polymer
AC5-2% Latex	Asphalt cement with 500 poises at 140 °F, modified with 2% latex
CRS-2P	Cationic, rapid setting, high viscosity emulsion modified with a polymer (If the number 1 is designated, it indicates low viscosity.)
CRS-2H	Cationic, rapid setting, high viscosity emulsion modified with a hard base asphalt
HFRS-2P	High-float, rapid setting, high viscosity emulsion with a polymer

Walubita et al. (*9*) developed a surface performance-graded (SPG) specification for the selection of surface treatment binders by relating binder material properties to surface treatment performance and associated distresses by monitoring 45 highway test sections across the districts. It turned out AC20 (15)-5TR type of binder has been the most widely used 40 percent of all sections.

In regard to aggregates, there are two main categories used to describe the aggregate used in Texas for seal coats. One is natural aggregate that include crushed gravel, crushed stone, and natural limestone rock asphalt. The other is synthetic aggregate that pertain to lightweight aggregate, which has been widely used recently due to its low specific gravity causing less windshield and vehicle damage along with

excellent skid-resistance (*8*). In terms of maximum particle size and gradation, Grade 3 aggregate is coarser than Grade 4 and 5 with a maximum particle size of 5/8 inch, and a Grade 4 has a maximum particle size of 1/2 inch. Generally, Grade 3 and 4 provides better performance in seal coats, but it also tends to be problematic with respect to noise and vehicle windshield damage. Grade 5 is rarely used compared to Grade 3 and 4 aggregates. According to the report (*9*), Grade 4 aggregate is the most widely used with portion of 64.5 percent based on the number of observed test sections followed by Grade 3 (33.3 percent). For aggregate type, the 50 percent of sections employed limestone and around 30 percent of section used lightweight aggregate. In addition, precoated aggregate has been prevailed over uncoated aggregate to mainly achieve better adhesion of the aggregate to asphalt cement binders and also to reduce the accumulation of dust on the surface of the aggregate. However, the use of precoated aggregate is not recommended for emulsion binder applications.

Tables 2 and 3 present typical TxDOT gradation specifications for Grades 3, 4, and 5 aggregates (*10*).

Table 2. Aggregate Gradation for Lightweight Aggregate.

	Grade 3	Grade 4	Grade 5
Retained 3/4"	0	0	0
Retained 3/8"	70	30	2
Retained #4	100	95	70
% passing #200	0	0	0

Table 3. Aggregate Gradation for Limestone, Gravel, and Sandstone Aggregate.

	Grade 3	Grade 4	Grade 5
Retained 3/4"	0	0	0
Retained 3/8"	90	35	2
Retained #4	100	98	60
% passing #200	0	0	0

Evaluation of Seal Coat Performance

Major distresses encountered during seal coat service are flushing and loss of aggregate due to insufficient bonding strength between aggregate and binder, inadequate binder or aggregate application rate, and improper curing period.

Estakhri et al. (*11*) developed a laboratory test method to determine curing rate of asphalt emulsions. From this study, the TTI cohesion test that designated to measure torque force applied to the binder samples at different curing times to record the variation of torque versus displacement until the torque remains constant indicating the sample has fully cured. The test provided two parameters to gauge adequate curing time called Curing Index and t_{95}. The curing index is the percentage of the total cure that has occurred at six hours, and t_{95} is the time required to reach 95 percent of the maximum torque. Based on these parameters, 75 or more cure index and 35 hours or less of t_{95} should be obtained to ensure curing time.

Similar study to investigate the influence of factors on the adhesive bond strength of the tack coat at the interface between pavement layers (*12*). Several test equipments were evaluated such as Florida DOT Shear tester, the UTEP Pull Off tester, and the Torque Bond test on a CSS-1 emulsion tack coat. It was found that while milling provided a significant improvement in bond at the interface between the existing surface and the new overlay, curing time had a minimal effect on the bond strength. With regards to evaluating test equipments, on the whole, the results from the FDOT Shear Tester were consistent compared to other tests conducted. However the results of this study are limited since only one type of material was tested and the variation of environmental condition was not considered.

Measuring texture depth was conducted to quantify transverse variable asphalt rates (TVAR), which is used as means of reducing wheel path flushing and consequent loss of texture and skid resistance (*13*). The Circular Track (CT) meter, the Outflow meter, and the Sand Patch tests were employed to determine textures at wheel path and outside of wheel path. The results indicated that differences in texture transversely can be useful in assessment of TVAR and successfully correlated with visually observed severity of wheel path flushing.

CHAPTER III DAMAGES AND COSTS ASSOCIATED WITH SHL MOVES

In this chapter, the researchers reviewed case studies monitored by the TxDOT engineers to identify pavement damage types due to SHL moves and estimate the costs to repair the damage.

Damages Associated with SHL Moves

Several case studies have been performed to evaluate pavement damages due to SHL moves. Chen et al. (*1, 14*) evaluated the routes before and after SHL moves at several locations with various field testing devices such as the falling weigh deflectometer (FWD), dynamic cone penetrator (DCP), and profiler. The readings from FWD and profiler were mostly identical before and after SHL moves, and no apparent structural damage was detected from the field survey. Nokes (*15*) also reported that visual crack surveys and Dynaflect data do not show any discernible short-term damage to the pavements after SHL moves made.

With regard to structural failure, a severe damage was recently reported from the Corpus Christi District in 2004. The SHL type was a hydrotreator reactor having 1,978 kips of GVW with 21-ft width and height and 117-ft length. The maximum tire load was 12,500 lb and most of tires weighed 6,250 lb. The move originated from Aransas Pass, Texas, on January 12, 2004, and was completed at Three Rivers on February 26, which was around 150 mile of travel. Along the route, around 7 mileage of FM 796 at the San Patricio County, which classified with load zoned road, was found to be the weakest section. The TxDOT engineers evaluated the route and found that the route was structurally inadequate to sustain such loads. Since there was no alternative route available, the move was allowed under agreement that the carrier should be responsible for whatever damage occurred. The route was generally composed of 2-in of asphalt concrete with multiple chip seals, 8-in of flexible base, and subgrade. The lane width was about 20-ft wide. Considering the width of SHL, the outer wheels appeared to travel either very close to the edge that has no shoulder or outside the edge of pavement. Figure 3 shows the variation of normalized deflection at the center of loading (W1) and 72-in from the load (W7) the FWD test results. The W1 ranged from 7.7 to 121.3 mils with an

overall average value of 65.4 mils, while W7 ranged from 1.7 to 5.6 mils with average value of 3.4 mils.

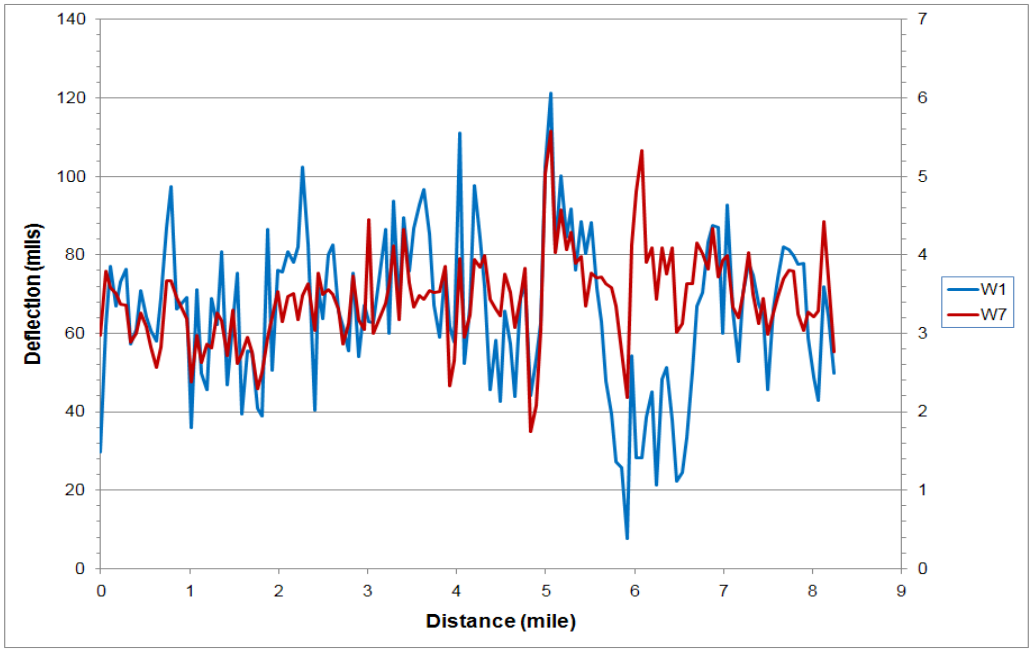

Figure 3. Normalized FWD Deflection on FM 796.

Researchers calculated the surface curvature index (SCI) and base curvature index (BCI) to evaluate structural condition along the route. The SCI is the difference between W1 and W2 (8-in from the load) and BCI is computed by subtracting W3 (16-in from the load) from W2. Figure 4 shows the distribution of two indices along the route. The Project 5-1712 conducted training classes on selecting rehabilitation options for flexible pavements along with CDs. *(16).* Researchers employed this tool to interpret structural condition and found that the route is fallen into very poor condition with respect to SCI and BCI since most of values were above 20 and 10 with a given surface layer thickness, respectively.

During this move, 8-in of wood mats were placed over culverts and bridges to prevent any damage. Severe pavement damage did occur, however, on FM 796 as shown in Figure 5. According to TxDOT engineers, the area received consecutive rainfall events close to moving day, thus the damage might be due to the loss of load bearing capacity of underlying materials induced by unexpectedly high moisture content. It

indicates that it is extremely important to take into account weather conditions to reduce the likelihood of structural damage, particularly for routes where exhibiting a relatively weak structural capacity or routes built on expansive clay soils that susceptible to moisture.

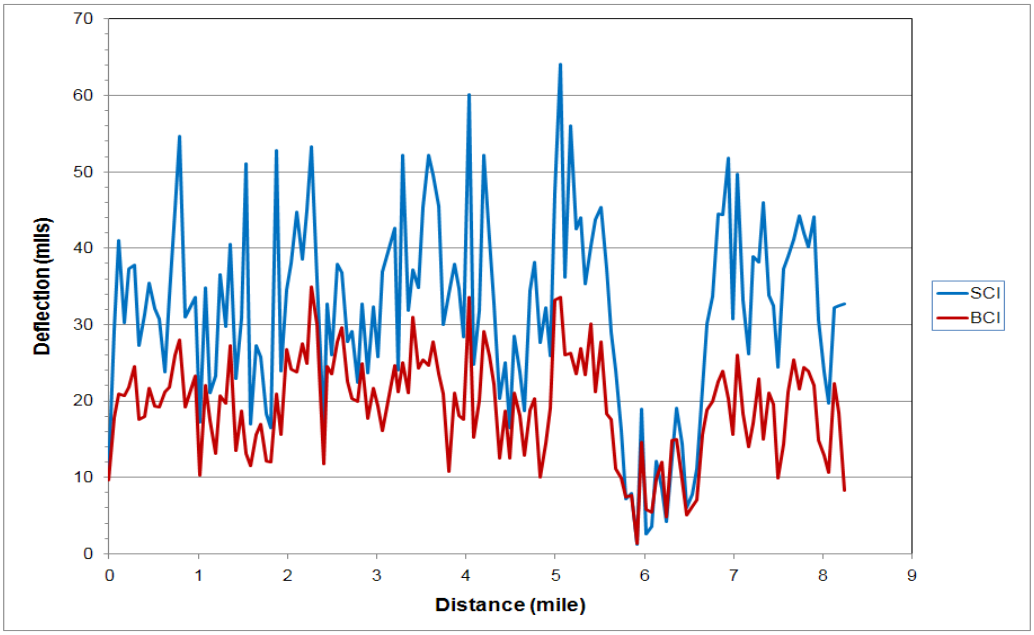

Figure 4. SCI and BCI on FM 796.

Figure 5. Severe Damage on FM 796.

The majority of SHLs have a wider width than normal trucks, so they often travel very close to the edge of the roadway. If the pavement is not supported with a paved shoulder or structurally sufficient lateral support, the route will sustain higher potential to the damage. Chen et al. (*14*) performed FWD testing on pavement edges and recommended at least 1 m of distance between the outer wheel and edge be kept to reduce the probability of damage. Satish et al. (*17*) conducted plate load tests at pavement edges, and found 0.9 m of shoulder width is sufficient with respect to structural support for flexible pavements. To mitigate structural failure with respect to superheavy loads, TxDOT has sponsored several research projects to develop procedures for the structure evaluation of superheavy load routes. Project 0-4519 conducted by Texas Transportation Institute verified the load-thickness design curves developed more than 50 years ago (*18*). From the verification, researchers found that the design shows some conservatism as used for checking the structural adequacy of a given pavement to sustain one application of the average of the ten heaviest wheel loads. The further verification of the current modified Texas Triaxial design method was achieved from the plate bearing test performed in both the field and laboratory. To evaluate load bearing capacity, researchers developed the *LoadGage* computer program with a modification of the Modified Triaxial (*MTRX*) Design Program developed from the Project 0-1869 (*19*) to accommodate a procedure to adjust strength properties depending on the moisture content difference which is associated with changes in soil suction change that is a major term to express strength properties based on findings of the project 0-1335. In addition, an extensive database containing field expected moisture contents for different types of soils with TTC for each county level was established using an integrated model of climatic effects, a compiled TTC database of TxDOT, and a soil report review. Figure 6 illustrates expected soil moisture contents across Texas climatic regions incorporated into the *LoadGage* program. The soils database and the moisture correction procedure incorporated in this program provides useful options that can be integrated into the superheavy load pavement review process to help minimize the need for triaxial testing and permit the evaluation of allowable wheel loads on proposed routes that realistically accounts for the effect of moisture on load bearing capacity.

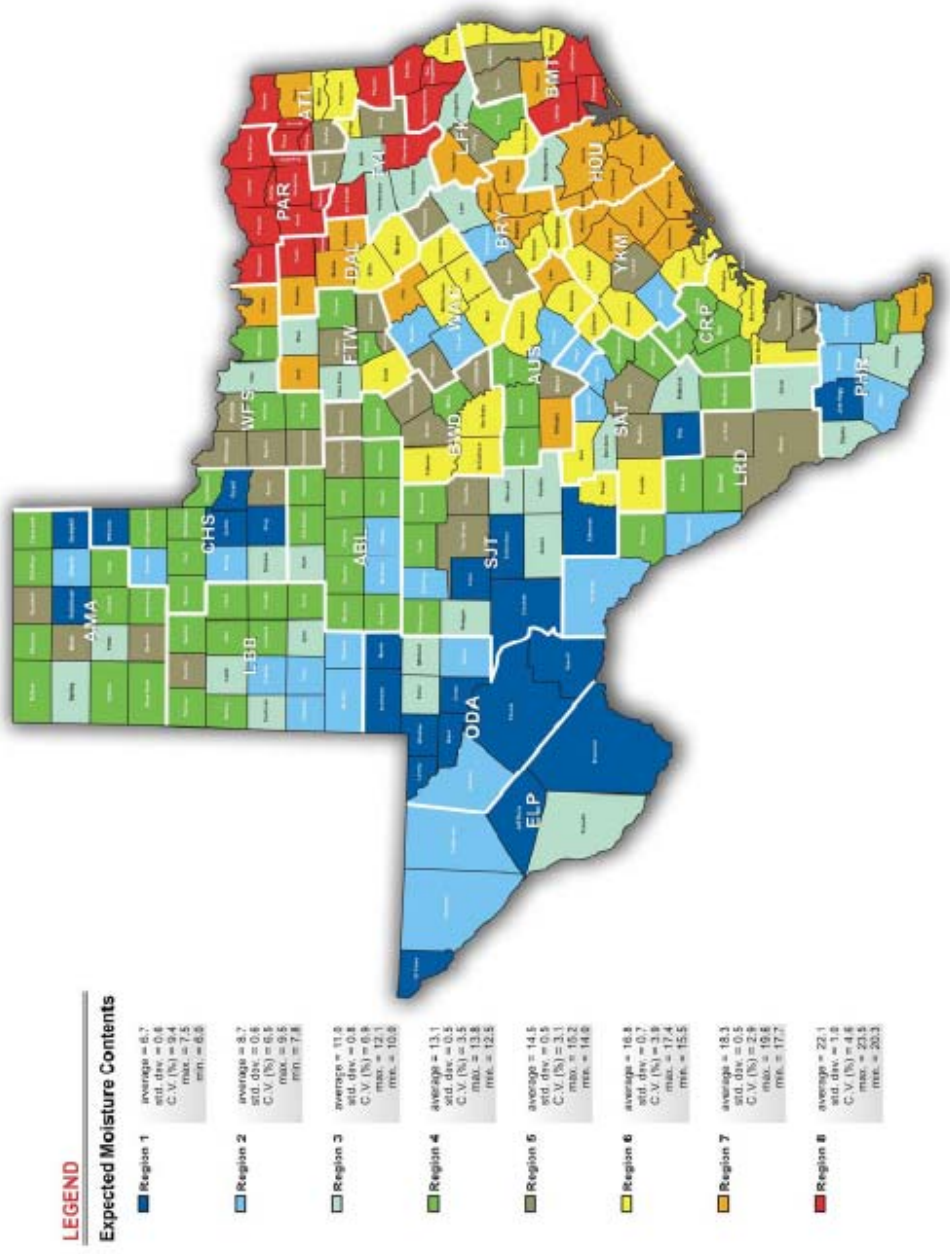

Figure 6. Variation of Expected Soil Moisture Contents across Texas (*18*).

Researchers made an attempt to analyze this route using *LoadGage* program with the given information. According to the soils database incorporated in *LoadGage*, the predominant soil in San Patricio County is identified as a CH soil with a Texas triaxial class of 5.2. Considering saturated subgrade soil conditions due to rainfall encountered prior to SHL moves, the field moisture content was set equal to the initial moisture content that represents capillary saturated condition, which is 19.4 percent of gravimetric water content. Researchers selected several sections to analyze based on the cumulative percentile of deflection (W1), shown in Figure 7. From this distribution, the locations corresponding to every 25 percentile were considered to represent existing condition of the route in this analysis. Table 4 shows the results of analysis using *LoadGage* program. The results indicated that most locations are likely to damage due to subgrade failure except a section that exhibits least deflection basin yielding a negative yield function. Greater positive yield function represents higher chances of damage. Researchers note from this limited verification that *LoadGage* might be useful to determine structural adequacy of a specific route since it is facilitating to analyze the route with moisture adjust option along with county level soil database tied to Texas Triaxial Classification (TTC) determining strength parameters without laboratory testing that requires substantial efforts to perform.

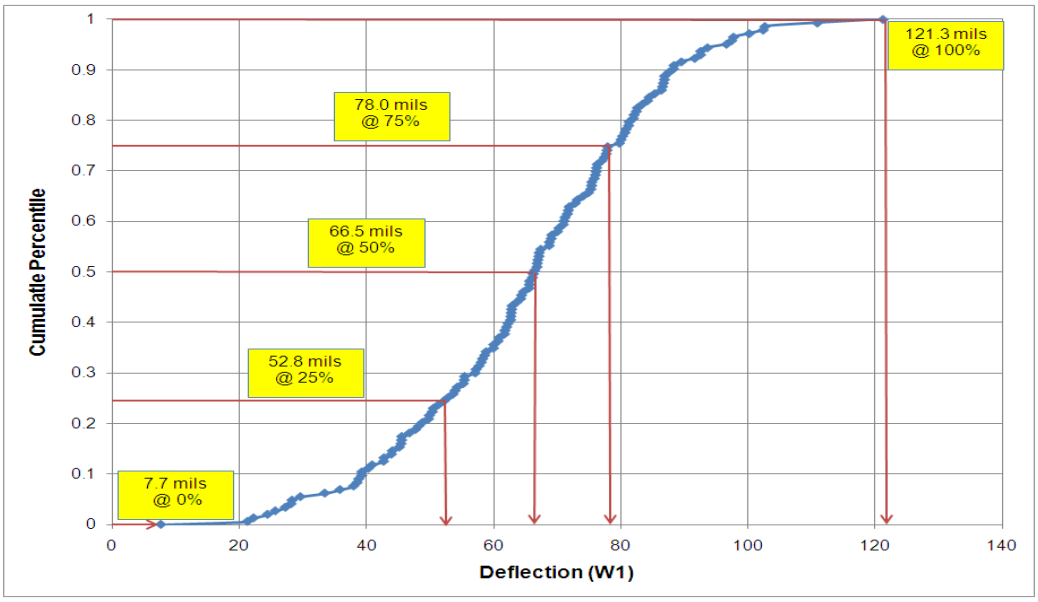

Figure 7. Cumulative Percentile of Deflection W1.

Table 4. Results of *LoadGage* Analysis.

W1 (mils)	W7 (mils)	AC (ksi)*	Base (ksi)*	Subgrade (ksi)*	Yield Function**	*LoadGage*
7.7	2.18	4170.9	671.4	11.4	-1.398	Pass
52.8	3.2	135.1	15.7	6.6	2.743	Fail
66.5	3.17	240.4	5.7	6.4	2.294	Fail
78.0	3.51	146.4	5.0	6.5	2.841	Fail
121.3	5.58	60.8	5.0	3.7	3.475	Fail

* FWD backcalculated modulus using MODULUS 6.0 program
** Mohr Coulomb yield function is calculated at the critical points. The value herein is the most critical one. The yield function is expressed as follows.

$$f = \frac{I_1}{3}\sin(\phi) + \sqrt{J_2}\sin\left(\theta + \frac{\pi}{3}\right) + \frac{\sqrt{J_2}}{3}\cos\left(\theta + \frac{\pi}{3}\right)\sin(\phi) - c\cos(\phi)$$

Where, I_1 = first stress invariant; J_2 = second deviatoric stress invariant; c = cohesion; ϕ = friction angle; and θ = Lode angle.

In addition, researchers carried out the analysis to determine the number of allowable load application with respect to pavement performances such as fatigue cracking and rutting based on Asphalt Institute (AI) equation. According to the current TxDOT procedure to evaluate pavement subjected to SHL moves as illustrated in Figure 2, should the number of allowable load application is less than 1000 with a given FWD load (9000 lbs with 5.9-in radius) then reroute be considered. The number of allowable load application is obtained as given equations.

$$N_f = 7.9488 * 10^{-9}\left(\varepsilon_t\right)^{-3.291}\left(E_{AC}\right)^{-0.854} \quad (1)$$

$$N_r = 1.365 * 10^{-9}\left(\varepsilon_{sg}\right)^{-4.477} \quad (2)$$

Where N_f *and* N_r = the number of allowable load application due to fatigue cracking and rutting, respectively; ε_t = tensile strain at the bottom of asphalt layer; ε_{sg} = compressive strain at the top of subgrade; and E_{AC} = asphalt modulus. Researchers used a layered elastic program BISAR to compute critical stains for above five locations considered in Table 4. Table 5 shows the results of this analysis. The results revealed that the current TxDOT procedure with respect to rutting criterion would be more applicable to determine structural adequacy. Two locations corresponding to 75 and 100 cumulative percentile of W1 yield the number of allowable load application due to rutting less than 1000. Another two locations corresponding to 25 and 50 percentile also exhibited close to 1000 implying that the locations would have a high probability of structural failure. The

results presented in Table 4 and 5 appear to be comparable representing the same order in magnitude in terms of yield function versus N_r.

Table 5. Results of AI Equations Used Analysis.

W1 (mils)	AC (ksi)	ε_t (10^6 με)	ε_{sg} (10^6 με)	N_f	N_r
7.7	4170.9	21.07	182.9	433,567,631	73,994,918
52.8	135.1	784.1	2177	54,949	1,131
66.5	240.4	1052	2057	12,769	1,458
78.0	146.4	1436	2341	7,004	817
121.3	60.8	2165	4441	3,841	46

As far as the seal coat damage, spreading water on the pavement surface appears to be effective in reducing surface shear force for at least plane segments (*1*). From the limited field observations, a tentative criterion on seal coat was established not to allow SHL to travel a route with a fresh seal coat within 5 weeks placed age (*1*).

Recent field observations conducted on FM 109, FM 1371, FM 2210, SH 43, and SH 56 showed most of the seal coat damage took place near vertical grades under high pavement temperatures as shown in Figure 8.

Figure 8. Seal Coat Damage along with Slope.

It should be also noted that FM 2210 route where placed with seal coat composed of CRS-2P and limestone aggregate in 2003 experienced seal coat damage due to SHL moves made in 2004 along with high pavement surface temperature. This indicates that

it might not be facilitating to regulate SHL moves on seal coat routes solely applying the current 5-week criterion. Case studies infer that most damage associated with SHL moves is seal coat deterioration rather than structural failure took place on FM 796 thus an emphasis was placed to evaluate seal coat damage mechanism and develop a guideline to control the damage in this study based on the findings from case studies and communication with project committee members.

Cost Associated to Repair Damage

Damage caused by the SHL moves needs to be repaired depending on severity of damage to provide a better ride quality for road-users and ensure performance within an expected life cycle. Researchers made an attempt to assess the cost to repair such damages in order to measure significance of regulating SHL moves effectively. Researchers contacted TxDOT maintenance division personnel to gather information on this concern. Table 6 shows statewide maintenance activities taken especially for pavement repair during FY09, provided by Mrs. Tammy Sims. As shown in the table, the major maintenance activity was associated with surface layer repair by means of overlay and seal coat in terms of total cost spent, even though the unit cost is relatively cheap. Researchers quantified unit cost per mile for several maintenance options considering a typical low-volume road geometry condition that has a higher potential damage as follows.

- Seal coat: Area per mile = 20 feet (lane width) * 5280 feet (length equivalent to 1 mile) = 105600 SF = 11721.6 SY. Thus, the unit cost would be around **$25,000/mile** (11721.6 SY * $2.13/SY).
- Overlay with maintainer: The unit cost would be around **$53,000/mile** (11721.6 SY * $4.54/SY).
- Base in place repair: Volume per mile = 20 feet (lane width) * 5280 feet (length equivalent to 1 mile) * 0.67 feet (8-in base thickness) = 70752 CF = 2617.8 CY. Thus, the unit cost would be around **$67,000/mile** (2617.8 CY * $25.44/CY).
- Edge repair: The unit cost would be around **$5,544/mile** (5280 LF * $1.05LF).
- Full depth removal/replacement: The unit cost would be around **$990,000**/mile (11721.6 SY * $84.38/SY).

Table 6. Statewide Maintenance Activities during FY09.

Unit	Description	Total Cost ($)	Total Amt of Work ($)	Statewide Unit Cost ($)
CY	BASE REMOVAL/REPLACEMENT	29,153,059.05	455,414.00	64.01
CY	BASE IN PLACE REPAIR	32,350,277.03	1,271,820.00	25.44
SY	UNPAVED ROAD MAINTENANCE	476,678.46	1,561,101.00	0.31
SY	LEVELING/OVERLAY W/ LAYDOWN	64,972,910.16	8,301,042.00	7.83
SY	LEVELING/OVERLAY W/ MAINTAINER	83,520,934.35	18,399,598.00	4.54
SY	LEVELING/OVERLAY WITH DRAG BOX	4,184,111.17	1,737,025.00	2.41
LM	SEALING CRACKS	16,225,552.10	23,778.00	682.38
SY	SEAL COAT	36,285,573.85	17,011,401.00	2.13
SY	ADDING/WIDENING PAVEMENT	13,110,422.03	2,485,505.00	5.27
SY	MILLING/PLANING	12,211,359.86	5,971,717.00	2.04
LF	EDGE REPAIR	18,965,213.57	18,096,298.00	1.05
SY	FULL DEPTH REMOVAL/REPLACEMENT	13,479,032.54	159,746.00	84.38
SY	RESHAPING UNPAVED SHOULDERS	9,299,536.08	29,679,155.00	0.31
SY	TRAFFIC CONTROL PLAN	36,344,800.89	-	0
SY	EMER. REPAIR TO BASE & SUBGRADE	1,963,302.08	-	0
SY	EMER. REPAIR TO ASPHALTIC SURFACES	1,399,477.08	-	0

Chen monitored SHL damages that occurred from 2002 to 2005 (*20*). SH56 and US377 in Paris District experienced fresh seal coat damage during summer in 2005 as shown in Figure 9. Consequently, it was reported that the carrier paid $265,717 for the damage repair. Considering mileage associated with seal coat damage, which is approximated 10 miles, the estimated repair cost turned out to be $250,000 based on FY 09 unit cost indicating that the assessment appears reasonable. In June 2005, FM1371 in Bryan District had a mild scraping of seal coat that has been several years old due to SHL moves with 6500 lbs of maximum tire load and 792 kips of gross vehicle weight. The maintenance forces fixed all damaged locations and sent two bills to the carrier. The total bill was $4,575.78.

Figure 9. SH56 and US377 Seal Coat Damaged Sections.

Researchers are of the opinion that the repair cost would vary case by case but it is evident that a logical guideline for SHL moves on fresh seal coats is imperative to minimize maintenance activities.

CHAPTER IV DEVELOPMENT OF A MECHANISTIC APPROACH

This chapter describes efforts to develop a mechanistic approach to model seal coat behaviors subject to different temperature and time conditions in order to determine extent of failure due to SHL moves. Employing fracture mechanism and aging model in asphalt binders was undertaken along with characterizing fundamental material properties such as surface energy, temperature-viscosity relationship, and volumetric properties. In addition, reviewing previous studies was conducted to determine properties film thickness and crack density to estimate tensile strength of seal coat mixture evaluated in this study.

Seal Coat Failure Mechanism

Considering representative phenomenon of peeling seal coats along the sloped pavement, researchers conceptualized the seal coat failure mode through a free body diagram as shown in Figure 10. From this diagram, it is feasible to estimate resistance force terms induced within the seal coats and fracture force components generated from wheel load as a function of different slope level, friction condition, and tire width.

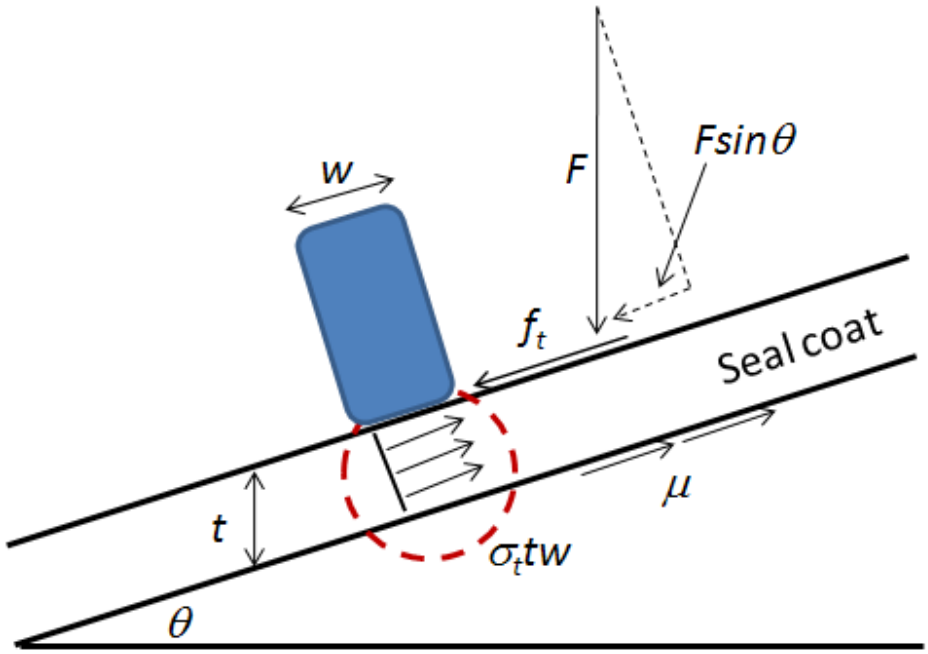

Figure 10. Free Body Diagram of Seal Coat Damage.

From the diagram, the Equation (3) can be considered based on the equilibrium force relationship. In the equation, the positive force term is applied along with the slope angle (θ).

$$\sum F = \sigma_t \cdot t \cdot w - f_t \cdot w - F \sin\theta + F \cdot \mu \cos\theta = 0 \tag{3}$$

From Equation (3), failure will occur if the tensile strength (σ_t) is less than the fracture pressure (right side term) induced by the tire on the pavement as shown in Equation (4).

$$\sigma_t \le \left[\frac{f_t}{t} + \frac{F}{t \cdot w}\left(\sin\theta - \mu \cdot \cos\theta\right) \right] \tag{4}$$

where, f_t = tire traction force per tire width; t = seal coat thickness; w = tire width; F = wheel load; and μ = friction between the seal coat and the underlying existing layer. It is advantageous in this formulation to use coefficient of μ as a calibration factor to simulate different stage of frictions tied to variation of temperature and aging.

From the given Equation (4), it calls for determining tensile strength of seal coats to evaluate damage potential. Since it is not feasible to measure tensile strength of the seal coat mixture from laboratory testing, researchers alternatively employed a fracture mechanics model to quantify tensile strength as a function of relevant material properties. Lytton (*21*) formulated tensile strength in terms of surface energy, crack density, crack length, asphalt mixture modulus properties (E_1 and m), and film thickness as given in Equation (5) for an adhesive fracture mode. Appendix A describes the derivations of this equation in more detail.

$$\left(\sigma_t\right)_{\max} = \left\{ \frac{8\pi}{3t\left(1 + \frac{E_f}{E_s}\right)} \left(\frac{m\overline{c^2}}{A} \right) \left[\Delta G_f^a \left(E_\infty + E_1 \left(\frac{t_l}{a_T} \right)^{-m} \right) \right] \right\}^{0.5} \tag{5}$$

where *m/A = crack density;* $\bar{c}$ = average crack length; G_f^a = total surface energy of mixture at adhesive fracture mode; E_f/E_s = ratio of fluid modulus to solid modulus in mixture (≈ 0.2); t_l = loading time; a_T = temperature correction factor; t = film thickness (microns); and E_∞, E_1, and m = asphalt mixture modulus coefficients (typically $E_\infty = 0$).

Material Characterization

Researchers made an attempt to determine inputs to calculate tensile strength of seal coats evaluated in this study. Five types of seal coat binders were selected and tested: AC20-5TR, AC20-XP, AC10-2TR, AC-15P, and CRS 2P. Grade 4 lightweight and limestone of Bridgeport in Texas were tested to obtain surface energy components. Other types of aggregate such as granite, sandstone, and gravel were also used for mixture designs to estimate volumetric properties.

Crack Density Function

Marek and Herrin (*22*) calculated crack density based on cavitation analyses by assuming a brittle model of crack failure for the HMAC specimen. In the analysis, an average microcrack length ($\bar{c}$) of 0.381 mm was used from 281 HMAC specimens. The microcrack density (*m/A*) was calculated using these data as a function of the number of cracks per specimen cross-sectional area to be 2.317 mm^{-2}. Since the typical HMAC has more potential to crack than seal coat materials due to its brittleness and it is not feasible to obtain the actual value, the decision was made to use the value in this study with conservative assumption.

Film Thickness

According to Burak and Agar (*23*), the asphalt film thickness has an influence on the moisture susceptibility of HMAC because it affects durability of the mixture. Generally, while thicker film thicknesses lead to more durable mixtures, brittle mixtures with thinner film thicknesses tend to crack, thus shortening the service life of the pavement. Kandhal et al. (*24*) reported that the asphalt binder film thickness less than 10 microns compacted to 8 percent air void content revealed accelerated aging based on the limited experimental study conducted. From this, an expression to quantify the minimum film thickness was given below.

$$Film\ Thickness(microns) = \frac{Air\ Void(\%) \times 4870}{4000} \quad (6)$$

In this study, the air void of AC20-5TR with lightweight aggregate mixture was 26.2 percent. Thus, the minimum film thickness is 32 microns. A typical film thickness of asphalt can be calculated using given Eq. (7).

$$FilmThickness\,(microns) = \frac{Weight\ of\ effective\ binder}{SA \times 1000 \times (Specific\ gravitiy\ of\ asphalt)} \qquad (7)$$

The calculated film thickness was 120 microns, and it was much thicker than typical asphalt film thickness because of extremely low surface area (SA) due to the absence of fine materials representing the typical gradation of Grades 3 and 4 aggregate used for seal coat construction as shown in Table 2 and 3. Examining Equation (5), thicker film thicknesses eventually yield to lower tensile strength. Lytton (*25*) reported the relationship between binder film thickness and failure type (adhesive and cohesive). Asphalt mixture damage takes place within the mastic (cohesive failure) or at the aggregate-mastic interface (adhesive failure). For thinner film thickness, the adhesive tensile strength is less than cohesive tensile strength. For the thicker film thickness, vice versa. It was found that around 60 microns of film thickness indicates the border of adhesive and cohesive failure zone as shown in Figure 11.

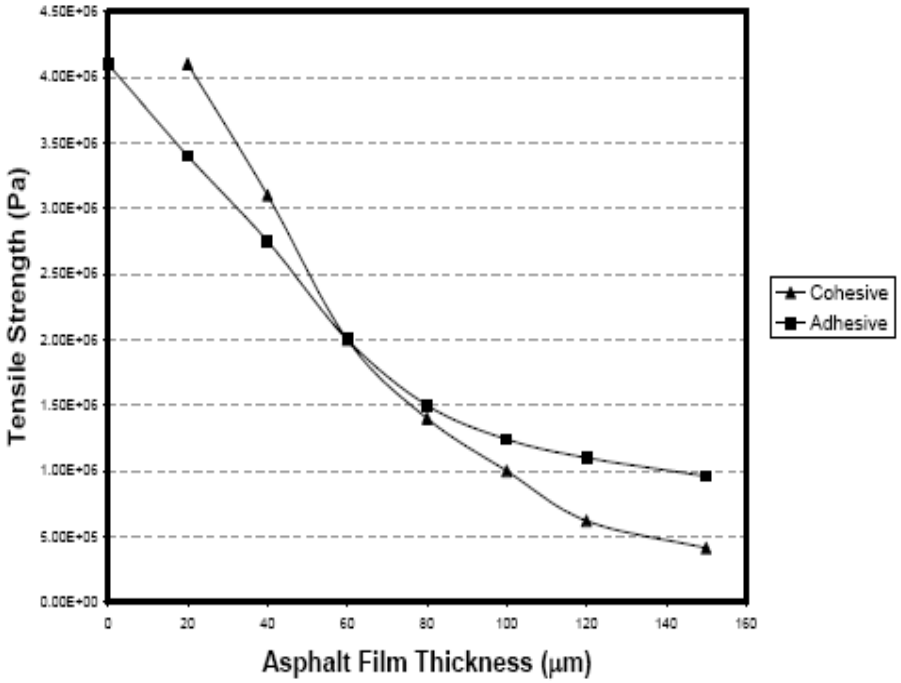

Figure 11. Film Thickness versus Tensile Strength (*25*).

Since the failure of seal coat observed from field sections is likely to the apart of aggregates from seal coat binder, it seems that the failure mode can be considered adhesive fracture mode. Therefore, the decision was made to use 60 microns of film thickness for a realistic assessment of tensile strength in this study.

Surface Energy

The development of fatigue cracking in asphalt material is associated with energy dissipation and storage on fracture surfaces as expressed in Equation (8) (*26*).

$$W = E_R D(t_\alpha) J_R \quad (8)$$

where, W is the work done per unit of each crack surface area created, E_R is the reference modulus used in determining the pseudostrain energy that is available to extend the track; $D(t_\alpha)$ is the viscoelastic creep compliance over a period t_α, the time equivalent for a crack to move a distance equal to the length (α) of the process zone ahead of the crack tip; and the J-integral J_r, is the pseudostrain energy release rate per unit crack area from one load cycle to the next. Thus, at the point of the pseudostrain energy released is greater than the required minimum energy for bond breakage, crack extension occurs (*27*).

Researchers at Texas A&M University developed the calibrated mechanistic approach with surface energy measurements (CMSE) approach to characterize HMAC materials both in terms of fracture and healing processes (*28, 29*). The surface energies in asphalt mixtures are composed of contributions from nonpolar short-range Lifshitz-van der Waals (LW) forces and longer-range polar acid-base (AB) forces mainly associated with hydrogen bonding (*30, 31, 32*). The polar acid-base surface energy is itself also a combination of the acid surface energy and the base surface energy. These polar forces typical of hydrogen bonding take longer to form and act perpendicular to the crack faces to actively pull them together, while the nonpolar tensile short-range and short-lived Lifshitz-van der Waals forces act in the plane of the crack face to form a contractile skin that resists healing (*30, 31, 32*).

The Wilhelmy Plate test and the Universal Sorption test was separately conducted to measure surface energy components of binder and aggregate, respectively (*33, 34)*.

The Wilhelmy plate test is measuring contact angles by immersing a binder coated slide into different types of probe liquid as shown in Figure 12.

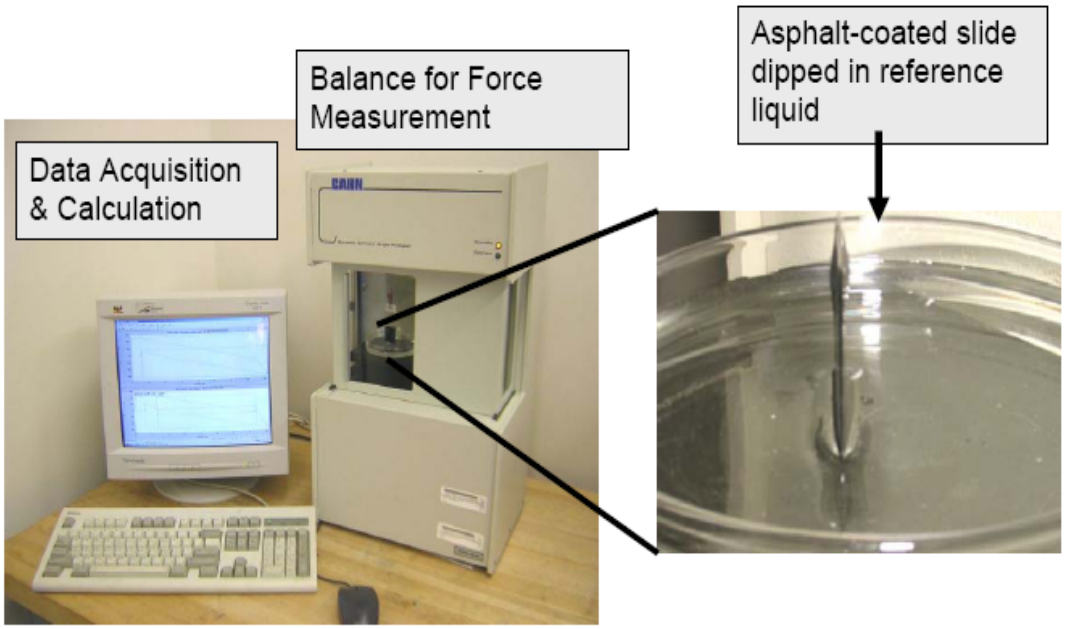

Figure 12. Wilhelmy Plate Test Set Up.

From this, the advancing and receding contact angles are recorded, respectively. In principle the both angles must be identical over a given solid surface. However it has been reported that hysteresis exists between advancing and receding angles due to surface roughness or chemical heterogeneity according to a previous study (*35*). Hefer et al. (*33*) recommend that the advancing angle be used for calculating total surface energy rather than the receding angle since more reasonable measurements were achieved especially in polar components. However other researchers (*36, 37*) state that the receding angle also can be used for surface energy estimation. Theoretically, while healing components are determined from advancing (wetting) condition, fracture components are found when receding (dewetting). Therefore, researchers used the receding angle for calculating total surface energy of seal coat binders in this study to reflect fracture mechanism of seal coats found in field observations. Surface energy components of aggregates are calculated from spreading pressures of three probe vapors on the aggregate surface using the Universal Sorption test (*34*) as shown in Figure 13. Theoretical basis and test procedure on these tests can be referred to the report written by Lytton et al. (*27*).

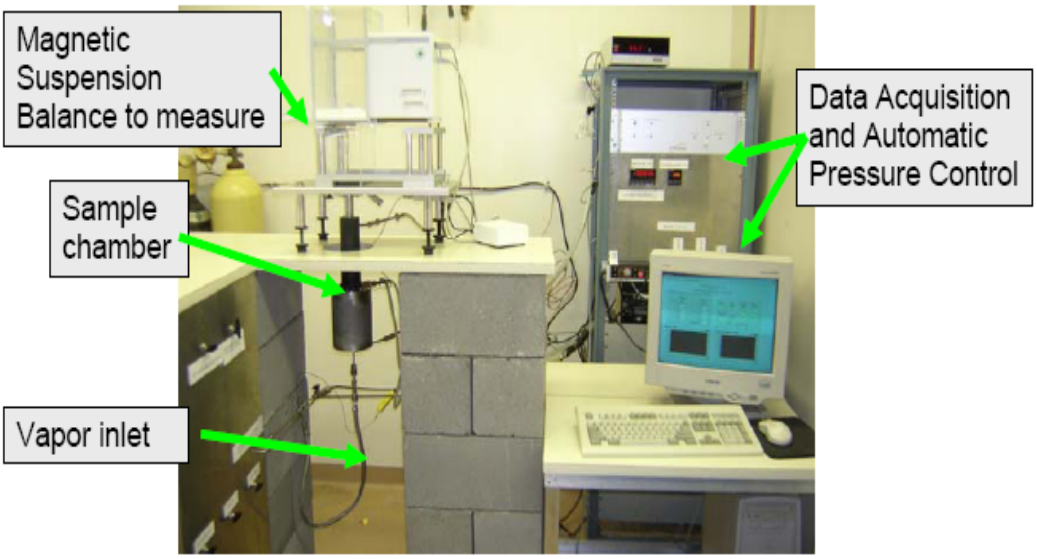

Figure 13. Universal Sorption Test Set Up.

From these tests, the ability of adhesion between the bitumen and aggregate at their interface in a dry and wet condition as follows:

$$\Delta G_{ab}^{dry} = 2\sqrt{\Gamma_a^{LW}\Gamma_b^{LW}} + 2\sqrt{\Gamma_a^{+}\Gamma_b^{-}} + 2\sqrt{\Gamma_a^{-}\Gamma_b^{+}} \quad (9)$$

$$\Delta G_{abw}^{wet} = \Gamma_{aw} + \Gamma_{bw} - \Gamma_{ab} \quad (10)$$

where the subscript a = aggregate; b = bitumen; and w = water. For any two phases represented by subscript "i" and "j"

$$\Gamma_{ij} = \Gamma_{ij}^{LW} + \Gamma_{ij}^{AB} \quad (11)$$

$$\Gamma_{ij}^{LW} = \left(\sqrt{\Gamma_i^{LW}} - \sqrt{\Gamma_j^{LW}}\right)^2 \quad (12)$$

$$\Gamma_{ij}^{AB} = 2\left(\sqrt{\Gamma_i^{+}} - \sqrt{\Gamma_j^{+}}\right)\left(\sqrt{\Gamma_i^{-}} - \sqrt{\Gamma_j^{-}}\right) \quad (13)$$

Whereas a higher magnitude of the absolute value of bond energy in dry condition indicates stronger adhesion between aggregate and binder less susceptible to moisture damage, a higher absolute bond energy in wet condition means greater potential for water

to displace interface between aggregate and bitumen (*27*). Previous studies (*27, 33, 34*) employed the compatibility ratio defined by the ratio of absolute dry adhesive energy to the wet adhesive energy in order to rank mixtures in terms of their moisture susceptibility. Higher compatibility ratio is desirable since it reflects high bond energy in dry condition and a lower release of free energy in presence of moisture.

Five types of binder and two types of aggregate were tested to measure surface energy components and the results were tabulated as presented in Table 7. For seal coat binders, several replications were made to check the variation of measurements of surface energy components. It resulted that each component was measured close enough to take average values for each material.

Table 7. Measured Surface Energy Components.

Binder Materials	**Ave. Surface Free Energy Components (ergs/cm^2)**				
	Γ_i	Γ_i^{LW}	Γ_i^{AB}	Γ_i^+	Γ_i^-
AC20-5TR (Wright Asphalt)	44.8	41.6	3.2	0.2	13.1
AC10-2TR (Valero)	48.1	42.7	5.4	0.4	18.2
AC20-XP (SH 30)	45.0	41.2	3.8	0.2	18.4
CRS-2P (Martin Asphalt)	50.4	39.6	10.8	2.1	14
AC15-P (Martin Asphalt)	55.6	51.6	4.0	0.2	20.4
Aggregate Materials	Γ_j	Γ_j^{LW}	Γ_j^{AB}	Γ_j^+	Γ_j^-
Lightweight (Bridgeport)	115.1	39.3	75.8	1.4	1027
Limestone (Bridgeport)	265.4	59.89	205.5	18.82	561.11

In addition, researchers included other types of aggregate that had been tested from previous studies conducted in TTI to calculate the total surface energy at adhesive fracture mode G_f^a of various seal coat mixtures that can be possibly considered in practice as presented in Table 8 using Equations (9) to (13). It was observed that the total surface energy substantially varied with different sources of aggregate in spite of the

same type of material. The total surface energies of mixtures composed of Limestone from El Paso and Traprock from Knippa generally exhibited higher magnitudes than other mixture combinations.

Table 8. Calculated Total Surface Energy of Seal Coat Mixtures.

Mixture Combinations	G_f (ergs/cm^2)	G_f (N*m/m^2)
LW* (Bridgeport)---Wright (2008) AC20-5TR	115.33	0.12
LW (Bridgeport)---Martin (2008) CRS-2P	179.26	0.18
LW (Bridgeport)---Valero (2008) AC10-2TR	131.13	0.13
LW (Bridgeport)---SH30 (2008) AC20-XP	117.52	0.12
LW (Bridgeport)---Martin (2009) AC15-P	129.42	0.13
LS* (Bridgeport)---Wright (2008) AC20-5TR	150.99	0.15
LS (Bridgeport)---Martin (2008) CRS-2P	198.47	0.20
LS (Bridgeport)---Valero (2008) AC10-2TR	168.03	0.17
LS (Bridgeport)---SH30 (2008) AC20-XP	157.32	0.16
LS (Bridgeport)---Martin (2009) AC15-P	171.56	0.17
LS (El Paso)---Wright (2008) AC20-5TR	200.81	0.20
LS (El Paso)---Martin (2008) CRS-2P	226.87	0.23
LS (El Paso)---Valero (2008) AC10-2TR	213.60	0.21
LS (El Paso)---SH30 (2008) AC20-XP	205.24	0.21
LS (El Paso)---Martin (2009) AC15-P	225.85	0.23
LS (Brownwood)---Wright (2008) AC20-5TR	122.70	0.12
LS (Brownwood)---Martin (2008) CRS-2P	162.89	0.16
LS (Brownwood)---Valero (2008) AC10-2TR	135.10	0.14
LS (Brownwood)---SH30 (2008) AC20-XP	125.66	0.13
LS (Brownwood)---Martin (2009) AC15-P	137.94	0.14
LS (Odessa)---Wright (2008) AC20-5TR	120.92	0.12
LS (Odessa)---Martin (2008) CRS-2P	166.37	0.17
LS (Odessa)---Valero (2008) AC10-2TR	133.81	0.13
LS (Odessa)---SH30 (2008) AC20-XP	123.40	0.12
LS (Odessa)---Martin (2009) AC15-P	135.33	0.14
LS (Caldwell)---Wright (2008) AC20-5TR	140.38	0.14
LS (Caldwell)---Martin (2008) CRS-2P	177.42	0.18
LS (Caldwell)---Valero (2008) AC10-2TR	151.93	0.15
LS (Caldwell)---SH30 (2008) AC20-XP	142.52	0.14
LS (Caldwell)---Martin (2009) AC15-P	156.88	0.16
GR* (Atlanta, TX)---Wright (2008) AC20-5TR	119.99	0.12
GR (Atlanta, TX)---Martin (2008) CRS-2P	153.11	0.15
GR (Atlanta, TX)---Valero (2008) AC10-2TR	130.37	0.13

Table 8. Calculated Total Surface Energy of Seal Coat Mixture (continued).

Mixture Combinations	G_f (ergs/cm^2)	G_f (N*m/m^2)
GR (Atlanta, TX)---SH30 (2008) AC20-XP	122.04	0.12
GR (Atlanta, TX)---Martin (2009) AC15-P	136.24	0.14
GR (Victoria, TX)---Wright (2008) AC20-5TR	140.91	0.14
GR (Victoria, TX)---Martin (2008) CRS-2P	181.11	0.18
GR (Victoria, TX)---Valero (2008) AC10-2TR	152.79	0.15
GR (Victoria, TX)---SH30 (2008) AC20-XP	142.76	0.14
GR (Victoria, TX)---Martin (2009) AC15-P	157.49	0.16
GN* (Wichita, TX)---Wright (2008) AC20-5TR	167.62	0.17
GN (Wichita, TX)---Martin (2008) CRS-2P	224.32	0.22
GN (Wichita, TX)---Valero (2008) AC10-2TR	189.13	0.19
GN (Wichita, TX)---SH30 (2008) AC20-XP	177.00	0.18
GN (Wichita, TX)---Martin (2009) AC15-P	192.47	0.19
SS* (Atlanta, TX)---Wright (2008) AC20-5TR	138.89	0.14
SS (Atlanta, TX)---Martin (2008) CRS-2P	174.14	0.17
SS (Atlanta, TX)---Valero (2008) AC10-2TR	151.95	0.15
SS (Atlanta, TX)---SH30 (2008) AC20-XP	143.30	0.14
SS (Atlanta, TX)---Martin (2009) AC15-P	157.19	0.16
TR* (Knippa)---Wright (2008) AC20-5TR	255.10	0.26
TR (Knippa)---Martin (2008) CRS-2P	590.83	0.59
TR (Knippa)---Valero (2008) AC10-2TR	320.48	0.32
TR (Knippa)---SH30 (2008) AC20-XP	256.07	0.26
TR (Knippa)---Martin (2009) AC15-P	268.31	0.27
RG* (Mulphy)---Wright (2008) AC20-5TR	118.63	0.12
RG (Mulphy)---Martin (2008) CRS-2P	169.36	0.17
RG (Mulphy)---Valero (2008) AC10-2TR	131.03	0.13
RG (Mulphy)---SH30 (2008) AC20-XP	119.49	0.12
RG (Mulphy)---Martin (2009) AC15-P	130.69	0.13

*LW = Lightweight; LS = Limestone; GR = Gravel; GN = Granite; SS = Sandstone; TR = Trap Rock; and RG = River Gravel

Relaxation Modulus Properties (E_1, m, t_1/aT)

Characterizing relaxation modulus properties of seal coat mixtures is a key aspect of this proposed mechanistic approach. In this study, an alternative method was employed to obtain relaxation modulus properties due to difficulty in molding specimens with seal coat mixture. For this, a dynamic modulus predicted equation developed by Witczak (*38*) as given equation (14), which is incorporated into the Mechanistic-

Empirical Pavement Design Guide (M-E PDG) program as a level 2 approach to establish the master curve without performing dynamic modulus laboratory test, was instead utilized to establish the master curve.

$$\log E^* = \delta + \frac{\alpha}{1 + e^{\beta + \gamma \log t_r}} \quad (14)$$

where, t_r is the time of loading at the reference temperature, and the model coefficients δ, α, β, and γ are defined as follows:

$$\delta = 3.750 + 0.029\, p_{200} - 0.002\left(p_{200}\right)^2 - 0.003\, p_4 - 0.058 V_a - 0.802\left(\frac{V_{beff}}{V_{beff} + V_a}\right) \quad (15)$$

$$\alpha = 3.872 - 0.002\, p_4 + 0.004\, p_{38} - 0.000017\, p_{38}^{\ 2} + 0.005\, p_{34} \quad (16)$$

$$\beta = -0.603 - 0.394 \log \eta_T \quad (17)$$

γ = parameter describing the shape of the sigmoidal function, 0.313351,

η_T = bitumen viscosity at the reference temperature (77 °F), 10^6 Poise.

It is observed that δ and α is functions of volumetric mixture properties, specifically:

- air voids content V_a (%),
- effective bitumen content by volume V_{beff} (%),
- cumulative percent retained on 3/4-inch sieve, p_{34} (%),
- cumulative percent retained on 3/8-inch sieve, p_{38} (%),
- cumulative percent retained on No. 4 sieve, p_4 (%), and
- cumulative percent retained on No. 200 sieve (%).

For the gradation inputs, Tables 2 and 3 are used. A dynamic shear rheometer (DSR) test and core rock air void measurement were conducted to obtain temperature viscosity relationship, air void, and effective asphalt content. The DSR test measured binder complex shear modulus (G* in Pascal) and phase angle (δ in degree) at different temperatures from 58 °C to 67 °C with 10.08 radian/sec frequency and established a temperature-viscosity relationship using given equations. Table 9 and Figure 14 presented the test results.

$$\eta = \frac{G^*}{10}\left(\frac{1}{\sin\delta}\right)^{4.8628} \quad (18)$$

$$\log\log\eta = A + VTS\log T_R \quad (19)$$

where

TR = temperature in Rankine at which the viscosity was estimated, and

A, VTS = regression parameters.

Once the viscosity-temperature relationship is identified, a viscosity at the reference temperature can be calculated using A-VTS coefficient relationship.

Table 9. DSR Test Results of Seal Coat Binders.

	AC20-5TR		AC20-XP		AC10-2TR		AC-15P		CRS-2P	
Temp. (°C)	**G* (Pa)**	**δ (°)**	**G* (Pa)**	**δ (°)**	**G* (Pa)**	**δ (°)**	**G* (Pa)**	**δ (°)**	**G* (Pa)**	**δ (°)**
58	3174	71.2	2930	77.8	2151	80.7	1710	71.2	2970	74.8
61	2369	72.3	2020	78.4	1409	81.4	1260	71.1	2120	75.0
64	1476	71.5	1430	78.5	999	81.4	944	70.9	1520	75.2
67	1093	71.7	1030	78.2	668	82.5	723	70.5	1120	75.4

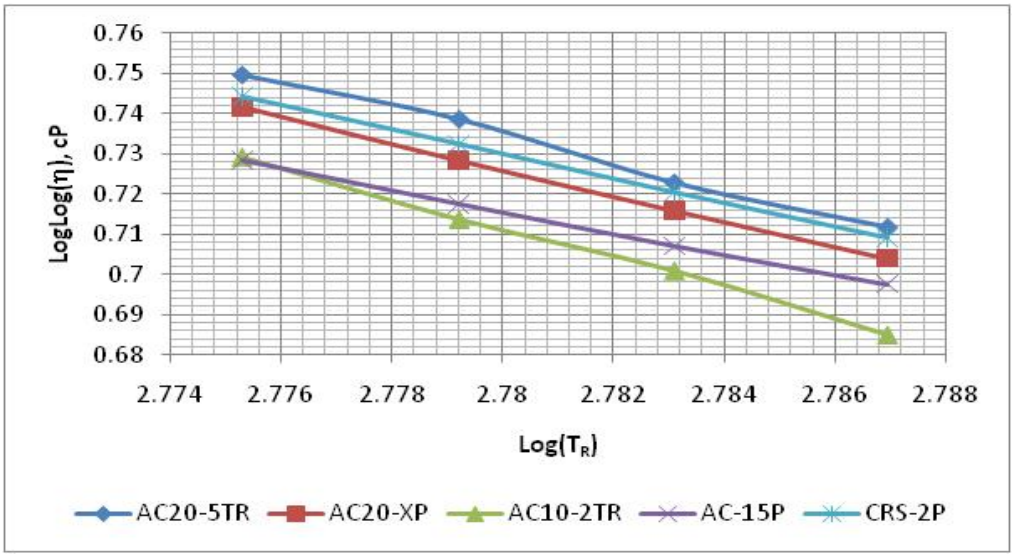

Figure 14. Temperature-Viscosity Relationship of Seal Coat Binders.

According to the plant sheet in Figure 15, the asphalt application rate and Grade 4 aggregate spread rate were assumed as 0.37 gallons per square yard and 1 cubic yard per 125 square yard, respectively, for the design experimental mixtures. Based on trials, the asphalt content was fixed at 5 percent of the total asphalt-aggregate mixture weight, which is equivalent to 10.5 percent of effective binder content in volume. A couple of samples using Grade 3 were also tried. For Grade 3 mixture, researchers used higher asphalt content 0.5 percent to compensate larger size of aggregate. With regards to gradation, aggregate was sized as follows based on (*11*):

- Grade 3: 0 percent by weight of retained on 1/2-inch sieve and 100 percent by weight of retained on 3/8-inch sieve, and
- Grade 4: 0 percent by weight of retained on 3/8-inch sieve and 100 percent by weight of retained on No. 4 sieve.

Samples were molded to a target air void of 20 percent in the Superpave gyratory compactor. However any of samples did not reach a target air void. The compaction was paused when the sample height appears to be constant. The cylindrical samples measured 4 inches in diameter and 6 inches in height as shown in Figure 16.

After compaction completed, the samples were capsulated by a plastic mold for 2 hours in the calibration chamber set to a room temperature 25 °C to prevent any possible collapse of the sample. In spite of this treatment, it failed to fabricate the mixture of CRS-2P since it was compacted too loose because of the characteristics of emulsions.

After curing, air voids of the molded samples were measured using the Corelok device. This device utilizes a controlled vacuum system to seal samples placed inside a plastic bag, which is then placed in a vacuum chamber. Under the vacuum, the bag conforms tightly around the sample, which prevents water infiltration. The volume of the sample is encapsulated within the bag and considered as the bulk volume, which is used to determine the bulk specific gravity. Air voids are then calculated by subtracting the ratio of the bulk specific gravity and maximum specific gravity from 100.

TEXAS DEPARTMENT OF TRANSPORTATION
DISTRICT BRYAN (17)

PROJ. NO. STP 2009(063), etc.
CSJ: 0049-15-011, etc.
HWY NO. FM 60
COUNTY Brazos
REF # 2

FORM 17-24 A

SUMMER 2009 REPORT SHOWING WORK PERFORMED

ENGLISH PROJECTS

ITEM DESCRIPTION			
ASPH AC-20-5TR OR AC-20XP	ITEM NO. 316-2532	LINE #250 ✓	DATE OF WORK: 7/8/09
AGGR TY PB OR PL GR4 SAC A	ITEM NO. 316-2414	LINE #245 ✓	DWR DATE:

GENERAL

LIMITS							ASPHALT				
DIST NO	STATION	STATION	L	W	AREA SY	TRK LDS	GAL START	GAL END	NET GAL	ASPH TEMP	G/SY
129	135+25 WBML	158+20 WBML	2295	11	2805		2260	1250	1010	350	.36
121	160+38 WBML	193+73 WBML	3335	11	4076		3940	2360	1580	350	.39
121	197+70 WBML	275+94 WBML	7824	12	10492		3940	560	3380	350	.32
121	144+02 WBS	158+20 WBS	1418	11	1733		2770			350	
121	160+38 WBS	193+73 WBS	3335	11	4076			650	2120	350	.36
	197+70 WBS	232+62 WBS	3492	10	3880		3770	2300	1470	350	.37
129	171+50 REER	192+05 REER	2055	16	3653		3940	2530	1410	350	.39
129	275+94 WBML	342+56 WBML	66662	12	8883		3660	650	3010	350	.34
121	342+56 WBML	374+22 WBML	3166	12	4221		3950	2540	1410	350	.33
121	374+22 WBS	318+62 WBS	5560	10	6178		2540	50	2490	350	.37
129	318+62 WBS	232+62 WBS	8600	10	9556		3860	80	3780	350	.40
121	374+22 EBML	286+72 EBML	8750	11	10694		4000	50	3950	350	.37
121	286+72 EBML	231+57 EBML	5515	11	6741		2400	50	2350	350	
129	436+39 REER	428+77 REER	762	20	1693		3960	3260	700	350	.41
					78521				28660		

ASPHALT DISTRIBUTOR CALIBRATIONS

DIST NO.	OWNER	MAKE/MODEL	SERIAL NO.	CAPACITY
1 P107	F.N. Ploch	Bearcat	51993	3750
2 P121	F.N. Ploch	Bearcat	2215	4200
3 P128	F.N. Ploch	Bearcat	111793	2040
4 P129	F.N. Ploch	Bearcat	21306	4200

HAUL TRUCK INFORMATION

TRUCK NO.	TRUCK MEAS. CY	NO. OF LOADS HAULED
P101	14	
P102	14	
P103	14	
P111	14	
P115	14	
P116	14	
P118	14	
P120	14	
P122	14	

104 x 14 = 1456 SY

PAYMENT INFORMATION

✓ AGGR. 1456 ✓ CY

✓ ASPH. 66220 ✓ GALLONS

AGGREGATE RATE

CY/SY 125.89

NO APPARENT MODIFICATIONS HAVE BEEN MADE IN THE ABOVE DISTRIBUTORS OR HAUL TRUCKS SINCE BEING CALIBRATED.

CALIBRATIONS ARE ON FILE AT THE DISTRICT CONSTRUCTIONS OFFICE.

COMMENTS:

▲ = No seal Bridges

■ = REER turns to Shoulder briefly

● = Shoulder turns to REER briefly

SHEET 2 OF 2

MEASURED, CALCULATED & REPORTED BY Philip Bullock

REPORT CHECKED BY D.Holman

Figure 15. Plan Sheet Example.

Figure 16. Molded Seal Coat Mixture.

Table 10 summarizes measured air voids of different combinations of mixture. Although a target air void was assigned 20 percent, all of measured values were over a target value. The least air void was obtained from limestone mixtures indicating better compatibility between aggregate and binder. For the mixture made of CRS-2P, researchers are of the opinion that higher air voids be assumed considering incompatibility between binder and aggregate with respect to compaction. Based on this, 30 percent of air void was assigned for CRS-2P mixture in establishing the mechanistic approach. It was found that Grade 3 aggregate mixture yielded a slightly higher air voids by around 1 percent even though limited number of samples were tested. It appears reasonable since a larger size of aggregate would tend to possess larger area of voids between binder and aggregates. Based on this, the mixture composed of Grade 5 that contains a larger portion of finer materials would expect to fill more voids resulting in fewer amounts of air voids and asphalt contents. In view of this, 1 percent of air voids added and subtracted to the air voids that obtained from Grade 4 mixtures to consider Grades 3 and 5 mixtures in the proposed mechanistic approach.

Table 10. Air Voids Measured.

Sample	Maximum Specific Gravity (gm/cm^3)	Bulk Specific gravity (gm/cm^3)	% Air Voids
Light Weight + AC10-2TR	1.504	1.102	26.7
Limestone + AC10-2TR	2.451	1.849	24.5
Limestone* + AC10-2TR	2.443	1.824	25.3
Sandstone + AC10-2TR	2.433	1.697	30.3
Light Weight + AC20-5TR	1.443	1.064	26.2
Sandstone + AC20-5TR	2.426	1.777	26.8
Limestone + AC20-5TR	2.444	1.924	21.3
Limestone* + AC20-5TR	2.450	1.898	22.5
Gravel + AC20-5TR	2.582	1.826	29.3
Light Weight + AC20-XP	1.443	1.023	29.1
Limestone + AC20-XP	2.451	1.839	25.0

Note: All aggregates are Grade 4 except denoted by * indicating Grade 3.

Consideration of Aging Effect

Asphalt binders experience aging after mixing and laydown during the service life due to oxidation, leading to the change of material properties of air voids and viscosity. Considering the characteristics of the predictive equation for dynamic modulus given in equation (14), the change of air void and viscosity along with aging is vital to determine the dynamic modulus of the mixture during its service life. In light of this issue, TxDOT has a tentative criterion stating that seal coats need to be cured for 5 weeks to minimize damage due to superheavy load moves. Therefore, an attempt was made to account for short-term aging effects to verify the criterion for the proposed mechanistic approach. To accomplish this, researchers employed a global aging system (*39*) which is also incorporated into the M-E PDG program. In this system, once the initial air void and viscosity properties are known, the properties after aging are calculated through the following four models:

- original to mix/laydown model,
- surface aging model,
- air void adjustment, and
- viscosity-depth model.

Using aged properties, a master curve is regenerated based on equation (14) and then E_1 and m values would be obtained in accordance with the curve using equation (20).

$$E(t) = E_1 t^{-m} \tag{20}$$

where t is a log reduced time in seconds.

The procedure is as follows:

- Estimate the mix/laydown viscosity ($\eta_{t=0}$, in cP) using the original value of η_{orig} (in cP) obtained from DSR testing.

$$\log\log(\eta_{t=0}) = a_0 + a_1 \log\log(\eta_{orig}) \tag{21}$$

$$a_0 = 0.054 + 0.004\,code \tag{22}$$

$$a_1 = 0.972 + 0.011\,code \tag{23}$$

where *code* is the hardening ratio with a recommended value of zero for average hardening resistance. The original viscosity at different temperatures is based on DSR test results using the following temperature-viscosity relationship.

$$\log\log(\eta) = A + VTS\log(T_R) \tag{24}$$

where T_R = Temperature in Rankine.

- From the surface aging model:

$$\log\log(\eta_{aged}) = \frac{\log\log(\eta_{t=0}) + At}{1 + Bt} \tag{25}$$

In Eq. (25), A is a function of the binder temperature T_R in °R, mean annual air temperature, and mix laydown viscosity, while B is a function of T_R. By substituting the mix laydown viscosity $\eta_{t=0}$, the aged viscosity $\eta_{t=aged}$ can be determined. The air void adjustment factor adjusts the viscosity form the surface aging model for air void effects using equation (26). The air voids adjustment factor, Fv, is a function of the air voids at the time of interest as shown in equation (27). The air voids at the time of interest can in turn be estimated from the initial air voids using equation (28).

$$\log\log(\eta_{aged})' = F_v \log\log(\eta_{aged}) \tag{26}$$

$$F_V = \frac{1 + 1.0367\times10^{-4}(VA)(t)}{1 + 6.1798\times10^{-4}(t)} \tag{27}$$

$$VA = \frac{VA_{orig} + \exp^{-1.0528\,t} - 1}{1 + 0.01406\,t + 0.00125\,t^{0.2307}\,Maat - 0.00325\,t\eta_{orig,77}} \tag{28}$$

where

VA_{orig} = initial air voids,

t = time in months,

$Maat$ = mean annual air temperature, °F,

$\eta_{orig,77}$ = original binder viscosity at 77 °F, MPoise (equal to 10^{-8} of cP).

- Using equation (14) with obtained aged binder viscosities and air void, construct a master curve and then obtain E_1 and m values by fitting equation (20) onto the master curve.

In order to check the developed procedure for estimating tensile strength, researchers conducted preliminary analyses on four mixtures characterized in this study with assumed various levels of temperature and curing period to verify their impact on the variation of tensile strength as well. They are (A) AC20-5TR with Grade 4 lightweight aggregate, (B) AC20-5TR with Grade 4 limestone (Caldwell), and (C) CRS-2P with Grade 4 limestone (Caldwell), and (D) CRS-2P with Grade 4 limestone (El Paso). The input values were tabulated to calculate tensile strength using equation (5) along with following above steps to find relaxation modulus properties E_1, m, t_1/aT in Table 11. It should be noted that aging effect on surface energy variation was not considered in this study. Lytton (*25*) investigated aging effect on surface energy through an accelerated laboratory aging process during 0, 3, and 6 months, which simulates equivalent field conditions: right after placing hot mix asphalt; 3 to 6 years aging; and 6 to 12 years aging in field, respectively. It was reported that dewetting (fracture) total surface energy decreases about 40 percent as the binder ages 6 month. Only 6 percent of reduction was observed from 0 to 3 months that is equivalent to 3 to 6 years aging in field thus an effect of aging on surface energy would be minimal in assessment of tensile strength of 5 weeks aged seal coats.

Table 11. Inputs Used to Estimate Tensile Strength.

Mixture	A	B	C	D
t (micron)	60	60	60	60
E_f/E_s	0.2	0.2	0.2	0.2
mc^2/A	0.3363	0.3363	0.3363	0.3363
ΔG_f^a (N*m/m^2)	0.12	0.14	0.18	0.28
V_a (%)	26.2	21.3	30	30
V_{beff} (%)	10.5	10.5	10.5	10.5
A-VTS	10.006-3.335	10.006-3.335	9.102-3.012	9.102-3.012

Figure 17 shows the shift of the master curve between the original and aged condition for AC20-5TR with lightweight aggregate mixture. For this comparison, a 130 °F of pavement surface temperature was assumed. The E_1 and m values were

obtained by fitting the master curve using equation (20). It was observed that E_1 value increased while the *m* value decreased as aging progressed. This trend is consistent with previous findings of a previous study conducted by Walubita (*40*). Considering four types of seal coat mixtures, the tensile strength was calculated at different levels of range of aging and temperature as shown in Figures 18 and 19. A pavement surface temperature of 130 °F and 1.25 months (5 weeks) of aging were assumed for each comparison. When it comes to the pavement surface temperature, all mixtures experienced drastic reduction in tensile strength due to the change of temperature shift factor that represents the sensitivity of bitumen properties to temperature variation. While highest tensile strength was obtained from mixture B, the lowest one from mixture C was obtained. In addition, the compatibility between limestone and AC20-5TR was superior to that of lightweight aggregate mixture as compared mixture A and B since mixture B exhibits higher total surface energy and lower air void. When the same source of limestone was mixed with AC20-5TR and CRS-2P as compared mixture B and C, higher tensile strength was achieved from the AC20-5TR mixture because a higher total surface energy of CRS-2P mixture comes to diminish advantage in compatibility due to a considerably larger air void. Comparison between mixtures C and D also indicates that the source of aggregate has a significant influence in controlling tensile strength primarily owing to the difference in surface energy. It reflects the observation that mixtures tend to gradually gain tensile strength along with short-term aging as shown in Figure 19. After 3 weeks aging, an incremental extent of tensile strength becomes alleviating as shown in Figure 20. From this, it is evident that higher pavement surface temperature and shorter curing period yields lower tensile strength that lead to a higher likelihood of failure based on the relationship between fracture pressure and tensile strength expressed by equation (4). Researchers are of the opinion that the proposed mechanistic approach to estimate tensile strength considering temperature and aging effects along with material characterization appears to be a promising tool to evaluate seal coat damages with a limited validation.

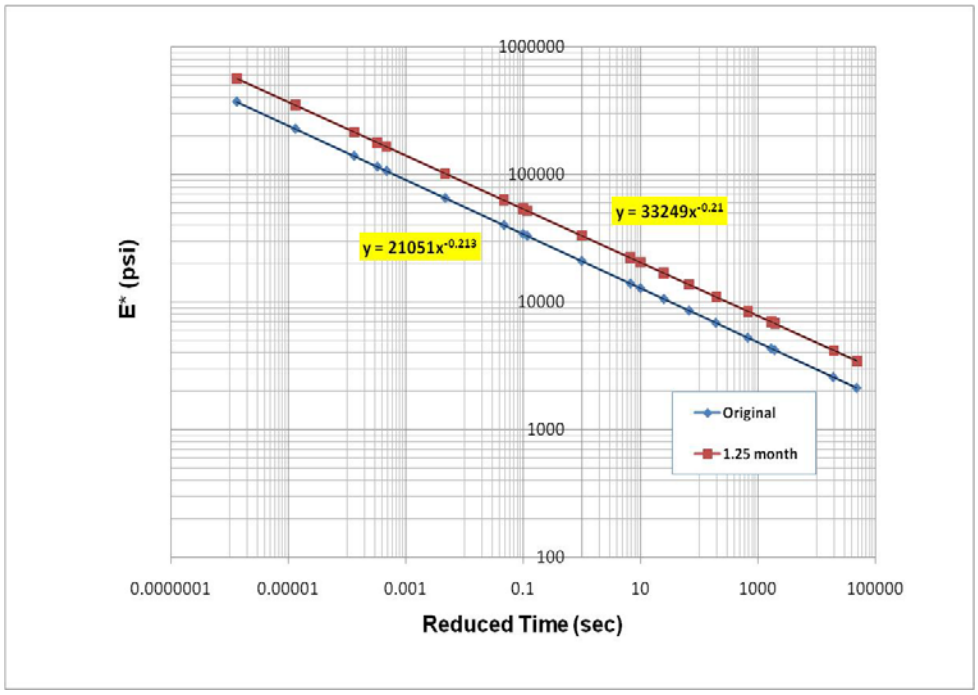

Figure 17. Shift of Master Curve from Original Condition to Aged Condition.

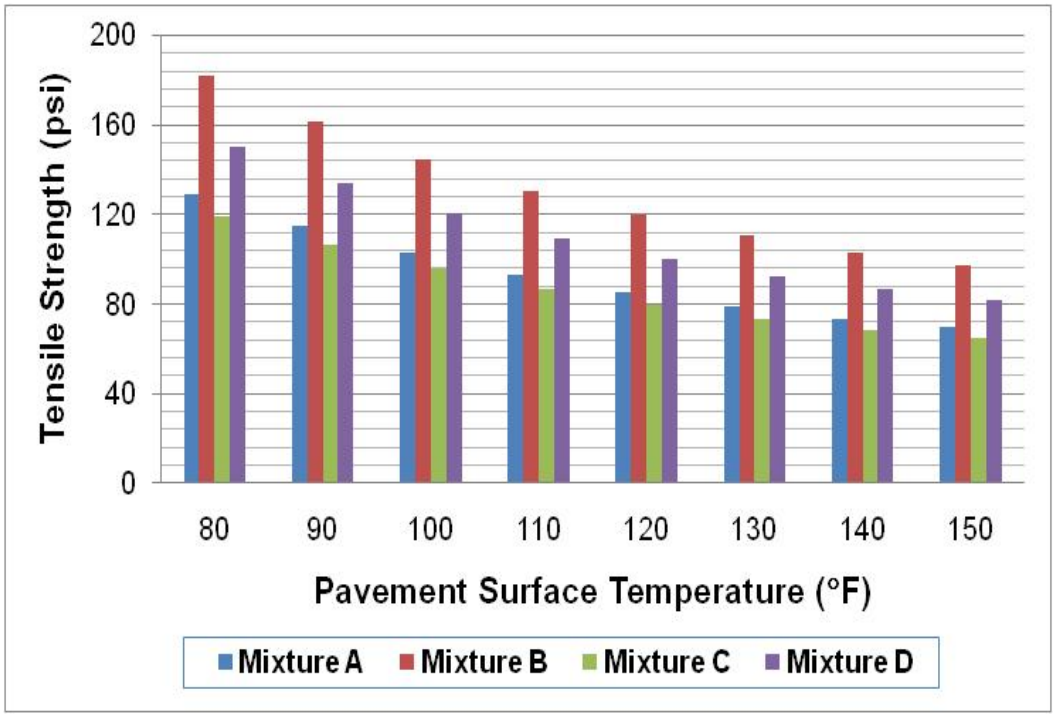

Figure 18. Variation of Tensile Strength with Pavement Surface Temperature.

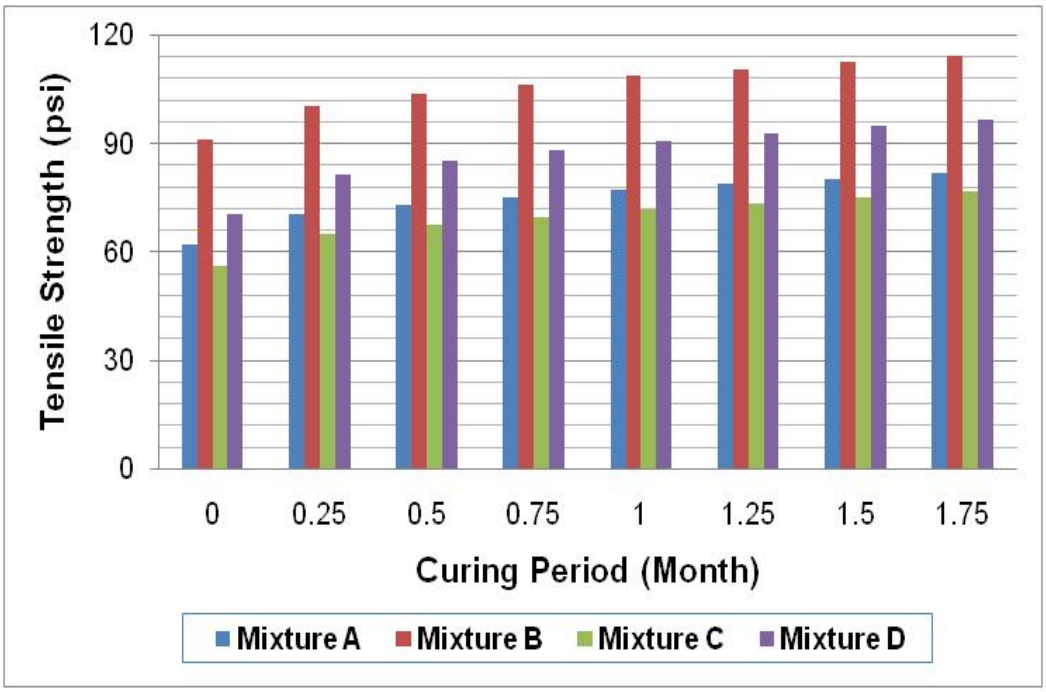

Figure 19. Variation of Tensile Strength with Curing Period.

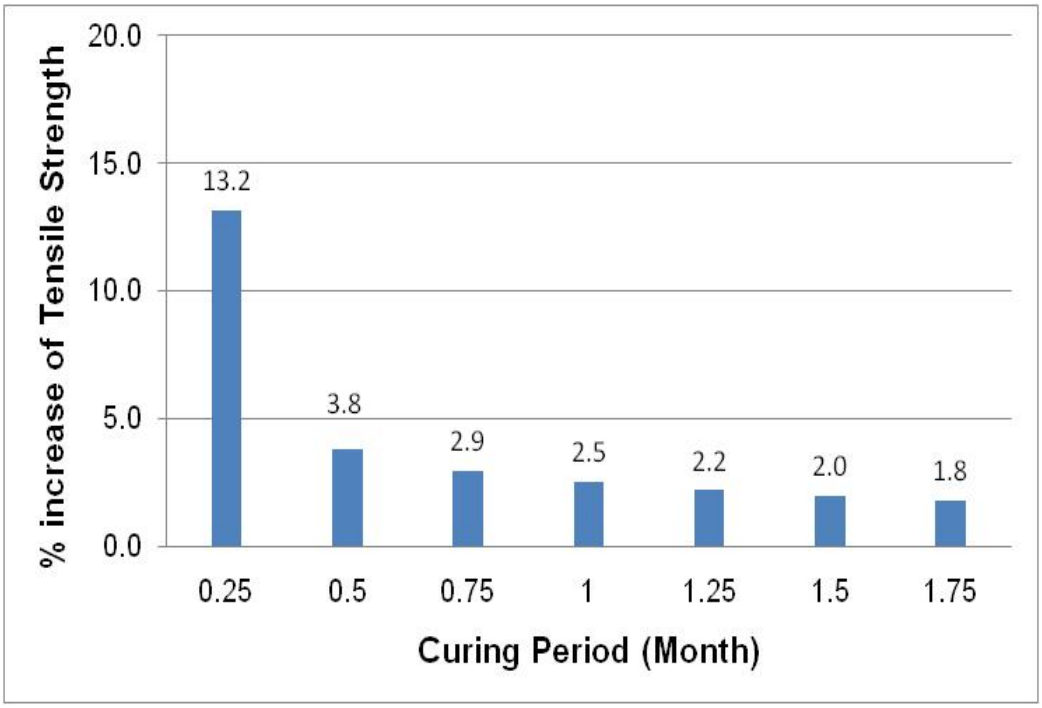

Figure 20. Percent of Increase in Tensile Strength along with Curing Period.

CHAPTER V FIELD TESTING AND VALIDATION

This chapter documents on validating the proposed mechanistic approach by means of field tests along with calibrations. Pilot field tests were conducted on selected test sections located in the Bryan and San Antonio Districts with operating test trucks equipped with a wheel force transducer. Test sections were identified in terms of seal coat placed date and type of seal coat materials that used to estimate failure ratio. Field measurements on slope, pavement surface temperature, damage rate, and wheel forces were made to quantify fracture pressure and tensile strength using the mechanistic approach. The sand patch testing was conducted to measure average texture depth in order to investigate the relationship between texture depth and seal coats performance. In addition, further validations of the calibrated mechanistic model were performed with case studies conducted by TxDOT.

Field Test during FY08

Through communications with TxDOT project monitoring committee, researchers identified four test routes in the Bryan District for field testing as shown in Figure 21.

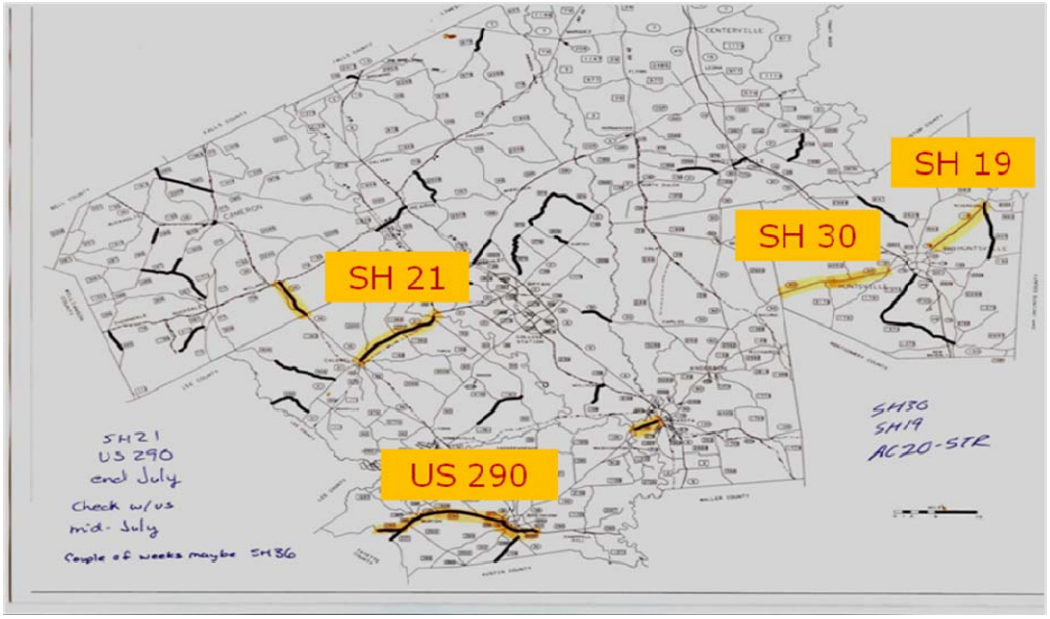

Figure 21. Test Routes Layout in Bryan District.

Field tests were planned to conduct at shoulder area not only to prevent damage within the travel lanes but also minimize routine traffic effects on the test results. During the initial survey, researchers measured pavement slopes using a digital protractor as shown in Figure 22. The device was laid over a straight level edge to minimize errors in reading due to irregular shape of aggregate.

Figure 22. Slope Measurement Using a Digital Protractor.

Table 12 presents the identified test locations for FY08 field tests. The slope readings in terms of degree were converted to the percentage as well since it is often to express pavement grade in percentages. While performing initial stage of field survey, researchers were making an effort to search appropriate instrument to measure wheel forces along the pavement slope. From the search, a heavy wheel force transducer from RS Technology was used for the purpose of measuring wheel forces in this study. The sensor system is designated for recording six components of wheel forces: longitudinal (F_x), lateral (F_y), and vertical forces (F_z); turn over moment (M_x), torque (M_y), and turning moment (M_z) as illustrated in Figure 23.

Table 12. Description of Test Locations in FY08.

Section ID	Seal Coat Placed Date	Material Type	Slope (°)	Slope (%)
SH19-L1	Week of July 7th, 2008	AC20-5TR + Grade 4 PL*	3.0	5.2
SH19-L2			3.0	5.2
SH19-L3			0.5	0.9
SH30-L1	Week of July 3th, 2008	AC20-XP + Grade 4 PL	2.5	4.3
SH30-R1			0.5	0.9
US290-L1	Week of July 14th, 2008	AC20-5TR + Grade 4 PL	2.0	3.5
US290-R1			2.2	3.8
SH21-L1	Week of July 14th, 2008	AC20-5TR + Grade 4 PL	2.3	4.3
SH21-R1			0.5	0.9
SH21-R2			2.0	3.5

*Precoated lightweight aggregate

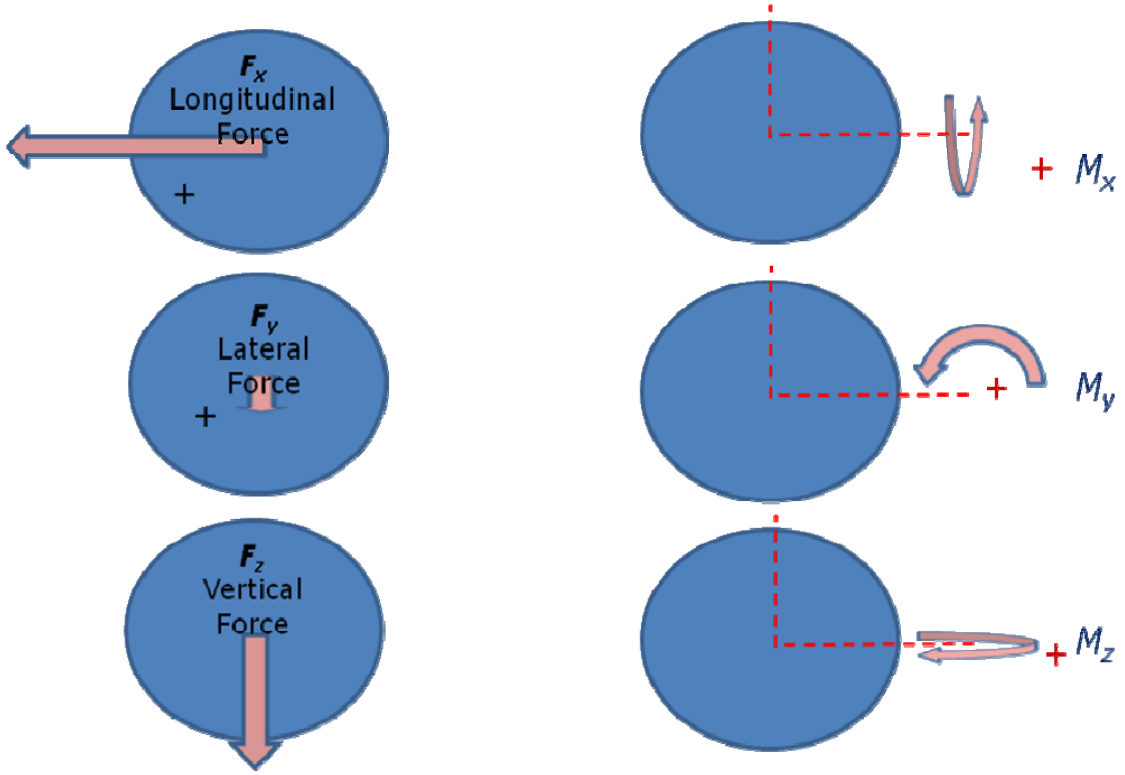

Figure 23. Measured Wheel Force and Moment Components.

The calibrated wheel force transducer was installed on the test truck and tested with static scale measurements to confirm the workability of the system shown in Figure 24.

Figure 24. Comparison of Wheel Force Transducer with Static Scale.

To achieve higher wheel loads, concrete block boxes were loaded onto the test truck close to the gross vehicle weight (GVW) of 80 kips, which is a legal limit. After completion of loading, the measured dual tire load was around 7500 lb, which is approximately equivalent to 3750 lb per tire that is much lighter than SHL's typical tire load. Although this condition is not deemed representative for simulating SHL behavior, a decision was made to proceed at the time of testing due to difficulty in obtaining permits for every test when higher wheel loads are achieved. To compensate this, researchers operated the test truck in different ways as follows: (1) normal driving; (2) low brake; (3) medium brake; and (4) hard brake to generate higher wheel forces. For the

normal driving condition, a driver drove the truck keeping a uniform speed along the test segment as shown in Figure 25. The total test pad was 60 ~ 90 ft length along the shoulder and three segments were evenly divided to accommodate different levels of brake. The test sequence is as follows. Pavement surface temperature was measured using an infrared sensor. The test truck was then driven with 30 mile per hour speed through the whole test segment with data collection. After the first run, different levels of brake were applied adjacent to the each segment border line right after normal driving was made. Figures 26 and 27 show an example of the trace of wheel forces and moments measured between normal driving and hard brake applied condition. It was observed that the magnitude of force terms, F_x and F_z, were almost identical during normal driving and F_y was stayed constant close to zero. With respect to the moment, only a small amount of torque moment M_y was generated during the operation since the brake was not applied purposely.

Whereas F_x and F_z were identical during normal driving condition, excessive wheel forces even up to 10 kips for dual tires were produced, which is 1.33 times greater than that of normal condition. Concurrently, higher torque moment M_y was obtained at the moment of brake applied.

Figure 25. Loaded Test Truck along the Test Segment.

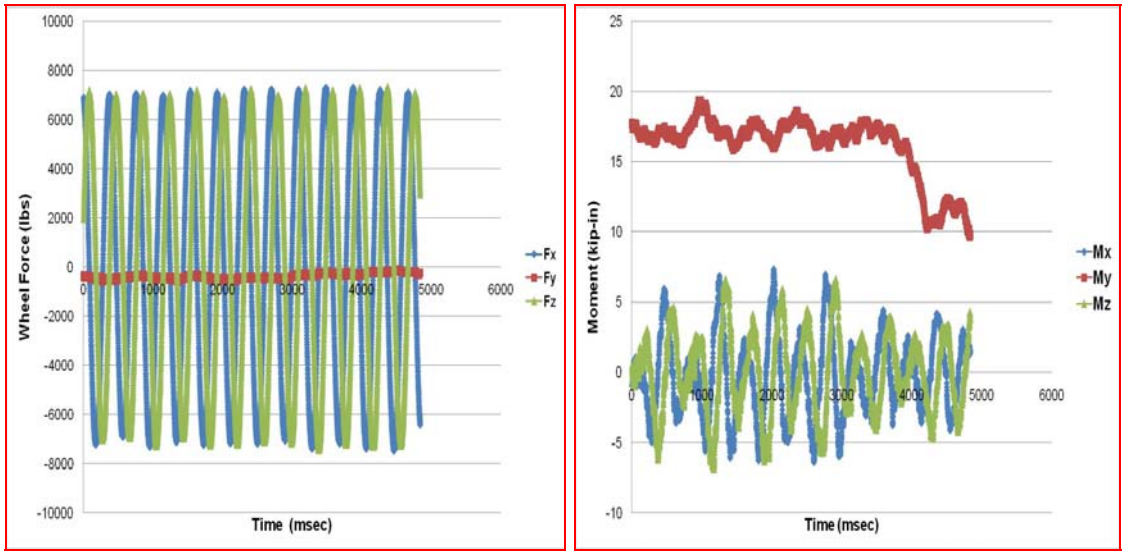

Figure 26. Measured Wheel Force and Moment from Normal Driving.

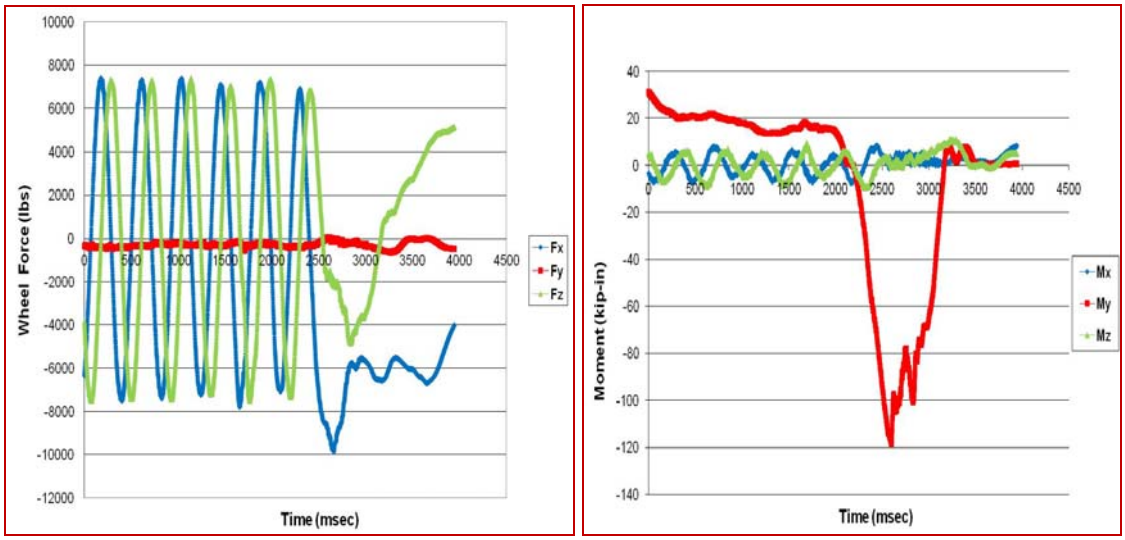

Figure 27. Measured Wheel Force and Moment from Brake Applied Driving.

Precise visual surveys were conducted whenever each run was made to rate the extent of damage before and after the truck passage with taking pictures. Three levels of damage were categorized: N for No damage, L for Low damage, and H for High damage. While a low level of damage causing little aggregate segregation accompanied with insignificant bleeding, a case where indicating larger number of aggregate segregation along with severe bleeding of binder was rated a high level of damage as illustrated in Figures 28 and 29.

Figure 28. Low Level of Damage.

Figure 29. High Level of Damage.

A series of tests was carried out at different dates and time within a day to cover various ranges of curing periods and pavement surface temperatures. A couple of FWD tests were done on SH21 and US290 test sections. During the FWD testing, pavement surface temperature and pavement temperature at depth of 1-inch were measured at the same time. Figure 30 shows the measured deflections and temperatures from SH21-L1 section. As expected, pavement surface temperature was generally higher than pavement temperature. The gap was maximized at 1:00 PM and the difference then approached to a constant level. With a given same time scale, the peak deflections increased proportionally as temperatures became higher. Based on this, researchers made a

decision to use pavement surface temperature as input for the proposed mechanistic model since it is easier to measure than pavement temperature and the behavior of seal coat is expected to be more sensitive to the variation of pavement surface temperature.

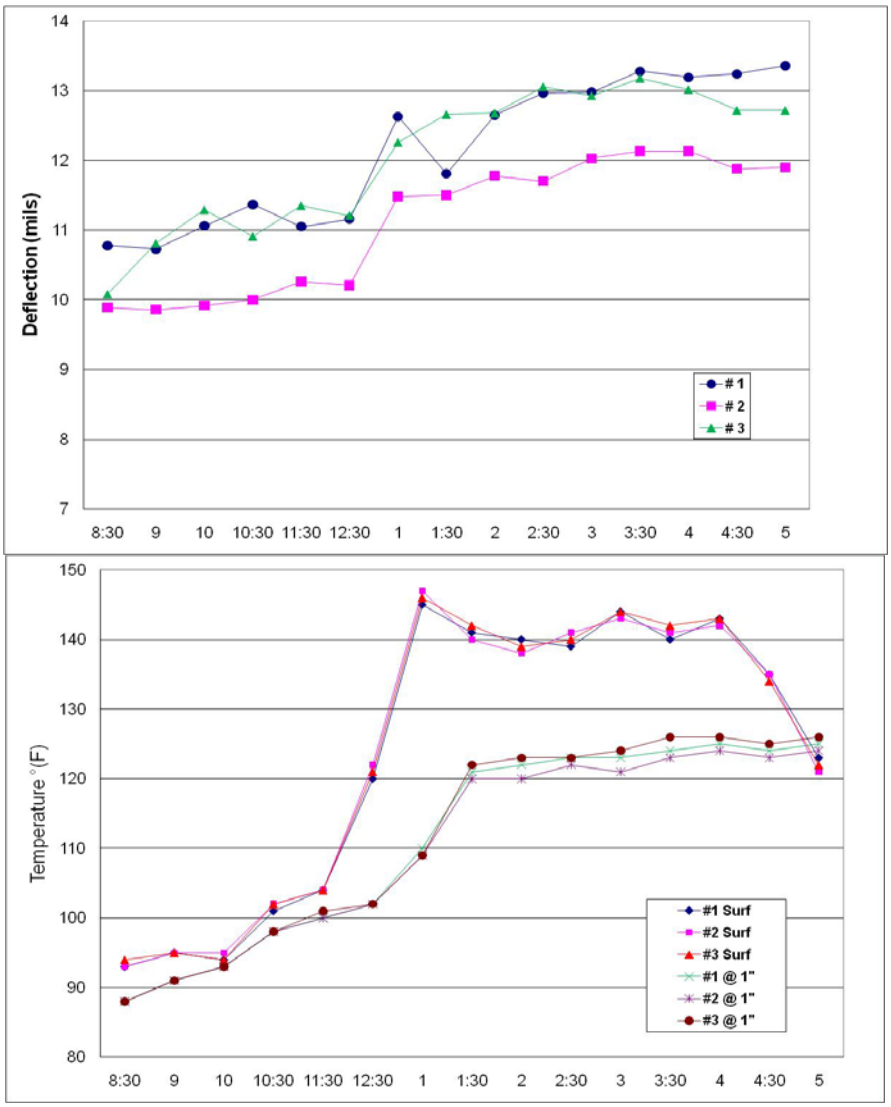

Figure 30. Relationship between Deflections and Temperature from FWD Tests.

Severe damage mostly occurred during afternoon when the pavement surface temperature increased up to 145 °F under medium to hard brake applied driving conditions. No discernable damage was detected either from normal driving condition

regardless of temperature and slope or from brake-applied driving when pavement surface temperature was below 110 °F as shown in Figure 31.

(a) (b)

Figure 31. Seal Coat Damage (a) Normal Drive (b) Brake-Applied Drive.

Researchers believe that tire load under 4 kips would not be critical when the truck is operated normally similar to most SHL moves. Pavement surface temperature over 120 °F seemed to be a threshold providing high damage potential when the brake was applied. It was also observed that the seal coat damage occurred even after a 5- weeks curing period when a hard level of brake was applied under high pavement surface temperature. An extent of damage was not differentiated between slope levels under high temperature condition. Overall, the damage was highly associated with the variation of temperature rather than the change of slope and curing period. It is worth noting that the severity of damage appears to be related to seal coat placed condition. That is, should the area of binder exposing to environmental condition become larger due to insufficient or irregular aggregate applications, it tends to accelerate binder's bleeding and aggregate segregation. To verify this, researchers performed the sand patch testing in accordance with ASTM E 965 and Tex 436-A to measure average texture depth along the wheel path as shown in Figure 32. It should be noted that all measurements were taken at

shoulders thus surface condition along the wheel path was close to intact condition unlike typical wheel paths within the travel lane because of negligible traffic effect.

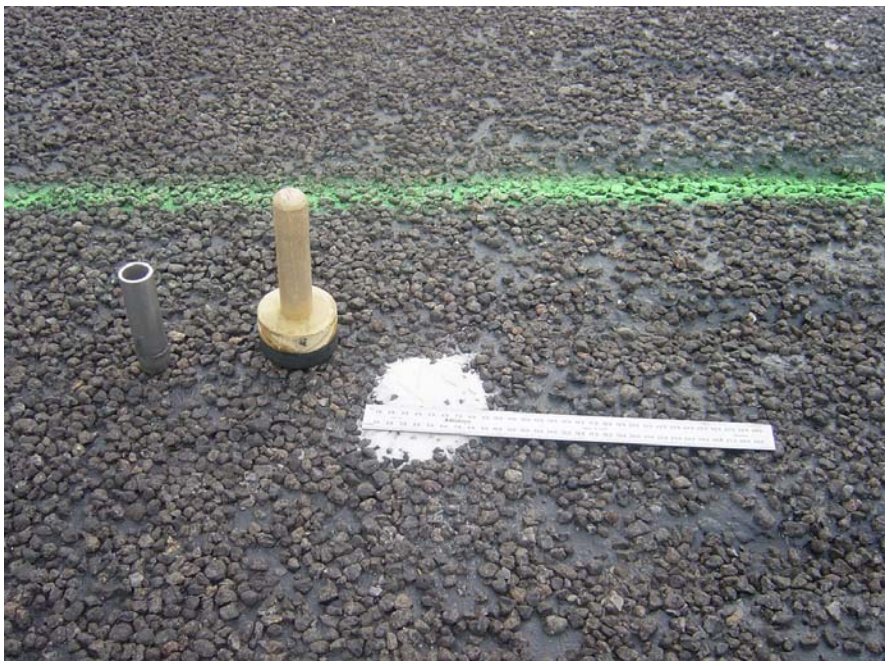

Figure 32. Sand Patch Test Conducted.

Three measurements at each test pad were made to obtain average texture depth. A standard volume of test sand is spread on the pavement surface until the tops of aggregate particles on the pavement surface have been reached (*13*). After then, four diameters at evenly spaced positions are measured to come up with averaged diameter of the area filled with test sand. With given averaged diameter, the texture depth in millimeter was calculated using a given equation.

$$T = \frac{4000V}{\pi D^2} \tag{29}$$

where T = texture depth, V = volume of sand, and D = average diameter. Figure 33 shows the measured texture depth of test sections. The texture depth of test sections typically ranged over 4 mm. Lower texture depth indicates that the surface is smoother because of larger diameter of sanded area representing more voids filled with aggregates. Contrary to this, higher texture depth is likely to provide more chances for binders to

expose to environmental conditions. The damage rate in SH30-L1 location was not as severe as observed in other sections.

Section ID	Ave. Texture Depth (mm)
SH19-L1	4.77
SH19-L2	4.38
SH19-L3	4.48
SH30-L1	3.04
SH30-R1	4.27
US290-L1	3.84
US290-R1	4.06
SH21-L1	4.00
SH21-R1	4.70
SH21-R2	4.71

Figure 33. Texture Depth Measured in FY08 Testing.

Validating the proposed mechanistic approach was performed with field measurements as presented in Table 13. With given information on measured wheel forces, curing period, pavement surface temperature, slope, and material properties of seal coat mixture characterized, the mechanistic model was employed to calculate fracture pressure and tensile strength for the field validation. During the validations, the coefficient μ was calibrated to achieve better correlations between calculated failure ratio (F/T) and damage rate as observed from field testing. Recognizing damage rate is highly associated with the variation of pavement surface temperature, researchers assigned individual coefficient corresponding to the temperature ranges. Table 14 presents the calibrated coefficients at initial stage of validation based on FY08 field testing. While the coefficient of 1 stands for excellent bond condition between aggregate and binder under low temperature, lower coefficient represents reduction in bond strength since binders tend to be soft with higher temperature.

Table 13. Field Validation Results of FY08 Tests.

Section	Age (weeks)	Temp. (°F)	Time	Fx (lb)	Fz (lb)	Damage Rate	Fracture (psi)	Tensile (psi)	Failure Ratio (F/T)
SH19-L1 (3.0°)	3	97	8:40 AM	7150	7000	N	66.2	102.6	0.6
	3	140	1:20 PM	8820	7820	H	209.8	71.1	3.0
	5	140.5	4:55 PM	9071	7520	H	267.3	74.2	3.6
	6	138.5	1:30 PM	8005	7412	H	151.2	76.7	2.0
SH19-L2 (3.0°)	3	102	9:15 AM	8045	8031	N	67.3	97.4	0.7
	3	146.5	1:30 PM	9017	8031	H	210.9	68.4	3.1
	5	138	5:15 PM	8013	7289	H	164.4	75.4	2.2
	6	133	1:45 PM	9135	7446	H	273.4	79.5	3.4
SH19-L3(0.5°)	3	133	1:45 PM	8920	8588	H	56.1	74.5	0.8
	5	138	5:30 PM	8108	7654	H	100.4	75.4	1.3
	6	135	1:45 PM	9219	8650	H	119.7	78.4	1.5
SH30-R1 (0.5°)	4	113	11:00 AM	7488	7351	L	76.1	71.8	1.1
	4	140	2:30 PM	9958	7700	H	340.3	58.3	5.8
	6	145	3:55 PM	11526	10050	H	280.7	59.2	4.7
	7	130	2:50 PM	9488	9270	L	84.7	66.7	1.3
SH30-L1 (2.5°)	4	113.5	11:15 AM	8439	8109	L	71.6	71.5	1.0
	4	140	3:00 PM	9419	8710	L	145.3	58.3	2.5
	6	142	4:10 PM	10325	9257	L	189.4	60.3	3.1
	7	130	3:00 PM	10277	10177	L	77.6	66.7	1.2
SH21-R2 (2.0°)	2	89.5	8:00 AM	7822	7822	N	30.9	108.6	0.3
	2	98.5	9:30 AM	8300	7496	N	127.2	98.2	1.3
	2	108.5	11:30 AM	10352	7323	L	381.7	88.7	4.3
	3	92.5	8:50 AM	9442	9442	N	47.7	107.9	0.4
	3	118	10:20 AM	7606	7494	N	67.1	83.7	0.8
	3	118	10:21 AM	7717	7676	N	60.4	83.7	0.7
	3	**150**	**2:30 PM**	**9850**	**7522**	**H**	**346.8**	**67.2**	**5.2**
	4	86.5	9:05 AM	8069	8021	N	37.0	118.5	0.3
	4	97	10:45 AM	8519	7870	N	111.8	105.1	1.1
	4	97	10:46 AM	7239	7330	N	26.9	105.1	0.3
	4	106	3:05 PM	9399	8624	L	139.3	95.8	1.5
	5	103	9:58 AM	9769	9188	L	121.2	100.8	1.2
	5	122	11:15 AM	10359	9980	L	125.8	84.7	1.5
	5	140	3:05 PM	8746	7714	L	196.5	74.5	2.6
SH21-L1 (2.3°)	2	90.5	8:15 AM	9015	9015	N	51.0	107.3	0.5
	2	96.5	9:40 AM	9860	8727	L	175.3	100.3	1.7
	2	110	11:35AM	9700	9651	L	81.5	87.4	0.9
	3	88.5	8:15 AM	9063	8739	N	75.8	113.0	0.7
	3	113.5	10:00 AM	7479	7700	N	36.1	87.1	0.4
	3	113.5	10:00 AM	7424	7273	N	74.1	87.1	0.9
	3	155	14:38	7472	7414	L	97.7	65.5	1.5
	3	155	14:39	7611	7515	L	103.3	65.5	1.6
	3	155	2:40 PM	10117	8467	H	287.6	65.5	4.4
	4	86	8:40 AM	8141	7846	N	68.5	119.2	0.6
	4	91.5	10:25 AM	9632	8295	L	195.5	111.7	1.8
	4	110	2:45 PM	10791	9071	L	262.6	92.2	2.8
	5	108.5	9:47 AM	9670	9649	L	67.6	95.5	0.7
	5	120	10:53 AM	10131	10004	L	104.0	86.1	1.2
	5	151	2:40 PM	8854	7755	H	217.7	70.0	3.1

Table 13. Field Validation Results of FY 08 Tests (Continued).

Section	Age (weeks)	Temp. (°F)	Time	Fx (lb)	Fz (lb)	Damage Rate	Fracture (psi)	Tensile (psi)	Failure Ratio (F/T)
SH21-R1 (0.5°)	2	92.5	8:40 AM	9550	9229	N	54.9	104.9	0.5
	2	95	9:50 AM	9209	8180	L	131.4	102.0	1.3
	2	111	11:46 AM	9449	7815	L	215.2	86.6	2.5
	3	90	8:35 AM	9442	9442	N	19.7	111.0	0.2
	3	118	10:10 AM	7282	7146	N	46.0	83.7	0.5
	3	118	10:12 AM	7256	7280	N	28.7	83.7	0.3
	3	150	2:50 PM	9523	8819	H	155.4	67.2	2.3
	4	86	8:50 AM	8984	8984	N	8.7	119.2	0.1
	4	92.5	10:35 AM	7246	7153	N	25.3	110.5	0.2
	4	92.5	10:37 AM	7239	7330	N	5.1	110.5	0.0
	4	92.5	10:39 AM	9255	8408	N	111.6	110.5	1.0
	4	111	2:56 PM	9449	8108	L	183.9	91.3	2.0
	5	105	9:05AM	9778	9437	L	68.0	98.8	0.7
	5	120	11:05 AM	12121	12076	L	113.6	86.1	1.3
	5	137	2:55 PM	9036	7947	H	172.9	75.9	2.3
US290-L1 (2.0°)	3	80	7:35 AM	8460	8460	N	33.4	125.3	0.3
	3	106	9:30AM	8254	8254	N	50.9	93.5	0.5
	3	124	11:25 AM	9857	7296	H	345.7	79.7	4.3
	3	134	11:30 AM	7316	7189	L	82.4	74.0	1.1
	3	134	11:32 AM	7268	7256	L	70.2	74.0	0.9
	3	142	1:30 PM	9321	8760	H	155.3	70.2	2.2
	3	140	3:00 PM	8967	8580	H	134.0	71.1	1.9
	3	144	4:30 PM	9200	8500	H	167.9	69.4	2.4
	4	134	11:30 AM	9234	8197	H	193.1	75.8	2.5
	5	108	11:50 AM	8976	8706	L	83.7	95.9	0.9
	5	110	1:35 PM	8578	8089	L	113.2	94.1	1.2
	6	121	12:35 PM	10710	10530	L	108.3	87.1	1.2
	6	140	1:27 PM	12453	11819	H	195.8	75.9	2.6
US 290-R1 (2.2°)	3	84	8:10 AM	9812	8888	N	141.3	119.3	1.2
	3	108	9:50 AM	8396	7246	L	175.4	91.7	1.9
	3	126	11:35 AM	8931	7148	H	260.9	78.4	3.3
	3	138	1:40 PM	7964	7205	H	155.7	72.0	2.2
	3	144.5	3:15 PM	9106	7500	H	261.0	69.2	3.8
	3	145	4:45 PM	8319	7715	H	152.0	69.0	2.2
	4	132.5	11:40 AM	10090	9595	H	149.9	76.6	2.0
	5	115	12:00 PM	8952	8429	H	122.8	89.9	1.4
	5	98	1:25 PM	8583	7524	L	158.7	106.2	1.5
	6	135	12:25 PM	9145	8737	L	131.8	78.4	1.7
	6	125	1:40 PM	8998	8688	L	112.8	84.4	1.3

Table 14. Calibrated Coefficient from Field Validation in FY08.

Pavement Surface Temperature (°F)	Coefficient (μ)
80 ~ 89	1.0
90 ~ 99	0.99
100 ~ 109	0.98
110 ~ 119	0.97
120 ~ 129	0.96
130 ~ 139	0.95
140 ~149	0.94
≥150	0.93

This shows an example procedure on how the failure ratio was calculated for one case, highlighted in red in Table 13.

- Given Condition : 3 weeks old of section SH21-R2

  Pavement Surface Temperature 150 °F, Slope 2.0° (3.5 %),

  9-inch tire width, 0.5-inch seal coat thickness

- Measured Wheel Force of dual tire: F_x = 9850 lb and F_z = 7522 lb were determined from Figure 27 based on absolute maximum value.
- Using equation (4), fracture pressure (right side of equation) is calculated as follows:

$$\left[\frac{f_t}{t}+\frac{F}{t\cdot w}\left(\sin\theta-\mu\cdot\cos\theta\right)\right]=\frac{(9850/2/9)}{0.5}+\frac{7522}{0.5*9}(\sin 2°-0.93\cos 2°)=346.8\,psi$$

- Using equation (5), tensile strength is calculated as follows:

$$\left(\sigma_t\right)_{\max}=\left\{\frac{8\pi}{3t\left(1+\frac{E_f}{E_s}\right)}\left(\frac{m\overline{c^2}}{A}\right)\left[\Delta G_f^a\left(E_\infty+E_1\left(\frac{t_l}{a_T}\right)^{-m}\right)\right]\right\}^{0.5}$$

$$=\left\{\frac{8\pi*0.3363}{3(60*10^{-6}m)*(1+0.2)}\left[0.118Nm/m^2*(210.43MPa)*(1299.72)^{-0.211}\right]\right\}^{0.5}$$

$$=463171.75\,MPa=67.2\,psi.$$

- Finally, the failure ratio is computed dividing the fracture pressure by tensile strength. That is, 346.8/67.2 = 5.2.

Figure 34 shows the range of failure ratio determined for each observed damage rate. Upper and lower arrow indicates corresponds to maximum and minimum values, and dots are averaged ones. Researchers believe that the proposed mechanistic approach realistically captures seal coat damage potential by exhibiting the trend that a higher failure ratio corresponds to a severe damage rate even though a wide range of variance in failure ratio was detected.

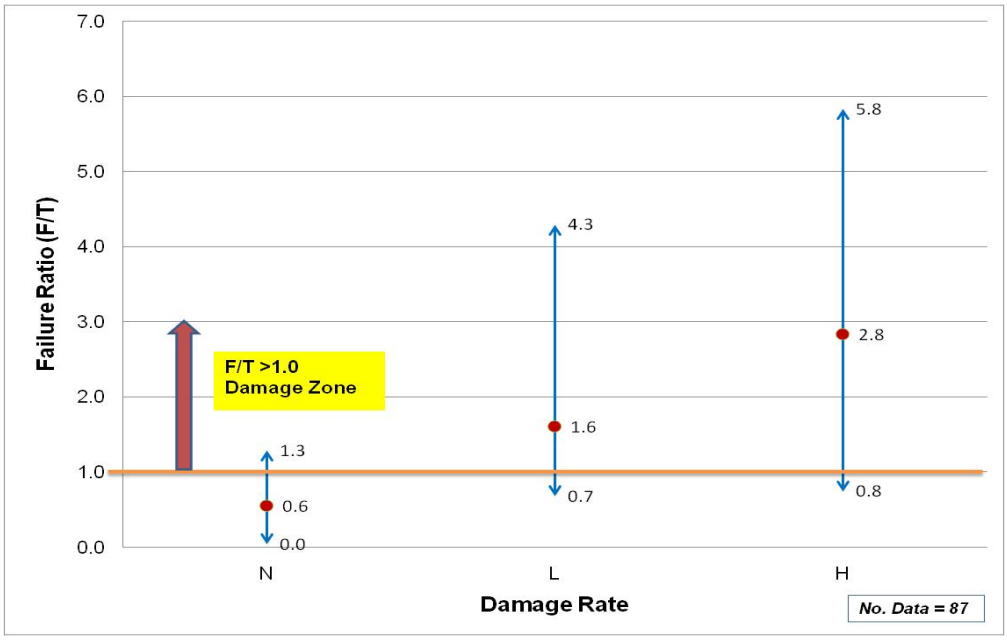

Figure 34. Relationship between Failure Ratio (F/T) and Damage Rate.

Besides field validations on seal coat damage, researchers conducted field tests on two routes in the Lubbock District to investigate the effect of SHL moves related to wind farm construction on pavement structural damage. Appendix B entails details of this task.

Field Test during FY09

Researchers conducted additional field tests in FY09 to recalibrate the mechanistic model based on following issues discussed with the project committee members:

- higher wheel load close to 6 kips per tire needs to be considered for more realistic calibration;

- different types of seal coat material need to be included for the recalibration; and
- further verification needed on surface condition and seal coat performance.

With the cooperation of TxDOT, test locations were indentified in the Bryan and San Antonio Districts as listed in Table 15. As noted, different types of seal coat materials such as CRS-2P, AC-15P, Grade 3 limestone, and Trap Rock, which is widely used in San Antonio area, were included. In addition, researchers added two locations, SH21-L1 and SH21-R2, that had been tested in FY08 and aged over 1 year at the time of testing to investigate the curing period effect on seal coat performance. These additions provided an opportunity to enhance the applicability of the mechanistic model through re-calibrations.

Table 15. Description of Test Locations in FY09.

Location	Section ID	Seal Coat Placed Date	Material Type	Slope (°)	Slope (%)
Bryan District	FM60-L1	Week of July 8th, 2009	AC20-5TR + Grade 4 PL	1.4	2.5
	FM60-R1			1.4	2.5
	SH21-L1	Week of July 28th, 2008		2.3	4.3
	SH21-R2			2.0	3.5
	SH21-R3	Week of July 9th, 2009		1.15	2.0
San Antonio District	FM1333	Week of May 18th, 2009	CRS-2P + Grade 3 Limestone	3.0	5.2
	FM476	Week of May 18th, 2009	CRS-2P + Grade 4 Trap rock	2.0	3.5
	FM463	Week of Aug 6th, 2009	AC-15P + Grade 5 Limestone	3.0	5.2
	US90	Week of Aug 6th, 2009	AC20-5TR + Grade 4 Trap rock	2.6	4.5

The most challenging task during FY09 test was to accommodate the test truck that is capable of imposing 6 kips of tire load on seal coats. To achieve this, researchers loaded two layers of concrete block boxes that had been used during FY08 testing onto

the test truck at the driving axle of trailer to concentrate higher wheel loads at corresponding axle location keeping the GVW below a legal limit of 80 kips for the Bryan District test as illustrated in Figure 35. The measured static scale of dual tires was 11,500 lb, which is approximately equivalent to 5750 lb per tire. The San Antonio District TxDOT engineers provided an annually-permitted test truck as shown in Figure 36. To achieve higher wheel forces, a milling machine filled with a water tank was loaded onto the trailer. The measured static scale of dual tires was 12,500 lb, which is approximately equivalent to 6250 lb per tire. The loaded GVW was 107,500 lb.

Figure 35. Test Truck for Bryan District Tests.

Figure 36. Test Truck for San Antonio District Tests.

During field testing in FY09, researchers operated the test truck in a normal driving condition without applying any brakes to generate excessive higher traction forces based on the discussion that most of SHLs do not behave in such a manner. Researchers also installed a wheel force transducer to check that static measured wheel force is properly loaded during the testing. Figure 37 shows the measured wheel force from the test trucks used for the Bryan and San Antonio District tests. Since the trucks were driven in normal condition, the F_x and F_z were almost identical during the data collection. While the envelope of measured F_x and F_z from the test truck used in the Bryan District was slightly lower than 12 kips solid line, the envelope measured from San Antonio tests generally above the 12 kips solid line, as consistent with the static scale measurements.

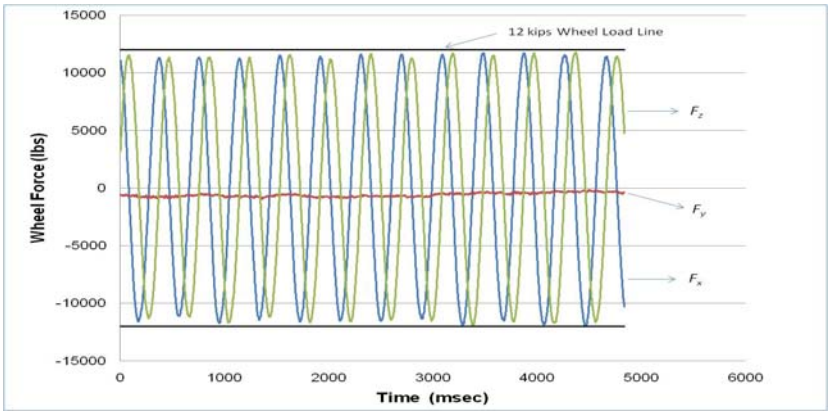

(a)

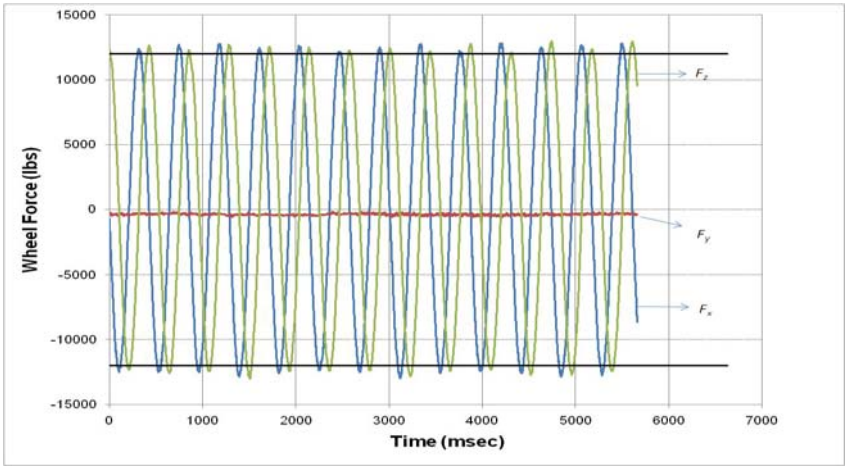

(b)

Figure 37. Measured Wheel Forces (a) Bryan District (b) San Antonio District.

The field tests were carried out in a similar way as FY08 field tests performed. During the validations, researchers made an effort to recalibrate the coefficient μ to fulfill better correlations between calculated failure ratio (F/T) and damage rate as observed from field testing. In addition, sand patch test to associate surface texture condition with seal coat performance was conducted.

From additional field validations, researchers confirmed that pavement surface temperature is the most critical factor in influencing seal coat damage. It should also be noted that the curing period is associated with the extent of damage. In particular, in spite of hot pavement surface temperature, tests sections on SH 21 that have been aged 1 year rarely revealed any specific damages as illustrated in Figure 38.

Figure 38. Comparison of Segment Before and After Test.

Fresh seal coated sections in FM60 and SH21 showed that the damage rate becomes slightly alleviated as the curing is progressed when compared within a similar temperature range.

The most severe damage was detected in FM1333 testing. The route was a surface treated load zoned road. According to the definition of TxDOT specification Item 316, surface treatments differ from a seal coat in that they are applied to a prepared compacted base not to a paved surface. Surface treatments composed of CRS-2P with Grade 3 limestone has been placed for two month directly over the flexible base layer in two month at the time of testing. Since there was no shoulder along the route, the test

was instead conducted within travel lanes with the permission of the San Antonio District. After the first passage of test truck was made under high pavement surface temperature around 140 °F, several locations along with wheel path came to flushing. During the back up of the test truck to an original location, the surface treatments severely failed as shown in Figure 39. It strongly indicated that special care needs to be taken to the surface treated load zoned roads for routing SHL moves particularly in the event of high pavement surface temperature and steep slope. It is interesting to report that no damage took place when the testing was conducted at the same location in the morning in the event of pavement surface temperature ranging from 80 to 100 °F.

Figure 39. Severe Damage of Surface Treatments.

At the vicinity of FM1333, the same age of FM 476 route was tested. The seal coats of this route were composed of CRS-2P with trap rock. The definition of trap rock is as follows according to the pocket note (*41*).

Traprock consists of various fine-grained, dense, dark colored igneous rocks, typically basalt or diabase; also called "trap." NOTE: This definition has been approved by the Specification Committee.

Researchers observed that the shape of trap rock is relatively plain so it appears to cover binders uniformly and to provide smoother surface conditions resulting in minimal

damage compared to the FM 1333 section. For the purpose of supporting this finding, researchers conducted the sand patch testing and calculated average texture depth as presented in Table 16. The average texture depth of FM 476 section was 1.2, which was significantly smaller than other sections indicating that areas where binders are exposed are sparser. It is also worth mentioning that the total surface energy value computed from two different mixtures used in FM1333 and FM476 exhibited that CRS-2P is better compatible with trap rock than limestone. Consequently, the total surface energy of trap rock mixture was 0.59 Nm/m^2, which is around three times greater than that of limestone mixtures.

Table 16. Texture Depth Measured in FY09 Testing.

Section	Average Texture Depth (mm)
FM 60-L1	3.07
FM 60-R1	3.17
SH 21- R2	3.83
FM 476	1.04
FM 1333	2.88
FM 463	2.91
US 90	2.93

Based on this finding, researchers came up with a new set of calibrated factors to consider different cases in terms of temperature, curing period, and surface condition as presented in Table 17 on the basis of additional field validation results presented in Table 18. The description of cases are as follows:

- Case I: Seal coat aged less than one year and texture depth above 3.0 mm. Area of binders filled with aggregates is sparse.
- Case II: Seal coat aged less than one year and texture depth below 3 mm. Area of binders filled with aggregates is predominant.
- Case III: Seal coat aged over one year.
- Case IV: Surface treated load zoned road.

Table 17. Calibrated Coefficients from FY09 Tests.

Temp.* (°F)	Age (month)	Case I		Case II		Case III		Case IV	
		μ_1**	μ_2**	μ_1	μ_2	μ_1	μ_2	μ_1	μ_2
80 ~ 89	0~0.24	1.0	0.95	1.0	0.95	1.0	-	1.0	0.9
90 ~ 99	0.25 ~ 0.49	0.99	0.97	0.995	0.97	1.0	-	0.99	0.92
100 ~ 109	0.5 ~ 0.74	0.98	0.99	0.99	0.995	1.0	-	0.98	0.94
110 ~ 119	0.75 ~ 0.99	0.97	0.995	0.985	1.0	1.0	-	0.97	0.96
120 ~ 129	1 ~ 1.24	0.96	1.0	0.98	1.0	1.0	-	0.95	0.98
130 ~ 139	1.25 ~ 1.49	0.95	1.0	0.97	1.0	0.99	-	0.93	0.98
140 ~149	1.5 ~ 1.74	0.94	1.0	0.96	1.0	0.98	-	0.92	0.98
≥150	1.75 ~ 1.99	0.93	1.0	0.95	1.0	0.97	-	0.91	0.98
	2.0 ~ 2.99		1.01		1.01		-		0.98
	3.0 ~ 11.99		1.02		1.02		-		0.98
	≥12		-		-		1.02		0.98

*Pavement surface temperature measured by an infrared sensor.

**μ_1 and μ_2 are calibrated coefficients depending on temperature and age, respectively.

Table 18. Field Validation Results of FY09 Tests.

Section	Age (weeks)	Temp. (°F)	Time	Fx (lb)	Fz (lb)	Damage Rate	Fracture (psi)	Tensile (psi)	Failure Ratio (F/T)
FM60-L1 (1.4°)	3	118.5	10:30 AM	12003	11948	N	91.3	83.3	1.1
	3	141.5	1:12 PM	11790	11848	H	118.6	70.4	1.7
	3	145.0	2:10 PM	11094	11067	H	120.3	68.9	1.8
	3	138.0	3:10 PM	11860	11729	H	125.9	72.0	1.8
	4	119.0	10:40 AM	11547	11487	N	81.8	85.0	1.0
	4	132.0	11:40AM	11466	11485	L	99.5	76.8	1.3
	4	141.0	1:40 PM	11311	11303	H	114.4	72.4	1.6
	4	150.0	2:40 PM	12045	11767	H	164.6	68.8	2.4
	5.5	112.5	10:15 AM	12015	11817	N	100.2	93.1	1.1
	5.5	127.0	11:05 AM	11377	11342	N	91.2	82.4	1.1
	5.5	138.0	12:20 PM	11218	11311	L	89.3	76.3	1.2
	5.5	140.5	1:10 PM	11458	11307	H	131.2	75.1	1.8
FM60-R1 (1.4°)	3	103.5	10:45 AM	11785	11686	N	80.7	95.9	0.8
	3	137.5	1:02PM	11841	11782	H	117.9	72.2	1.6
	3	140.5	2:00 PM	11721	11798	H	115.8	70.8	1.6
	3	145.0	3:00 PM	11941	11964	H	124.0	68.9	1.8
	4	119.5	10:30 AM	11794	11518	N	107.4	84.7	1.3
	4	137.0	11:30 AM	11825	11717	L	116.5	74.3	1.6
	4	140.0	1:30 PM	11875	11697	H	138.3	72.8	1.9
	4	149.0	2:30 PM	12069	11821	H	147.8	69.1	2.1
	5.5	109.0	10:05 AM	11458	11307	N	78.0	96.1	0.8
	5.5	125.0	11:00 AM	11960	11720	N	118.3	83.7	1.4
	5.5	135.0	12:10 PM	12049	11964	L	116.0	77.8	1.5
	5.5	140.5	1:00 PM	11709	11566	H	132.9	75.1	1.8

Table 18. Field Validations in FY09 Testing (Continued).

Section	Age (weeks)	Temp. (°F)	Time	Fx (lb)	Fz (lb)	Damage Rate	Fracture (psi)	Tensile (psi)	Failure Ratio (F/T)
SH21-L1 (2.3°)	Over 1 year	104.0	9:21 AM	12034	12026	N	30.4	152.1	0.2
		138.0	3:30 PM	11601	11578	N	44.9	117.5	0.4
		105.0	9:10 AM	11732	11763	N	25.1	150.7	0.2
		145.0	1:30 PM	11775	11670	N	68.9	112.8	0.6
SH21-R1 (2.0°)	Over 1 year	104.0	9:40 AM	11586	11547	N	25.8	152.1	0.2
		145.0	3:44 PM	11984	11782	N	73.7	112.8	0.7
		107.0	9:30 AM	12026	11895	N	37.3	148.0	0.3
		147.0	1:40 PM	11960	11767	N	72.5	111.69	0.7
SH21-R3 (1.15°)	3	116.5	10:00 AM	11887	11775	N	89.4	84.8	1.1
	3	143.5	4:02 PM	11817	11991	L	99.3	69.5	1.4
	4	109.0	9:40 AM	12038	11802	N	86.6	93.1	0.9
	4	150.0	3:00 PM	11721	11864	L	116.2	68.8	1.7
	5.5	107.0	9:50 AM	11427	11477	N	48.4	98.1	0.5
	5.5	145.0	2:00 PM	11346	11392	L	102.1	73.1	1.4
FM1333 (3°)	8	140.0	4:00 PM	12378	12208	H	237.7	76.0	3.1
	8	85.0	7:40 AM	12389	12463	N	98.7	125.5	0.8
	8	100.0	9:40 AM	12269	12424	N	117.4	106.4	1.1
FM 476 (2°)	8	150.0	4:25 PM	12034	12397	L	154.6	125.8	1.2
	8	91.5	8:25 AM	12540	12354	N	92.1	202.7	0.5
	8	96.5	8:50 AM	12459	12366	N	81.3	192.3	0.4
FM 463 (3°)	3	140.0	1:53 PM	12251	12424	N	115.9	89.5	1.3
	3	118.0	11:10 AM	12405	12119	N	131.0	104.4	1.25
	3	130.0	11:50 AM	12185	12397	N	96.4	95.6	1.0
US 90 (3°)	3	140.0	3:30 PM	12215	12203	N	135.3	105.3	1.3
	3	88.0	8:46 AM	12996	12775	N	102.6	168.7	0.6
	3	98.0	9:35 AM	12737	12145	N	152.9	150.7	1.0

Figure 40 shows that the relationship between failure ratio and damage rate observed from the field testing. It was observed that the recalibrated mechanistic model fairly captures the variation of damage rate across sections tested. Researchers categorized three zones based on the results. Theoretically, the failure ratio greater than one means the seal coat damages occur. However researchers recommend that a failure ratio up to 1.2 appears to be safe for routing SHL moves based on field validations. Therefore, rerouting may not be an option in such cases. When the failure ratio is distributed between 1.2 and 1.6, low to medium levels of damages are likely to occur, thus rerouting would be an option as long as alternative routes are available. Rerouting or rescheduling of SHL moves should be considered when the failure ratio is greater than 1.6. During the field validations, researchers noted that following findings as well.

- Measured longitudinal wheel force (F_x) and vertical wheel force (F_z) were fairly close in the magnitude. Noted that the test truck was operated

normally without creating abrupt high torque forces by applying brakes. Figure 41 compares two forces. The F_x was overall slightly larger than F_z by a factor of 1.008 because the test truck was operated along the slope. Researchers incorporated this finding into the proposed model by setting the traction force f_t multiplied by a factor of 1.008 to the maximum tire load (F) denoted in equation (3).

- Researchers measured the pavement surface temperature during the field testing conducted in summer (July and August) in the Bryan and San Antonio Districts. Table 19 shows the measured temperatures corresponding to testing time were tabulated in Table 19. It might be useful in gauging pavement surface temperature for evaluating damage potential in the absence of temperature data when the routing inspection is imperative.
- Researchers had an opportunity to follow a real super heavy load move made on July 24, 2009. The moves of were routed from Tomball to the Oklahoma line. The gross vehicle weight was 514 kips with a maximum tire load of 5 kips. The move just passed through fresh seal coated section of SH 21 toward FM 60 at 6:00 AM. The measured pavement surface temperature was 80 °F, and no damage was occurred.

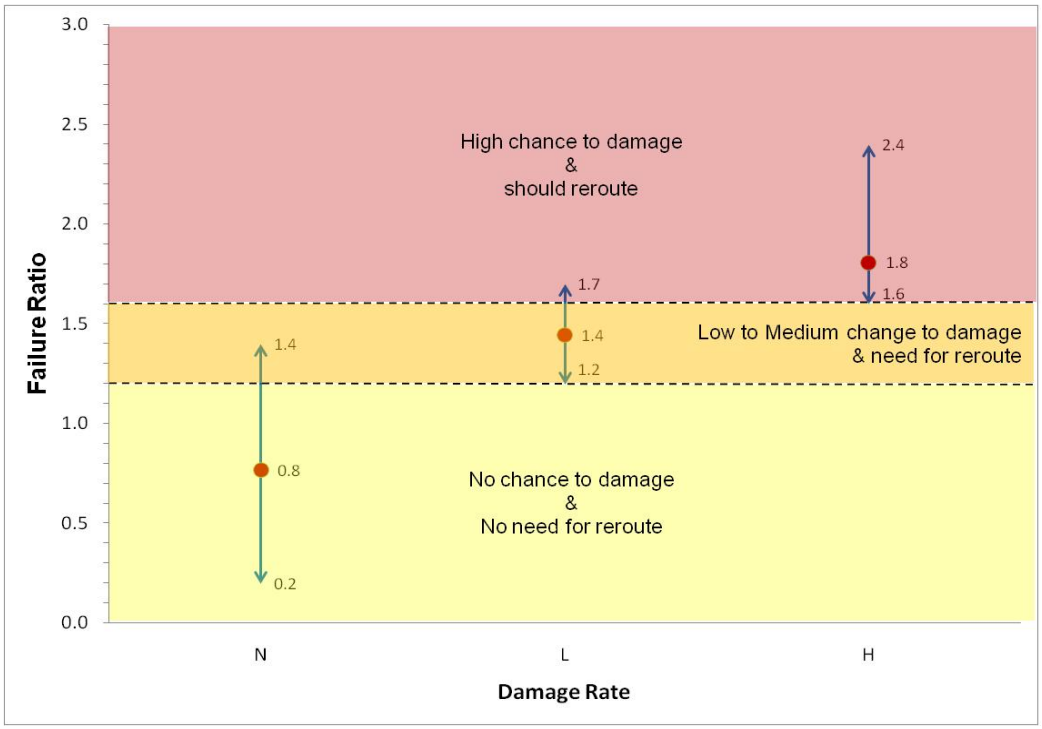

Figure 40. Failure Ratio versus Damage Rate from FY09 Field Tests.

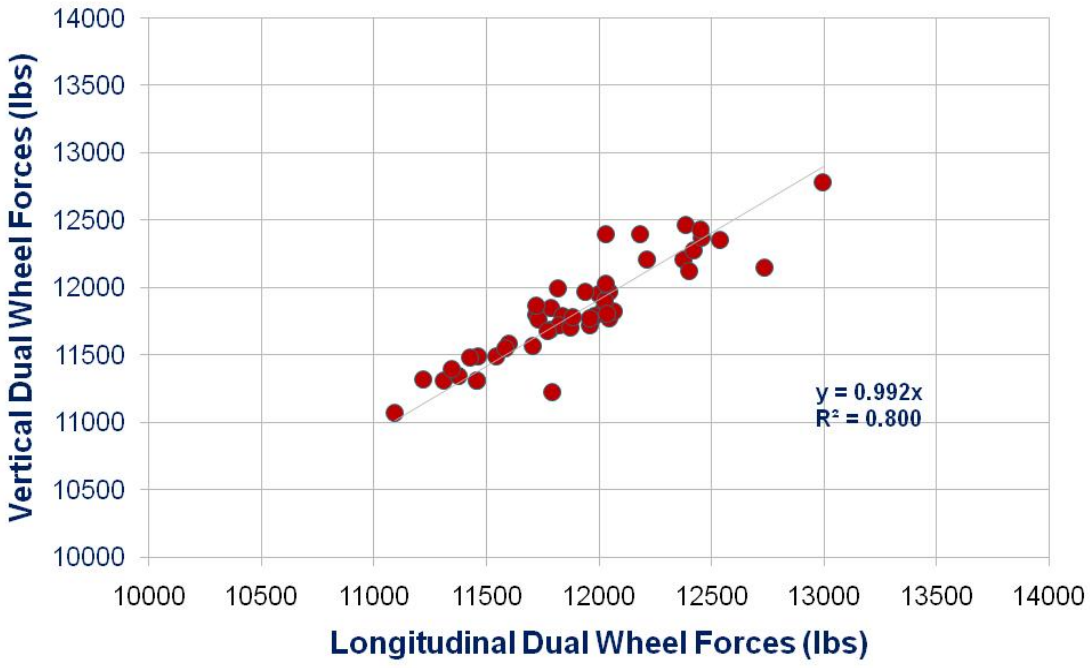

Figure 41. Relationship between Vertical and Longitudinal Wheel Forces.

Table 19. Pavement Surface Temperature Range versus Time.

Temperature (°F)	Time
80 ~ 90	7:00 am ~ 9:00 am
90 ~ 100	9:00 am ~ 10:30 am
100 ~ 110	10:30 am ~ 11:00 am
110 ~ 120	11:00 am ~ 11:30 am
120 ~ 130	11:30 am ~ 12:00 pm
130 ~ 140	12:00 pm ~ 1:30 pm
140 ~	1:30 pm ~ 5:00 pm

The researchers developed a Microsoft Excel® spreadsheet program, known as the Mechanistic-Empirical Seal Coat Damage Evaluation Program (M-E SDEP), to evaluate seal coat damage potential incorporating the recalibrated mechanistic model along with established database on material properties identified. Researchers included a user manual of this program in Appendix C in this report.

Further Validations Based on Case Studies

Several case studies were employed for further validations of the recalibrated mechanistic model using M-E SDEP. This section documents test location, field survey, available data, and the results of validations of model. Chen et al. (*20, 42*) monitored the following sections to identify the cause of seal coat damages due to SHL moves.

SH 43 – Tyler District

- Route: From Henderson to Marshall along with SH43 on June 24, 2002
- Load Condition: GVW was 736,000 lb with 5 kips of maximum tire load
- Seal coat: 3-week old, AC15-5TR with Grade 4 aggregate but type of rock is not known
- Slope: 2.4 ~ 5.2 percent
- Weather: high and low temperature was 89°F and 68°F
- Damage: occurred along with wheel path
- Evaluation inputs
    - Material = 3 weeks aged AC20-5TR with Grade 4 limestone (Bridgeport)/Lightweight aggregate

- Slope = 5.0 percent
- Maximum tire load = 5 kips
- Pavement surface temperature = 140 °F
- Case I and II

- Evaluation results

Case I: Failure ratio = 1.41
Damage Rate = L
Probability of Failure = 67.1 percent
Reroute is considered

Case II: Failure ratio = 1.13
Damage Rate = N
Probability of Failure = 56.1 percent
Reroute is not considered

FM 2210 –Fort Worth District

- Route: From Bridgeport to Gibtown along with FM 2210 on April 1, 2004. FM2210 is a load zoned road with surface treatments. GVW limit is 58420 lb.
- Load Condition: 5625 lb of maximum tire load. Two moves made. The first load was made in the morning; the second move was around 2:30 PM.
- Seal coat: 1 year, CRS-2P with Grade 4 limestone
- Slope: 1.0 ~ 4.2 percent
- Weather: high and low temperature was 81°F and 46°F
- Damage: the aesthetics and skid resistance of the road were destroyed. In addition, there were localized areas where the seal coat stuck to the tires and peeled off.
- Evaluation inputs
  - Material = 1 year aged CRS-2P with Grade 4 limestone (Bridgeport)
  - Slope = 4 percent
  - Maximum tire load = 5625 lb

- Pavement surface temperature = 130 °F
- Case IV

- Evaluation results

  Case IV: Failure ratio = 1.42
  Damage Rate = L
  Probability of Failure = 67.5 percent
  Reroute is considered

US 285 –Odessa District

- Route: US 285 on May 30, 2003
- Load Condition: 663 kips of GVW, 14,900 lb of maximum tire load
- Seal coat: 2-week
- Slope: flat
- Weather: Not known
- Damage: Numerous locations had 0.6-1.5 m (2-5 ft) long streaks of seal coat peeling off, and the longest one found was 24 m (80 ft)
- Evaluation inputs
  - Material = 2 weeks aged AC20-5TR with Grade 3 limestone (Odessa)
  - Slope = 1.0 percent
  - Maximum tire load = 14,900 lb
  - Pavement surface temperature = 135 °F
  - Case I and II

- Evaluation results

  Case I: Failure ratio = 2.96
  Damage Rate = H
  Probability of Failure = 92 percent
  Reroute should be considered

Case II: Failure ratio = 2.02
Damage Rate = H
Probability of Failure = 81.9 percent
Reroute should be considered

FM 109 –Yoakum District

- Route: FM 109 on August 10, 2004
- Load Condition: 670 kips of GVW and 8000 lb of maximum tire load.
- Seal coat: 3 month of CRS-2P with Grade 4 limestone
- Slope: 9 percent
- Weather: hot summer
- Damage: peeling of seal coats
- Evaluation inputs
    - Material = 3 month aged CRS-2P with Grade 4 limestone (Caldwell)
    - Slope = 9.0 percent
    - Maximum tire load = 8 kips
    - Pavement surface temperature = 145 °F
    - Case I and II

- Evaluation results

Case I: Failure ratio = 3.54
Damage Rate = H
Probability of Failure = 94.9 percent
Reroute should be considered

Case II: Failure ratio = 3.03
Damage Rate = H
Probability of Failure = 92.5 percent
Reroute should be considered

SH 56 –Paris District

- Route : SH 56 on August 22, 2005
- Load Condition: 367 kips of GVW and 5800 lb of maximum tire load.
- Seal coat: 1 week
- Slope: 1.8 ~ 2.4 percent
- Weather: high average temperature 92 °F
- Damage: slightly peeling of seal coats
- Evaluation inputs
    - Material = 1 week aged AC20-5TR with Grade 4 limestone aggregate (Bridgeport)
    - Slope = 2.4 percent
    - Maximum tire load = 5.8 kips
    - Pavement surface temperature = 150 °F
    - Case I and II

- Evaluation results

Case I: Failure ratio = 1.92
Damage Rate = H
Probability of Failure = 80.2 percent
Reroute should be considered

Case II: Failure ratio = 1.64
Damage Rate = H
Probability of Failure = 73.8 percent
Reroute should be considered

CHAPTER VI ESTABLISHING DATABASE AND GUIDELINE

The researchers established an extensive database compiling paper-based routing inspection sheets that originally collected by the construction division of TxDOT for evaluating the routes. This work provides an opportunity to provide a baseline for reviewing or modifying the current guideline in terms of truck loads, identifying primary locations receiving SHL moves, counting a number of seal coat sections or load zoned areas, and so on. Upon establishing the database, researchers proposed a guideline for regulating SHL moves based on the findings from field validations of the developed mechanistic approach.

SHL Database

Currently, SHL movers are required to obtain a permit from the motor carrier division (MCD) of TxDOT, providing information such as company name, transport type, and vehicle weight with loading diagram. With given information, the MCD document super heavy route inspection form including route information. In this study, researchers made an effort to convert 243 pages of paper-based data on SHLs that have been collected during the past 5 years into an electrical formant file as shown in Figure 42.

Based on the established database, researchers conducted statistical analyses to figure out the factors that should be considered for developing a guideline. Figures 43 to 48 show the results of statistical analyses. Here is a summary of statistical analyses conducted:

- The GVW of SHLs ranged from 135 to 2550 kips. The GVWs corresponding to 50, 75, 95 cumulative percentile are 654, 746, and 1130 kips, respectively. It appears that the current GVW limit of 500 kips for evaluating pavements is reasonable since 92.5 percent of SHLs exceeds 500 kips of GVW based on cumulative percentile shown in Figure 43.
- The maximum tire load of SHLs ranged from 1828 to 15,768 lb. The maximum tire loads corresponding to 50, 75, 95 cumulative percentile are

5500, 6150, and 7200 lb, respectively. Considering pavement damage is highly associated with tire or axle load rather than GVW, it appears that the current maximum tire load limit of 5000 lb for evaluating pavements is reasonable since 73.7 percent of SHLs is loaded over 5000 lb of tire load based on cumulative percentile shown in Figure 44.

- The portion of routes with seal coated segments is found to be 42 percent as shown in Figure 45. Only 28 percent of route did not include seal coat pavements. Considering 30 percent of unknown routes for the presence of seal coat, it is likely to be extrapolated that at least half of routes had a chance to encounter seal coated pavement, thus it seems to support a need to develop a guideline for regulating SHLs on seal coat routes.
- Figure 46 indicates that a primary portion with respect to travel distance from SHLs is occupied with a short (less than 50 miles) and long distance (over 300 miles). Practically, since it is more facilitating to monitor and evaluate a short distance route than longer route, it is deemed that a guideline will be effective controlling SHLs when seal coated pavements are within a relatively short distance route.
- Chen et al. (*42*) reported that SHLs equipped with push truck have advantages particularly in slope areas resulting in reducing considerable torque forces between tire and seal coat surface. Figure 47 suggests that the portion of SHLs with push truck be increased to alleviate seal coat damage potential.
- According to Figure 48, Houston is a major city receiving SHL moves. Itmight be necessary to monitor SHLs in Houston, Yoakum, and San Antonio Districts and implement the guideline for these areas at the initial stage.

From the overview of established SHL database, researchers recognized that a guideline for regulating SHLs on seal coats needs to be developed and made an effort to outline a guideline to incorporate the calibrated mechanistic model along with field validation results. Following section documents on the development of guideline.

No.		1
File Code		t\h brown-den-pon
Transport Company		H. Brown Crane & Rigging
Date		2/30/2004
Re-Route		N
Load Information	Load Description	Transformer
	Oil Related	
	Power Related	Y
	Energy Related	
	Other	
Width		13'
Height		20'
Length		100'
Gross Weight		493,000
Payload Weight		377,996
Max Tire Load (lbs/tire)		4,385
Travel Distance Related	Starting City	Denton
	Ending City	Ponder
	Travel Distance	7
	<50 mile	Y
	50~100 mile	
	100~300mile	
	>300mile	
Load Zone	Traveled Distance	25.14
	Load Zone Highways	FM156
Critical Route	Highway Name	
	Lowest Distress Scores	
Seal Coat		N
Loading Diagram	Push Truck (Y or N)	N
	Driving Truck Axle load	15000;19000;19000;19000
	Driving Truck Tire Load	7500;4750;4750;4750
	Push Truck Axle Load	
	Push Truck Tire Load	
	Trailer Load per Line	35083;35083;35083;35083;35083;35083;35083;35083;35083;35083;35083;35083
	Trailer Axle Load	17542;17542;17542;17542;17542;17542;17542;17542;17542;17542;17542;17542
	Trailer Load/Tire	4385;4385;4385;4385;4385;4385;4385;4385;4385;4385;4385;4385
	Lateral Load (lbs/inch)	516;516;516;516;516;516;516;516;516;516;516;516
Scanned Loading Diagram		079_T_h brown-pon-den.pdf

Figure 42. Snapshot of SHL Database.

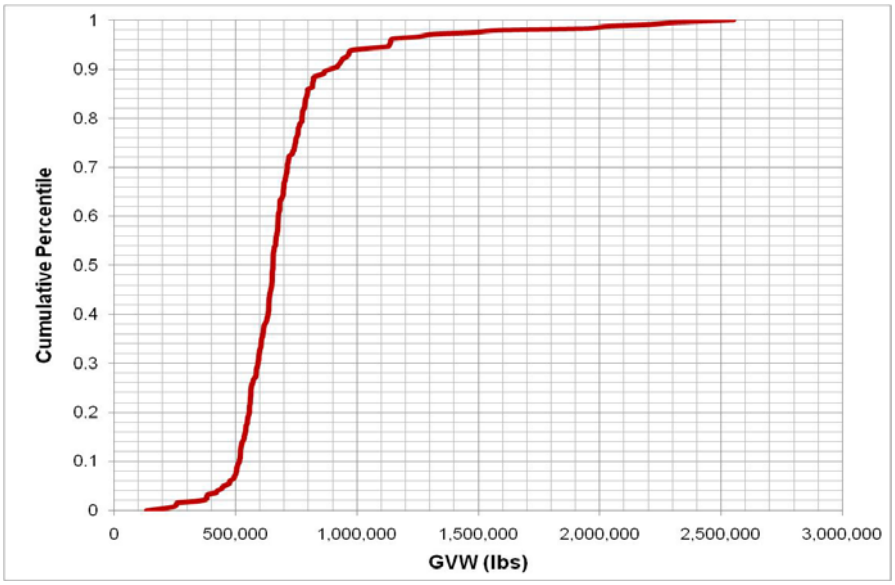

Figure 43. Cumulative Percentile of GVW.

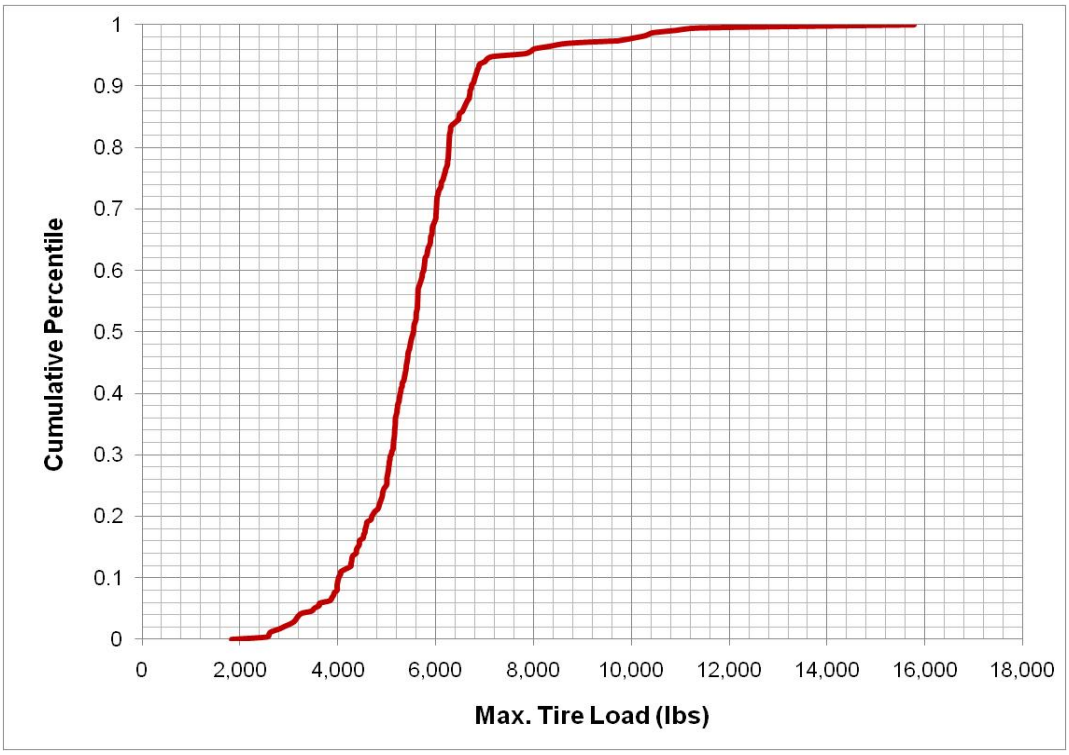

Figure 44. Cumulative Percentile of Maximum Tire Load.

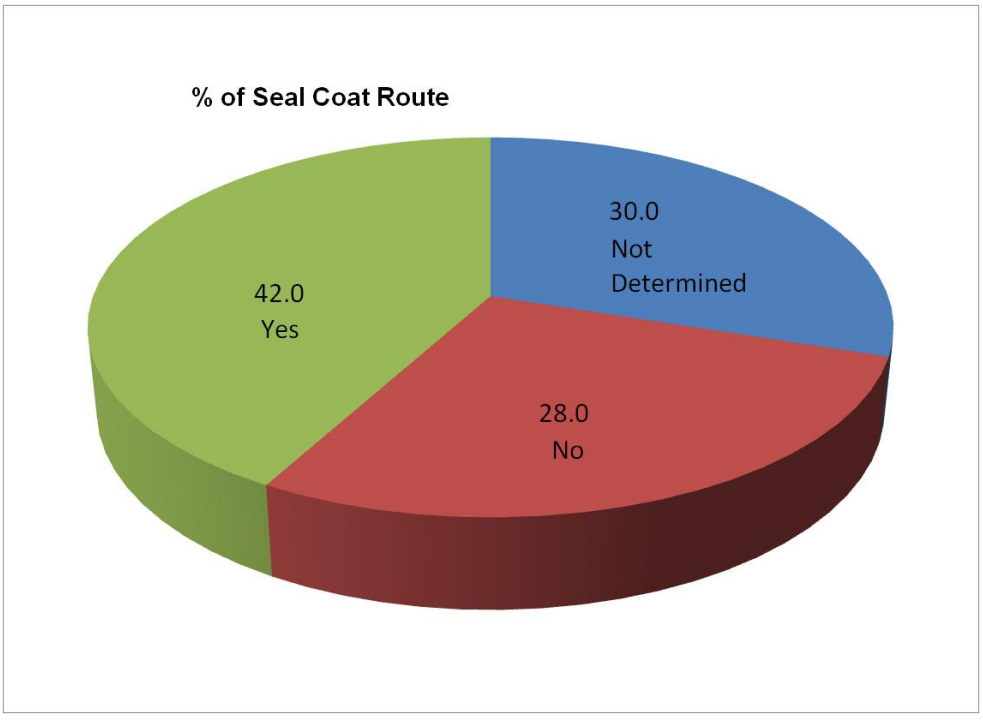

Figure 45. Percentage of Routes including Seal Coat.

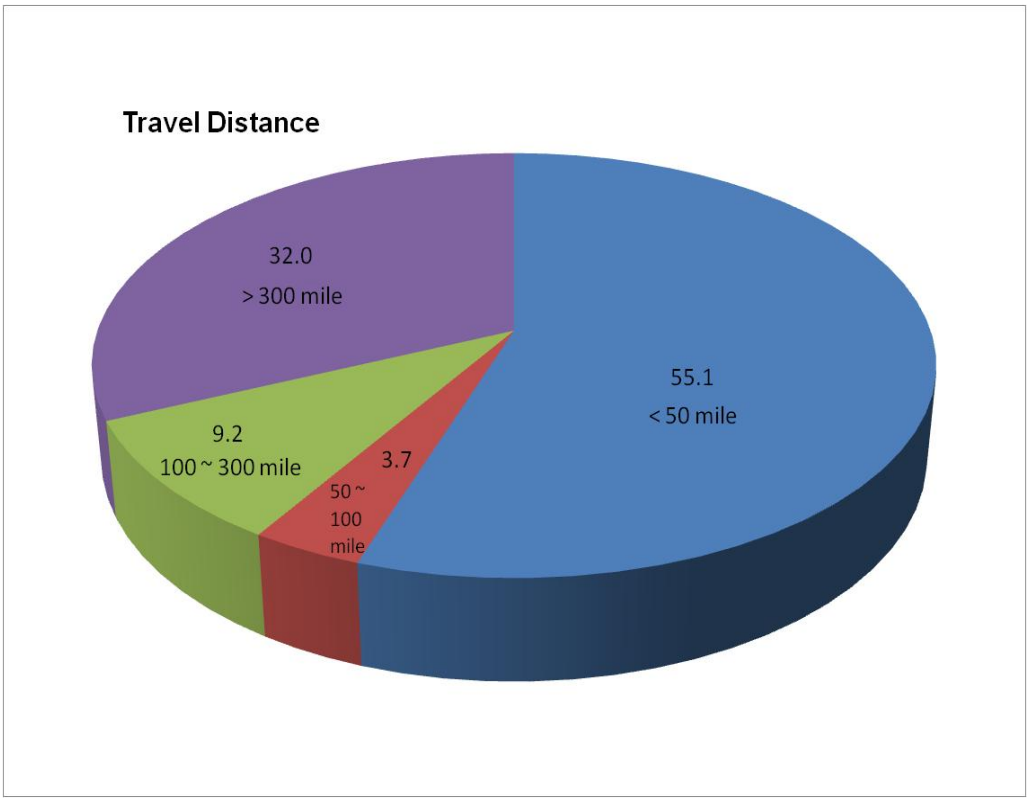

Figure 46. Percentage of Travel Distance.

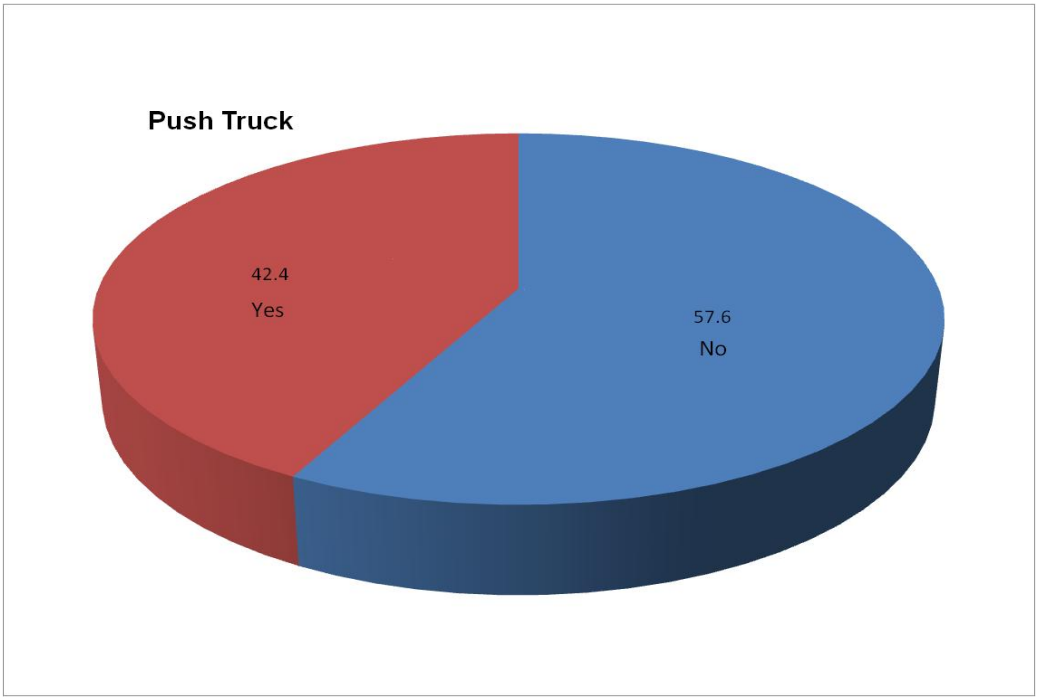

Figure 47. Percentage of SHL with Push Truck.

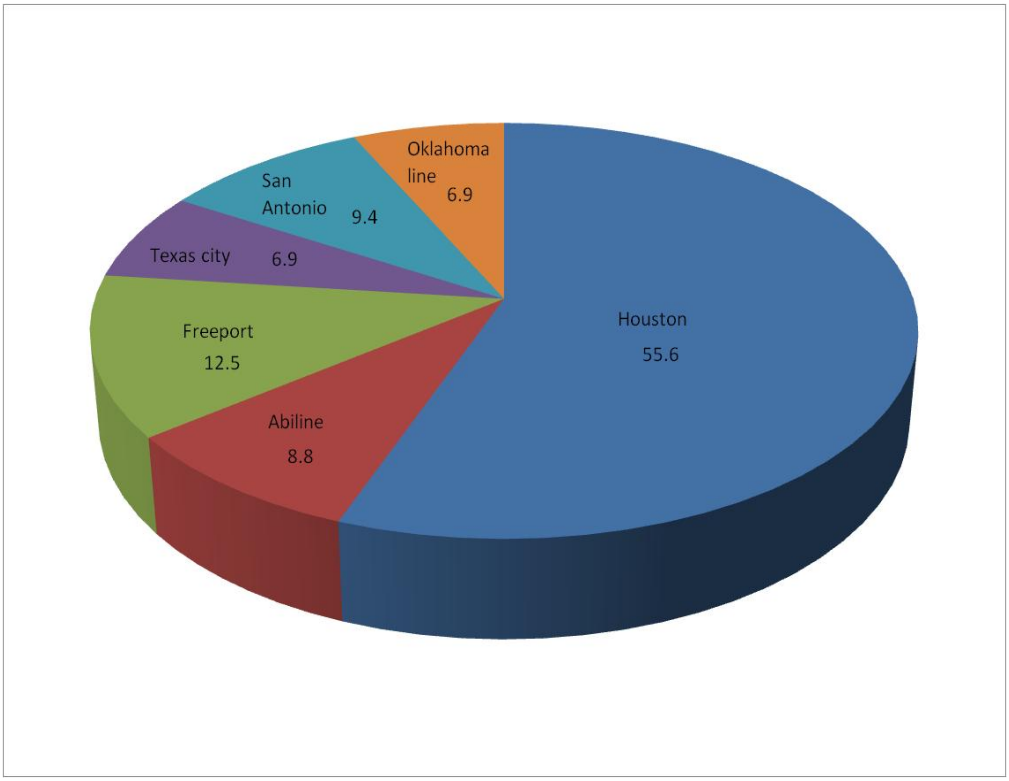

Figure 48. Percentage of Major City Traveling SHL Moves.

Outline of Guideline

The researchers came up with an outline of guideline as shown in Figure 49. With respect to loading limit, a plot was generated to provide relationship between GVW and tire load a shown in Figure 50. Six cases where experienced seal coat damages that reported from case studies were included as well. Most of SHLs were highly populated within the range of 500 to 700 kips of GVW with 5 to 6 kips of maximum tire load. In view of this, researchers recommend that SHLs (over GVW of 254 kips according to the TxDOT's definition) with a maximum tire load exceeding 5000 lb be considered for the seal coat damage evaluation since wheel load is found to be a more critical factor than GVW directly associated with seal coat damage and other parameters such as pavement surface temperature, slope, curing period, and seal coat material also play a significant role in yielding seal coat damages interactively.

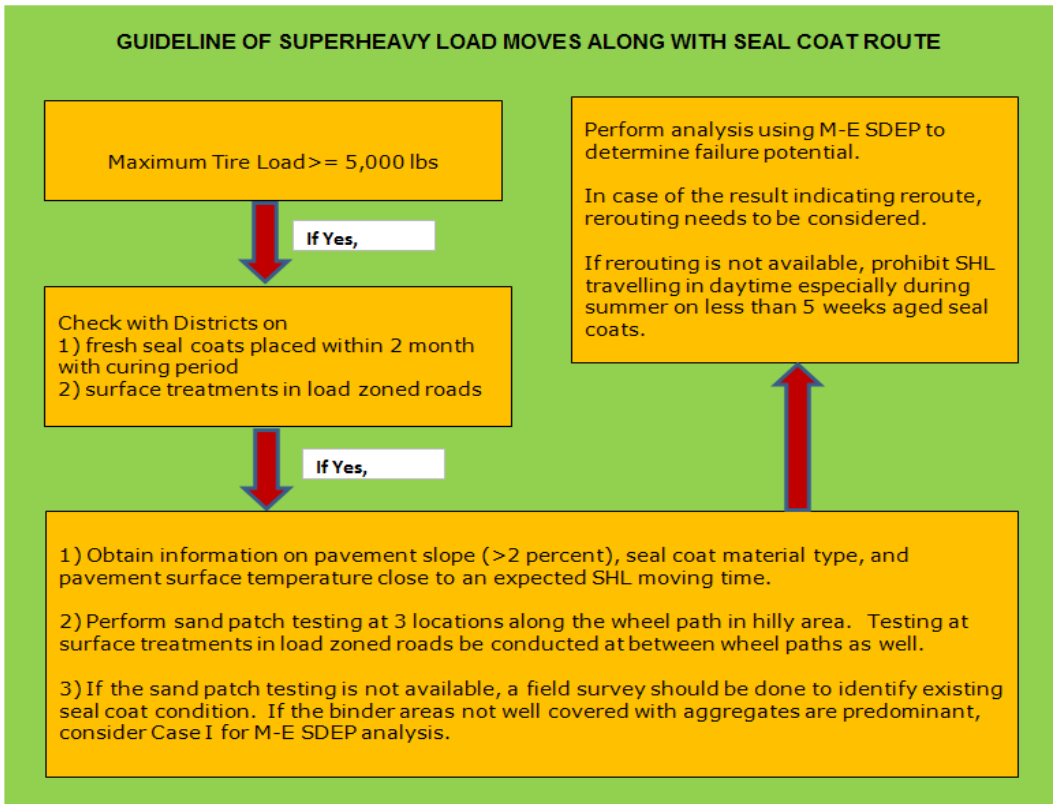

Figure 49. Proposed Guideline of SHL Moves on Seal Coat Routes.

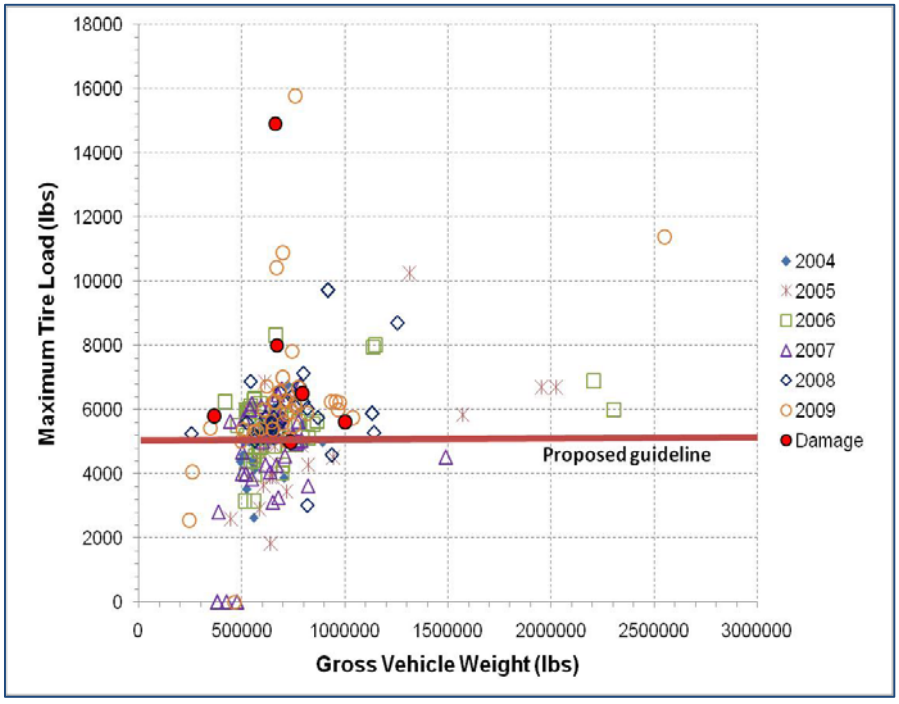

Figure 50. Maximum Tire Load versus GVW.

It is substantially important to coordinate with the Districts to identify the presence of fresh seal coats along the route in this guideline. Seal coats less than 2 months should be considered for route evaluation using M-E SDEP. However it should be noted that even old aged seal coat routes exhibited damage based on field case studies particularly in surface treatments of load zoned roads. This case also needs to be considered for the evaluation.

Once seal coat routes falling into such conditions are identified, it is required to obtain the following information from the Districts on pavement slopes, especially slopes greater than 2 percent, seal coat material type, and pavement surface temperature close to an expected SHL moving time. In addition to gathering the information, researchers recommend performing sand patch testing in accordance with Tex 436-A at three locations along the wheel path to obtain the average texture depth especially located at hilly area. In case where the route has two lanes without a shoulder, the test needs to be conducted between wheel paths as well since it is not uncommon the width of SHL exceeds a typical lane width of 12 ft. If the sand path testing cannot be achieved, a field survey should be substituted to identify seal coat conditions. When it is deemed that binders are not sufficiently covered with aggregates due to either excessive binder application or higher texture depth over 3 mm, the analysis using M-E SDEP should be carried out under Case I condition to accommodate such a condition.

After completion of analysis using M-E SDEP program considering all inputs, a decision needs to be made on rerouting depending on the results of analyses. To assist in making decision, M-E SDEP provides failure potential in terms of failure probability and damage rate resulting in rerouting decision. If the results indicate rerouting, an alternative route needs to be evaluated. Should the rerouting be restrained due to other factors, researchers strongly recommend prohibiting SHLs from traveling in daytime especially during summer along with less than 5 weeks aged seal coats.

CHAPTER VII FINDINGS AND RECOMMENDATIONS

Seal coat damage in a roadway system has become a prevalent problem for TxDOT along with a rapid growth of superheavy load moves. In line with this issue, project 0-5270 aimed to develop a logical guideline for SHL moves to minimize seal coat damages and achieve the cost effective pavement preservation goal. To accomplish this objective, researchers carried out a comprehensive work plan that covered the following tasks:

- Reviewing current TxDOT and other state's practices on overweight/SHL regulation, TxDOT seal coat specification, and previous literatures dealing with damage evaluations due to SHLs,
- Proposing a preliminary mechanistic approach to evaluate seal coat damage along with identification of critical parameters and material characterization,
- Conducting pilot field tests to validate the proposed mechanistic approach,
- Calibrating a preliminary mechanistic approach and develop a Microsoft Excel spreadsheet based tool, and
- Establishing a single electronic source of SHLs database collected by the TxDOT during the past 5 years for the pavement review to overview the current SHL procedure.

Based on the research conducted, the following conclusions are noted:

- The review of guidelines in several highway agencies indicated that most DOTs regulate SHLs in a sound manner for bridges but clear guidelines for pavement evaluation are not well established.
- Texas is one of leading states dealing with a number of SHL moves. Consequently, TxDOT is equipped with the most well-defined guidelines among states reviewed. However, a lack of logical guidelines on seal coat routes due to SHL moves was identified. A criterion that prevents SHLs from moving on fresh seal coat less than five weeks is only applicable up to date in this respect.
- Researchers identified typical types of seal coat binder and aggregate used in Texas. For binder, asphalt cement modified with a polymer is mostly utilized

with Grade 4 precoated aggregate. Emulsified binder like a CRS-2P has been occasionally used because of its rapid setting with non-coated aggregate.

- The review of case studies of SHL moves conducted by TxDOT revealed that structural failure due to SHL was not a major concern except the case where the existing route exhibits a structurally poor condition or encounters heavy rains prior to SHL moves. Most of the damage has been related to seal coat failures when SHL traveled under hot temperatures, hilly areas, and fresh seal coats.
- Researchers conducted a case study on structural failure along with FM 796 in Corpus Christi District. Interpreting FWD data showed structurally inadequate condition of the route at the time of receiving the SHL move. Employing LoadGage program and the current TxDOT procedure tied to the allowable number of load application exhibited comparable results indicating the route possessed a high potential to be damaged.
- An effort was made to estimate cost associated with repairing such damages due to SHL moves based on communication with TxDOT maintenance division personnel. Maintenance activities taken during FY 09 revealed that the most common maintenance type was repairing surface layer by means of seal coat and overlay. Based on the information, researchers quantified repair cost for several maintenance options and verified with limited cases that reported to TxDOT.

From this perspective, researchers made an effort to develop a mechanistic approach to evaluate seal coat damage potential and following achievements were made:

- Researchers came up with a free body diagram shown in Figure 10 to simulate interaction between wheel load and seal coats with a certain given slope. From this, two force terms are quantified. One is called fracture pressure, which is calculated from wheel load, slope, seal coat thickness, tire width, and friction coefficient. The other force term is tensile strength within seal coats that is considered resistance force to the fracture pressure. When the fracture pressure exceeds tensile strength, seal coat damage tends to occur as given in equation (4).
- A key component in the mechanistic approach is to quantify the tensile strength of seal coat. Since it is not feasible to conduct laboratory testing due to difficulty in

molding samples like a typical hot mix asphalt mixture, in lieu of this, researchers employed a fracture mechanics based formula given in equation (5) to estimate tensile strength.

- To estimate tensile strength from the formula, researchers made an attempt to obtain surface energy and relaxation modulus properties via laboratory testing. The Universal Sorption and Wilhelmy plate tests were carried out to measure surface energy components of aggregates and binders, respectively. Grade 4 lightweight and limestone aggregate from Bridgeport were successfully characterized with five types of binders: AC20-5TR, AC10-2TR, AC20-XP, AC-15P, and CRS 2P. With given tested data from this project, researchers integrated measurements of other types of aggregates from different sources that obtained from previous studies conducted by TTI so as to accommodate various combinations of seal coat mixtures that possibly can be considered in practice.
- Characterizing relaxation modulus properties to estimate tensile strength was conducted coupling an asphalt modulus predicted equation given in equation (14) and a global aging model. A series of laboratory testing was conducted to obtain temperature-viscosity relationship, air void, and asphalt content in order to provide input variables to generate master curve using equation (14). From this, a temperature shift factor can be obtained. Researchers then applied the global aging model to shift master curves at any given time frame. Once a master curve is generated, relaxation modulus properties can be obtained by fitting equation (20) onto the master curve.
- Researchers performed preliminary analyses for testing the proposed mechanistic approach. Different types of seal coat mixtures were considered to check whether tensile strength is estimated realistically. Analyses showed that tensile strength varied reasonably with the change of temperature and curing period. In addition to this, it was found that tensile strength is significantly sensitive to material types and properties.

Researchers conducted a pilot field testing in the Bryan and San Antonio Districts during summer seasons of 2008 and 2009 to validate the proposed mechanistic model and following findings were drawn.

- During this project, two sets of field testing were conducted. In the first fiscal year, field testing was performed at four fresh seal coated routes in the Bryan District for initial calibration of the mechanistic model. Grade 4 precoated lightweight aggregate was used in all sections with AC20-5TR and AC20-XP. During the second fiscal year, two routes in the Bryan District and four routes in the San Antonio District were tested. This test provides an opportunity to examine an effect of different types of seal coat mixtures and longer curing periods up to 1 year on seal coat behavior resulting in recalibrating the mechanistic model.
- To accomplish field testing, researchers set up the test truck installed with a wheel force transducer system to measure wheel forces during the test. Tests were conducted at different curing periods and times within a day to cover the change of pavement surface temperature. Prior to collecting data, slope and pavement surface temperature measurements were conducted for every testing and visual scanning of test segments was then conducted to rate damages caused by the test truck passage. The damage was rated into three levels: None, Low, High, depending on extent of aggregate peeled off. In addition to this, sand patch testing was conducted along the wheel path to measure average texture depth.
- During the first year test, the tire load of test truck was only around 3750 lb that was much lower than typical SHLs tire load. To compensate this condition, researchers operated the test truck with brake after normal driving so that a high level of torque force equivalent to 5000 lb was generated from applied brakes.
- First set of test results indicated that pavement surface temperature was the most influential factor controlling seal coat damages. No discernable damage was detected in the morning test even if high torque force was applied. Pavement surface temperature below 110 °F appears to be a threshold giving less chance of damage based on field observation. In terms of tire loading, it was confirmed that tire load below 4000 lb would not be problematic as long as SHLs move normally.

Researchers calculated failure ratio with given information on measured wheel load, slope, temperature, and material properties to relate with observed damage rate. From this, first set of calibration was achieved shown in Table 14 and Figure 34.

- Researchers achieved a higher tire load around 6000 lb during the second year test. During this test, the test truck was operated normally without applying brakes to generate torque forces. Seal coats that tested in this period aged from 3 weeks to 1 year. Material types varied AC20-5TR with lightweight aggregate, AC20-5TR with Trap rock, AC-15P with limestone, CRS-2P with limestone, and CRS-2P with Trap rock.
- Second set of test results showed that seal coat curing period and seal coat mixture combination are also important factors considered in assessment of seal coat damage potential. One year aged section in SH21 that had been tested during the first year performed well without causing severe damage even under hot temperatures. Researchers also noted that the damage rate becomes alleviated as curing period increases. The most severe damage was occurred at surface treatments in FM 1333 as shown in Figure 39. A special care should be taken to evaluate surface treatments in load zoned roads.
- FM463 and US90 in the San Antonio District performed well even though they were fresh seal coats that were only around 3 weeks old at the time of testing. It infers that mixture combination and quality of construction are crucial in determining seal coat damage potential. Sand patch test results indicate that the segments with higher texture depth is prone to damage because of larger binder areas not covered with aggregates leading to a higher probability of the binder to be exposed to harsh environmental conditions.
- In a similar way, researchers validated and recalibrated the mechanistic model, and came up with calibration factors as presented in Table 17. Calibration factors were established under four cases taking into account different levels of temperature, curing period, texture depth, and seal coat type. Researchers then developed a Microsoft Excel based program Mechanistic-Empirical Seal Coat Damage Evaluation Program to incorporate the recalibrated mechanistic model.

M-E SDEP was tested with several case studies and provided a realistic estimation of seal coat damage compared to observed results.

- Researchers established a database integrating routing inspection sheets that have been collected by TxDOT in the past 5 years for pavement evaluation in routing SHLs. Statistical analyses on the database recommend that establishing a logical guideline for SHL on seal coats be encouraged since the portion of routes including seal coat and a short distance travel less than 50 miles was close to 50 percent among considered routes.
- Researchers outlined a guideline as shown in Figure 49. The guideline presents steps to be taken for evaluating seal coat routes anticipating for SHL moves. In the guideline, coordinating with districts is a key aspect to collecting available information that required running M-E SDEP.

Considering the findings from this project, researchers offer the following recommendations on TxDOT's continuing implementation of this guideline:

- TxDOT should consider funding a follow-up implementation project to enable the guideline and M-E SDEP developed in this project to be applicable considering a substantial increase in SHL travels across the state in these days. Further validations of the M-E SDEP program should be expected with additional case studies that will take place in the near future. Recognizing importance of seal coat material properties on seal coat performance, the current database on viscosity-temperature relationship, volumetric properties, and surface energy can be extended to other available sources of materials used in practice.
- Researchers believe that the guidelines be linked to Texas Permit Routing Optimization System (TxPROS), which is being developed by the motor carrier division (MCD) of TxDOT. The task will be conducting to improve the current guideline parallel to TxPROS during the implementation project.

REFERENCES

1. Chen, D.H., Bilyeu, J., and Chang, J.R. "A review of the Superheavy Load Permitting Programme in Texas," The International Journal of Pavement Engineering, Vol. 6, No. 1, 2005, pp. 47-55.

2. Pocket Notes. "Permitting Over Sized Loads in Texas" http://www.dot.state.tx.us/iheep2009/presentations/9B_TexasPermitRoutingOptimization_RayHutchinson.pdf, 2009.

3. Pocket Notes. "Rules of Department of Transportation," Missouri Department of Transportation (www.sos.mo.gov/adrules/csr/current/7csr/7c10-25.pdf), 2008.

4. *Pavement Design Guide.* Texas Department of Transportation (TxDOT), Austin, TX, 2006.

5. Rodier, C.J., Shaheen, S.A., and Cavanagh, E. "Virtual Commercial Vehicle Control Stations for California: A Review of Legal and Institutional Issues," California PATH Research Report, 2005.

6. *Roading Network Control Manual.* New Zealand Transit, 2003.

7. Estakhri C., and Senadheera, S. "The Updated TxDOT Seal Coat and Surface Treatment Manual- Summary," Research Report, No. FHWA/TX-05/5/1787-03-1, Texas Transportation Institute, College Station, TX, 2003.

8. *Seal Coat and Surface Treatment Manual.* Texas Department of Transportation (TxDOT), Austin, TX, 2004.

9. Walubita L.F., Epps, M.A., and Glover, C.J. "A Surface Performance-Graded (SPG) Specification for Surface Treatment Binders: Development and Initial Validation," Research Report No. FHWA/TX-05/0-1710-2, Texas Transportation Institute, College Station, TX, 2005.

10. *Standard Specification for Construction of Highways, Streets and Bridges*. Texas Department of Transportation (TxDOT), Austin, TX, 1995.

11. Estakhri. C.K., Saylak, D., Button, J.W., and Jenkins, P. "Investigation of Laboratory Test Methods to Determine Curing Rate of Asphalt Emulsion," Research Report, FHWA/TX-92-1157, Texas Transportation Institute, College Station, Texas, 1991.

12. Tashman, L., Nam, K., and Papagiannakis, T. "Evaluation of the Influence of Tack Coat Construction Factors on the Bond Strength between Pavement Layers," Research Report, WA-RD 645.1, Washington Center for Asphalt Technology, Pullman, Washington, 2006.

13. Krugler, P.E., Estakhri,C.K., Chang-Albitres, C.M., and Sasser, C.H. "Synthesis Study on Transverse Variable Asphalt Application Rates For Seal Coats," Research Report, FHWA/TX-09-0-5833-1, Texas Transportation Institute, College Station, Texas, 2009.

14. Chen, D.H., Fernando, E.G., and Murphy, M. "Application of Falling Weight Deflectometer Data for Analysis of Superheavy Loads," Journal of Transportation Research Board 1540, 1995, pp.83-90.

15. Nokes, W.A. "Superheavy Overloads: NDT Pavement Deflection Compared to Predictions Based on Backcalculated Moduli," Nondestructive Testing of Pavements and Backcalculation of Moduli, ASTM STP 1206, 1989, pp. 574-588.

16. Scullion, T. "Selecting Rehabilitation Options for Flexible Pavements: Training Classes and CDs," Implementation Project 5-1712 Summary Report, Texas Transportation Institute, College Station, Texas, 2005.

17. Satish C., Mehndiratta, H.C., and Chennapragada, U.K. "Structural Adequacy of Flexible Pavements with Types and Widths of Shoulders," Journal of Transportation Engineering, ASCE, Vol. 132, No.1, 2006, pp. 69-75.

18. Fernando E.G., Oh, J., Ryu, D., and Nazarian, S. "Consideration of Regional Variations in Climatic and Soil Conditions in the Modified Triaxial Design Method," Research Report 4519-2, Texas Transportation Institute, College Station, 2007, TX.

19. Fernando E.G., Liu, W., Lee, T., and Scullion, T. "The Texas Modified Triaixal (MTRX) Design Program," Research Report 1869-4, Texas Transportation Institute, College Station, 2001, TX.

20. Chen D.H. "Summary of SHL Damage 2002 to 2005," Unpublished Memorandum, 2010.

21. Lytton, R. Class Notes (CVEN 613). Department of Civil Engineering, Texas A&M University, College Station, Texas, 2006.

22. Marek, C.R., and Herrin, M., "Tensile Behavior and Failure Characteristics of Asphalt Cements in Thin Films," Proceedings of the Association of Asphalt Paving Technologists, AAPT, Atlanta, February 26-28, 37, 1986, pp.386-421.

23. Burak, S., and Agar, E. "Effect of Asphalt Film Thickness on the Moisture Sensitivity Characteristics of Hot-Mix Asphalt," Journal of Building and Environment, Vol.42, 2007, pp.3621-3628.

24. Kandhal P.S., and Chakraborty S., "Effect of Asphalt Film Thickness on Short and Long Term Aging of Asphalt Paving Mixtures," Research Report, NCAT Report No. 96-01, 1996.

25. Lytton, R. “Adhesive Fracture in Asphalt Concrete Mixtures,” In J. Youtcheff (Ed.), submitted for publication, 2004.

26. Schapery, R.A., “Correspondence Principles and a Generalized J Integral for Large Deformation and Fracture Analysis of Viscoelastic Media,” International Journal of Fracture, Vol. 25, 1984, pp.194-223.

27. Lytton, R., Masad, E.A., Zollinger, C., Bulut, R., and Little, D. “Measurements of Surface Energy and Its Relationship to Moisture Damage,” Research Report, FHWA/TX-05-0-4524-2, Texas Transportation Institute, College Station, Texas, 2005.

28. Lytton, R. L., Uzan, J., Fernando, E.G, Roque, R., Hiltunen, D., and Stoffels, S. “Development and validation of performance prediction models and specifications forasphalt binders and paving mixes,” Report SHRP-A-357, Strategic Highway Research, 1993.

29. Little, D., Lytton, R, Si, Z., Xin, D., and Kim, Y. R. “Crack phenomenology: Formation and healing - Task K findings”, Interim Report, Texas Transportation Institute, College Station, Texas, 2000.

30. Good, R.J., and Van Oss, C.J. “The Modern Theory of Contact Angles and the Hydrogen Bond Components of Surface Energies,” Modern Approaches to Wettability, M.E. Schrader and G. Loeb, eds., Plenum Press, New York, 1992.

31. Si, Z. “Characterization of Microdamage and Healing of Asphalt Concrete Mixtures,” *Ph.D. Dissertation*, Texas A&M University, College Station, Texas, 2001.

32. Cheng, D. “Surface Free Energy of Asphalt-Aggregate System and Performance Analysis of Asphalt Concrete Based on Surface Energy”, Ph.D. Dissertation, Texas A&M University, College Station, Texas, 2002.

33. Hefer, A.W., Bhasin, A. and Little, D.N. “Bitumen Surface Energy Characterization Using a Contact Angle Approach,” Journal of Materials in Civil Engineering, ASCE, Vol. 18, No. 6, 2006, pp.759-767.

34. Bhasin, A.W., and Little, D.N. “Characterization of Aggregate Surface Energy Using the Universal Sorption Device,” Journal of Materials in Civil Engineering, ASCE, Vol. 19, No. 8, 2007, pp.634-641.

35. Kwok, D.Y., Gietzelt, T., Grundke, K., Jacobasch, H.J., and Neumann, A.W. “Contact Angle Measurements and Contact Angle Interpretation. 1. Contact Angle Measurements by Axisymmetric Drop Shape Analysis and a Goniometer Sessile Drop Technique,” *Langmuir*, American Chemical Society, Vol.13, No. 10, 1997, pp. 2880-2894.

36. Jacobasch, H.J., K. Grundke, S. Schneider, and F. Simon, "Surface Characterization of Polymers by Physico-Chemical Measurements," J. Adhes., 48, 1995, pp. 57-73.

37. Chibowski, E, "Surface Free Energy of a Solid from Contact Angle Hysteresis," Adv. Colloid Interface Sci., 103, 2003, pp. 149-172.

38. Witczak, M.W. and Fonseca, O.A. "Revised Predictive Model for Dynamic (Complex) Modulus of Asphalt Mixtures," Transportation Research Record 1540, Transportation Research Board, Washington, D.C., 1996, pp. 15-23.

39. Mirza, M.W. and Witczak, M.W. "Development of a Global Aging System for Short and Long Term Aging of Asphalt Cements," Journal of the Association of Asphalt Paving Technologists, Vol. 64, 1995, pp. 393-430.

40. Walubita, L.F., "Comparison of Fatigue Analysis Approaches for Predicting Fatigue Lives of Hot-Mix Asphalt Concrete (HMAC) Mixtures," Ph.D. Dissertation, Texas A&M University, College Station, Texas, 2006.

41. Pocket Notes. "Trap Rock," (http://onlinemanuals.txdot.gov/txdotmanuals/glo/t.htm)2009.

42. Chen D.H., Bilyeu, J., and Li, Z. "Field Evaluation of Damages from Super Heavy Load Moves," ASCE Geotechnical Special Publications No. 193, 2009, pp 187-192.

APPENDIX A DERIVATION OF TENSILE STRENGH

This chapter presents the derivation of tensile strength used in the mechanistic model according to the reference (*16*).

From the stress-strain curve relationship, stress can be expressed as

$$\sigma_t = E^{'}\varepsilon_t \tag{A1}$$

where σ_t = tensile strength; ε_t = tensile strain; and E' = apparent modulus.

For uniform strain condition, the apparent modulus E' is expressed as

$$E^{'} = E\left[1-\frac{2\pi^2}{t}\left(\frac{m}{A}\right)\frac{\bar{c}^3}{t}\right] \tag{A2}$$

where t = film thickness; m/A = crack density; and $\bar{c}$ =critical crack length.

For adhesive fracture condition, the critical crack length is obtained as

$$\bar{c}_{crit} = \frac{4\Delta G_f^a E_f}{3\pi\sigma_t^2\left[1+\frac{E_f}{E_s}\right]} \tag{A3}$$

where E_f, E_s = the modulus of fluid (asphalt) and the solid (aggregate), respectively; ΔG_f^a = the total adhesive fracture surface energy of the mixture.

The crack propagation conditions can be considered either $\frac{m\overline{c^2}}{A}$ is constant or m is constant. In this study, the crack density function is considered as constant thus the tensile strength based on uniform strain and adhesive fracture is expressed as combining equations (A1), (A2), and (A3)

$$\sigma_t = E^{'}\varepsilon_t = E\left[1-\frac{2\pi^2}{t}\left(\frac{m}{A}\right)\frac{\bar{c}^3}{t}\right]\varepsilon_t = E\left[1-\frac{2\pi^2}{t}\left(\frac{m\bar{c}^2}{A}\right)\frac{4\Delta G_f^q E_f}{3\pi t\sigma_t^2\left[1+\frac{E_f}{E_s}\right]}\right]\varepsilon_t \tag{A4}$$

The above equation can be rearranged as below

$$\sigma_t^3 - E\sigma_t^2\varepsilon_t + \frac{8\pi}{3t(1+\frac{E_f}{E_s})}\left(\frac{m\bar{c}^2}{A}\right)\left(\Delta G_f^a E_f\right)E\varepsilon_t = 0 \tag{A5}$$

Putting $\frac{8\pi}{3t(1+\frac{E_f}{E_s})}\left(\frac{m\bar{c}^2}{A}\right)\left(\Delta G_f^a E_f\right)$ is equal to R in equation (A5), and simplifying, gives

in elastic condition

$$\sigma_t^3 - E\varepsilon_t\sigma_t^2 + RE\varepsilon_t = 0 \tag{A6}$$

Differentiating equation (A6) yields

$$3\sigma_t^2\frac{\partial\sigma_t}{\partial\varepsilon_t} - 2E\sigma_t\varepsilon_t\frac{\partial\sigma_t}{\partial\varepsilon_t} - E\sigma_t^2 + RE = 0 \tag{A7}$$

Rearranging equation (A7) gives

$$\frac{\partial\sigma_t}{\partial\varepsilon_t}\left[3\sigma_t^2 - 2E\sigma_t\varepsilon_t\right] = E\sigma_t^2 - RE \tag{A8}$$

Therefore,

$$\frac{\partial\sigma_t}{\partial\varepsilon_t} = \frac{E\left(\sigma_t^2 - R\right)}{\sigma_t\varepsilon_t\left(\frac{3\sigma_t}{\varepsilon_t} - 2E\right)} \tag{A9}$$

This equation reveals that the maximum tensile strength occurs when $\sigma_t = R^{1/2}$ and the maximum secant modulus is when $\frac{\sigma_t}{\varepsilon_t} = \frac{2}{3}E$.

Considering viscoelastic condition for asphaltic materials,

$$E_f = E_\infty + E_{1f}\left(\frac{t_l}{a_T}\right)^{-m} \tag{A10}$$

Therefore, the maximum tensile strength is expressed by substituting equation (A10) into R term defined in equation (A6) as follows.

$$\sigma_{t\max} = R^{1/2} = \frac{8\pi}{3t\left(1+\frac{E_f}{E_s}\right)}\left(\frac{m\bar{c}^2}{A}\right)\left(\Delta G_f^a\left(E_\infty + E_{1f}\left(\frac{t_l}{a_T}\right)^{-m}\right)\right)^{0.5} \tag{A11}$$

APPENDIX B FIELD TEST RESULTS OF FM 97/28

Due to recent rising concerns related to energy, the number of wind turbine units increased gradually in Texas. Among districts in Texas, wind turbines are actively being constructed in Abilene, Amarillo, Lubbock, Odessa, and San Angelo. A case study was conducted to evaluate pavement damage due to repeated superheavy load moves related to wind turbine construction in Floyd County.

The construction schedule was early May through October in 2007. During this period, pavement maintenance issues on FM97 and 28 raised due to excessive rainfall of 8 inches in May/June 2007 along with repeated applications of haul trucks. To evaluate damage, forensic data using FWD and profiler had been collected on FM97/28 on July 11 and December 6, 2007. The first wind turbine arrived on September 24, 2007, as shown in Figure B1. Prior to forensic data collection, the routes experienced localized damages such as edge failure and rutting because of structurally poor conditions, high moisture content level, and lack of lateral support. According to the pavement evaluation score on this route, whereas the average score in FY08 of FM 97 was reduced from 100 to 52 compared to FY07, the score dropped from 94 to 76 in FM 28 between FY07 and FY08.

Figure B1. Shipping of Wind Turbine.

The pavement structure history on tow routes are as follows:

FM 97

- 1949: 18 ft wide, 2C surface treatment over a 6-inch flex base with sandy loams subgrade.
- 1954: 20 ft wide, 2C surface treatments
- 1995: 26 ft wide, 2C prime coated with a 6-inch stabilized base with 5 percent fly ash.
- Seal coats: 1954, 1958, 1960, 1964, and 2001.

FM 28

- 1956: 20 ft wide, 2C surface treatment over a 6-inch flex base with sandy loams subgrade.
- Seal coats: 1961 and 2001.

Below figures compare pavement condition before and after SHL moves made at an individual monitoring location with comparison of measured transverse profiles. Based on field observations on forensic data, it was concluded that:

- an increased number of haul trucks during construction of wind turbine contributed to the majority of pavement damage such as rutting and edge failure;
- excessive rainfall during the early stage of construction appeared to cause the damage by weakening soil bearing capacity; and
- repeated loads transporting turbines and cranes during the construction did not cause additional rutting between July and December during the period that data had been collected. No discernable damage was detected from field survey. This indicates that pavement structural failure is highly related to the moisture condition that controls load bearing capacity of underlying materials especially in surface treated pavements.

(a) (b)

Figure B2. FM 97 Location 1 on Milepost 336. (a) July 11th; (b) December 6th.

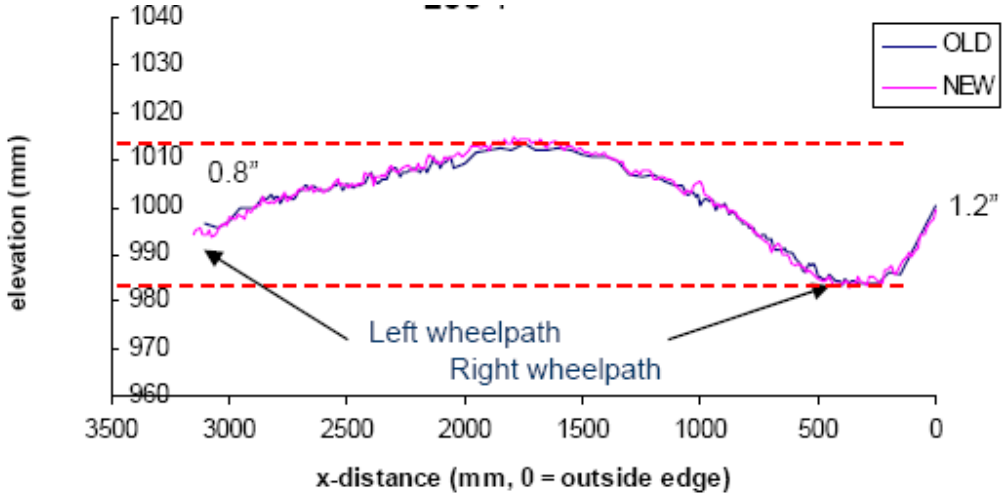

Figure B3. Comparison of Transverse Profile of FM 97 Location 1.

(a) (b)

Figure B4. FM 97 Location 2 on Milepost 336+60. (a) July 11th; (b) December 6th.

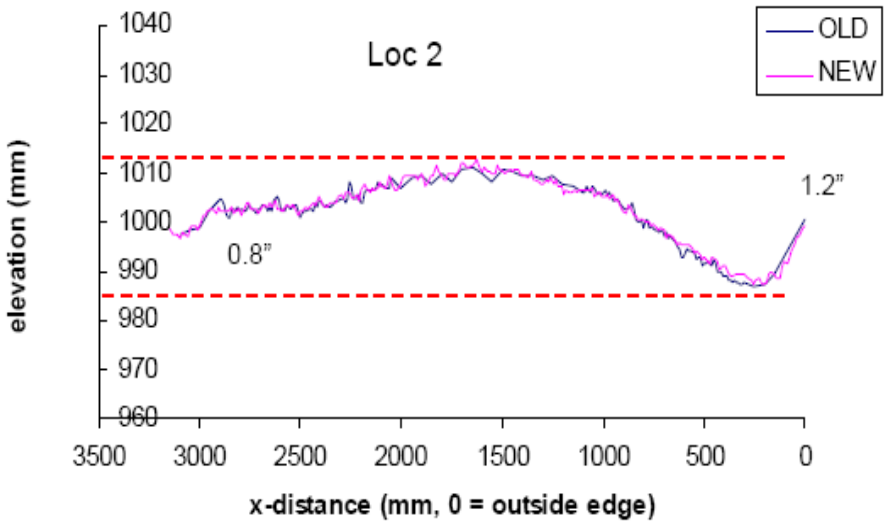

Figure B5. Comparison of Transverse Profile of FM 97 Location 2.

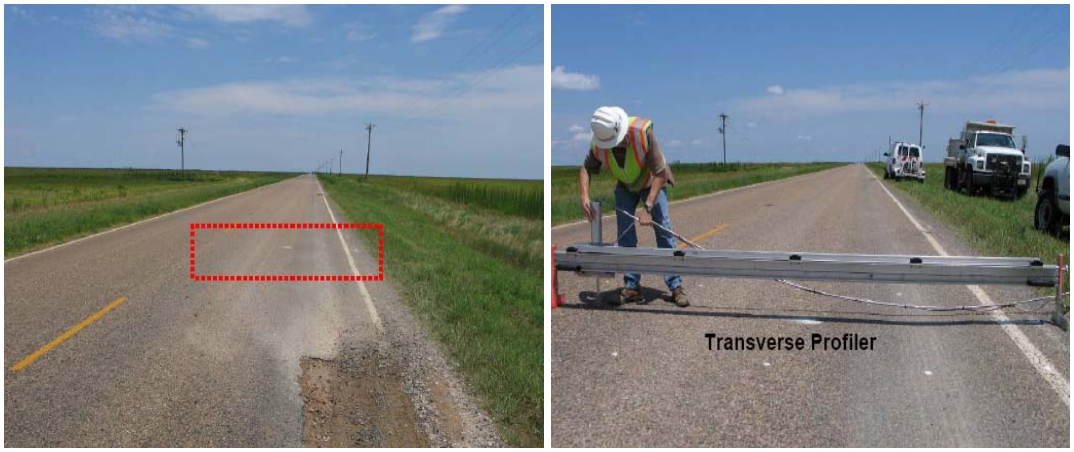

(a) (b)

Figure B6. FM 97 Location 3 on Milepost 336-2040'. (a) July 11th; (b) December 6th.

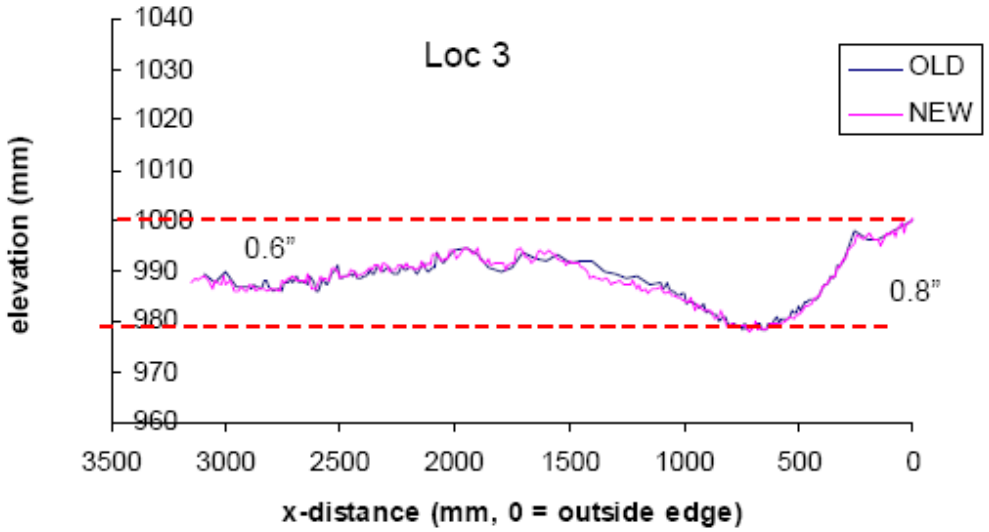

Figure B7. Comparison of Transverse Profile of FM 97 Location 3.

(a) (b)

Figure B8. FM 28 Location 1 on Milepost 186+900' (a) July 11th; (b) December 6th.

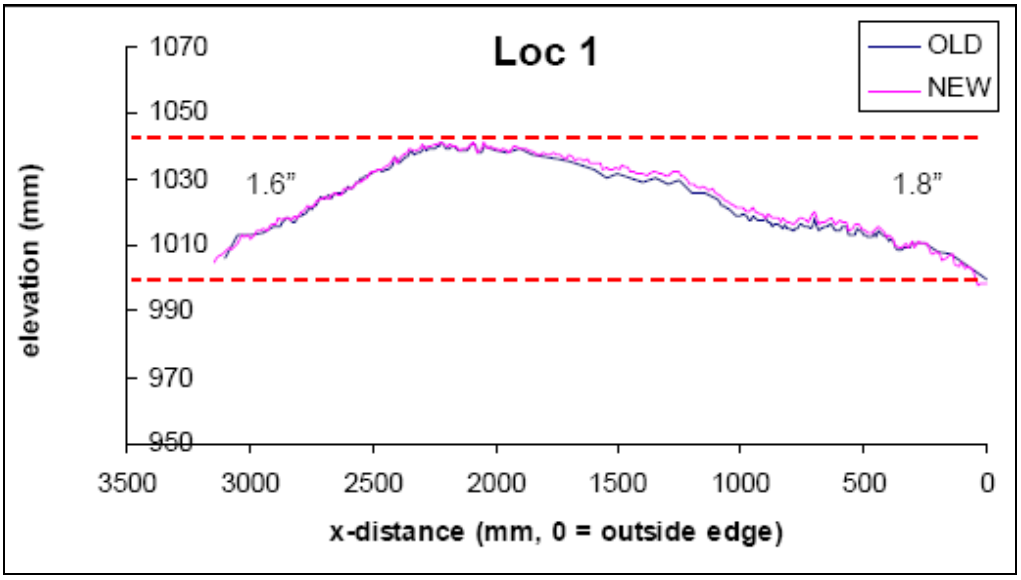

Figure B9. Comparison of Transverse Profile of FM 28 Location 1.

(a) (b)

Figure B10. FM 28 Location 2 on Milepost 182+2100' (a) July 11th; (b) December 6th.

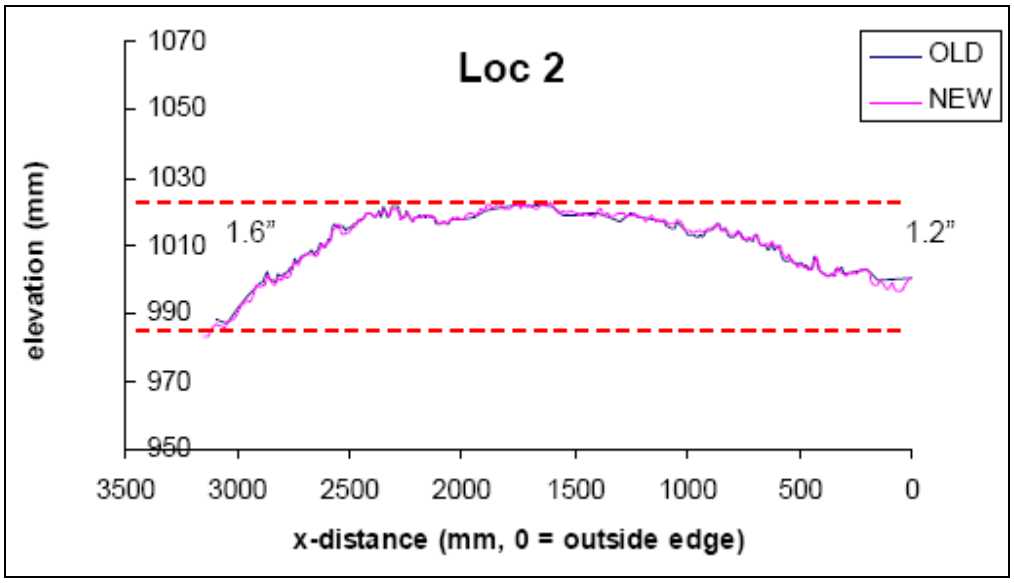

Figure B11. Comparison of Transverse Profile of FM 28 Location 2.

(a) (b)

Figure B12. FM 28 Location 3 on Milepost 182+5400' (a) July 11th; (b) December 6th.

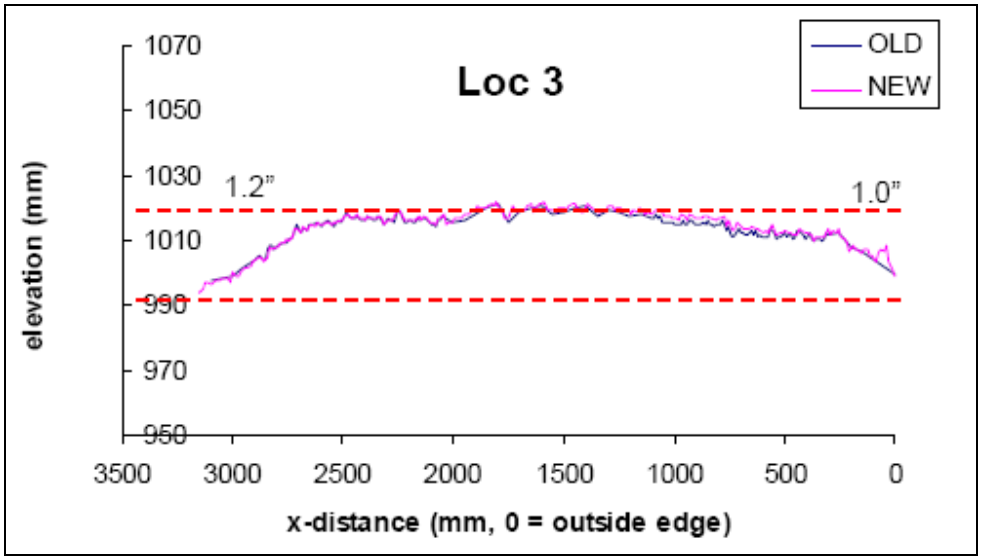

Figure B13. Comparison of Transverse Profile of FM 28 Location 3.

APPENDIX C M-E SDEP USER'S MANUAL

1) Open "M-E SDEP" Microsoft Excel file. There are three worksheets. For a brief explanation on these worksheets, refer to "*READ ME*." Go to the first worksheet is labeled "Calculate Failure Ratio" as shown in Figure C1. Select a case that considered for the analysis and fill input cells on age (month), pavement surface temperature (F), maximum tire load (lb), tire width (in), and slope (%). Slope in degree will be converted to slope in percent. Once all inputs are entered, go to "Calculate tensile strength" worksheet. As far as pavement surface temperature, typical temperature range corresponding to time in summer season can be obtained from the note.

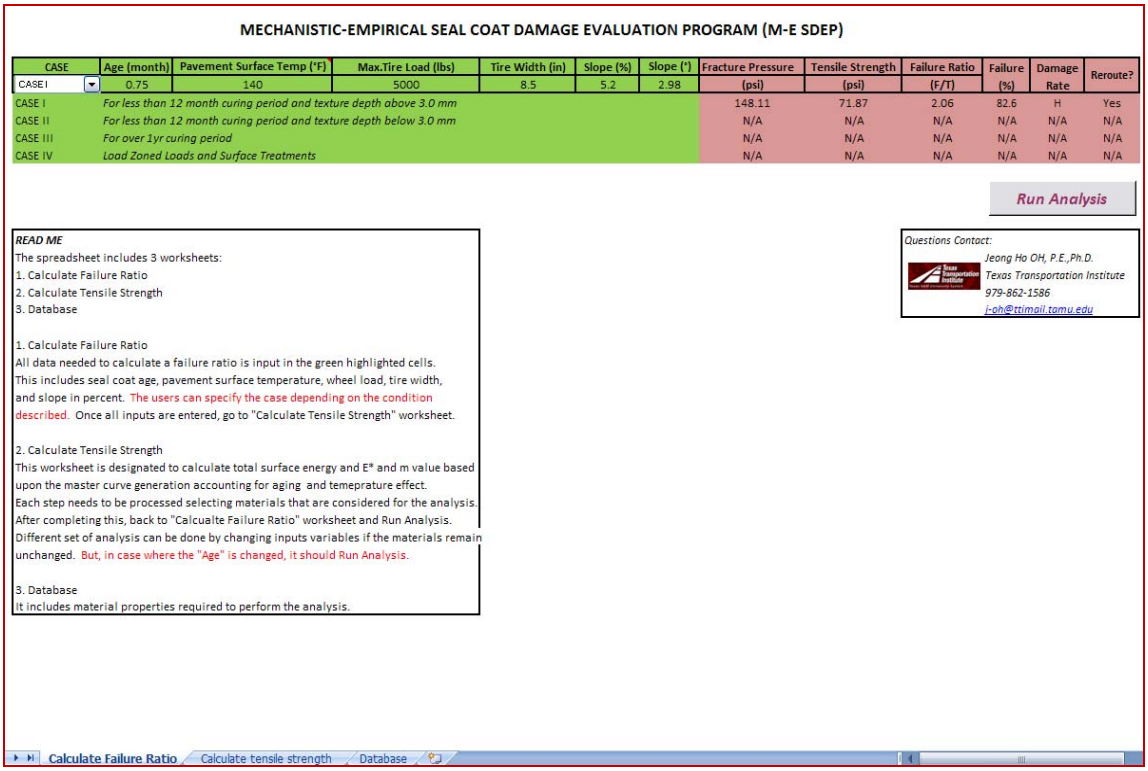

Figure C1. Snapshot of Input Screen on "Calculate Failure Ratio" Worksheet.

2) In "Calculate tensile strength" worksheet, follow steps from top to bottom. In original to mix/lay-down model, select seal coat binder type as shown in Figure C2. Next enter mean annual air temperature (Maat) in surface aging model. MAAT at a specific location considered can be determined based on the map provided.

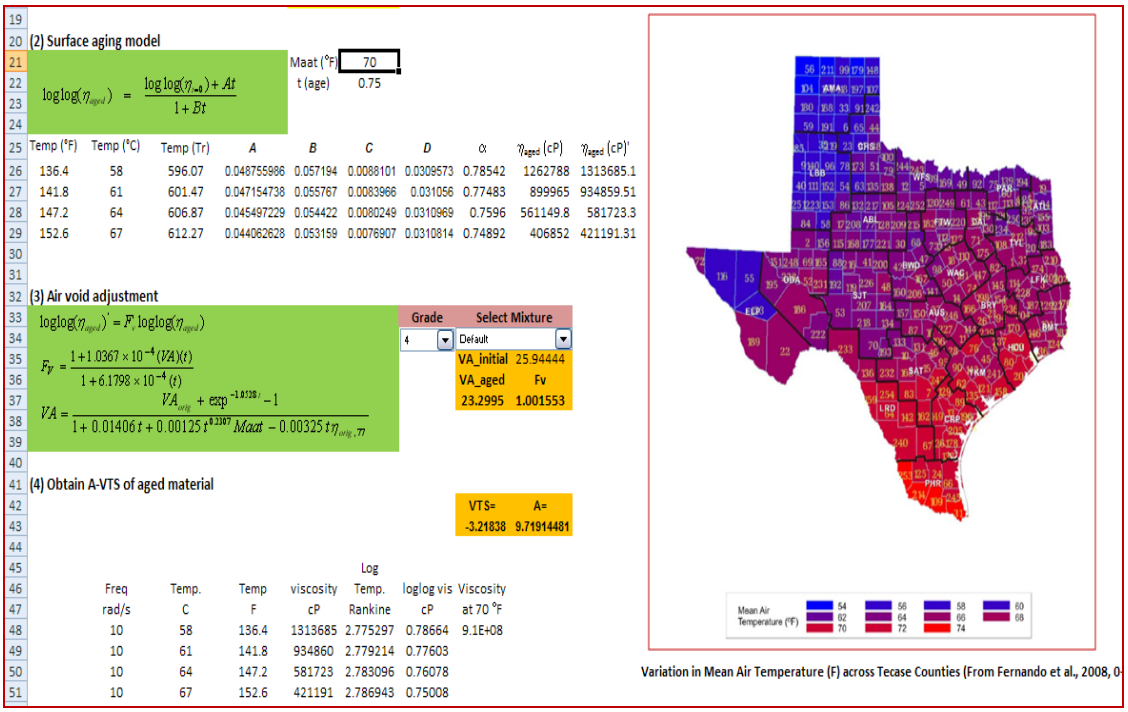

Figure C2. Select Binder Type for A-VTS Coefficient Calculation and MAAT.

3) In air void adjust step, select aggregate Grade (3, 4, and 5) and mixture combination to assign initial air void of the mixture. LW stands for lightweight aggregate, LS for limestone, GR for granite, and SS for sandstone. If the mixture is not available in the list, select default in the list. Mixture with CRS-2P can be considered by choosing CRS-2P mixture from the list.

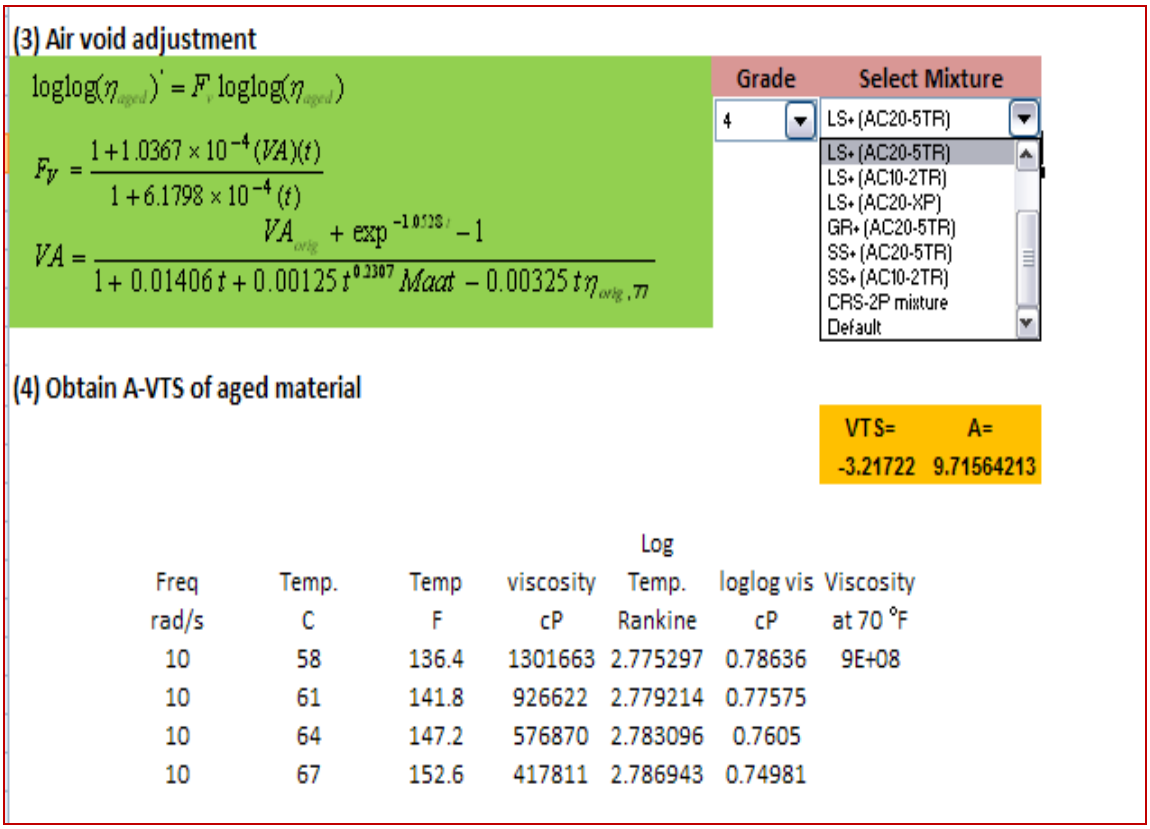

Freq rad/s	Temp. C	Temp F	viscosity cP	Log Temp. Rankine	loglog vis cP	Viscosity at 70 °F
10	58	136.4	1301663	2.775297	0.78636	9E+08
10	61	141.8	926622	2.779214	0.77575	
10	64	147.2	576870	2.783096	0.7605	
10	67	152.6	417811	2.786943	0.74981	

Figure C3. Select Aggregate Grade and Mixture Type.

4) Next, select aggregate type and grade to assign gradation inputs for generating a master curve. The type of aggregate and gradation should be consistent with information specified in air void adjustment step shown in Figure C3. Among the list, TR stands for Trap rock.

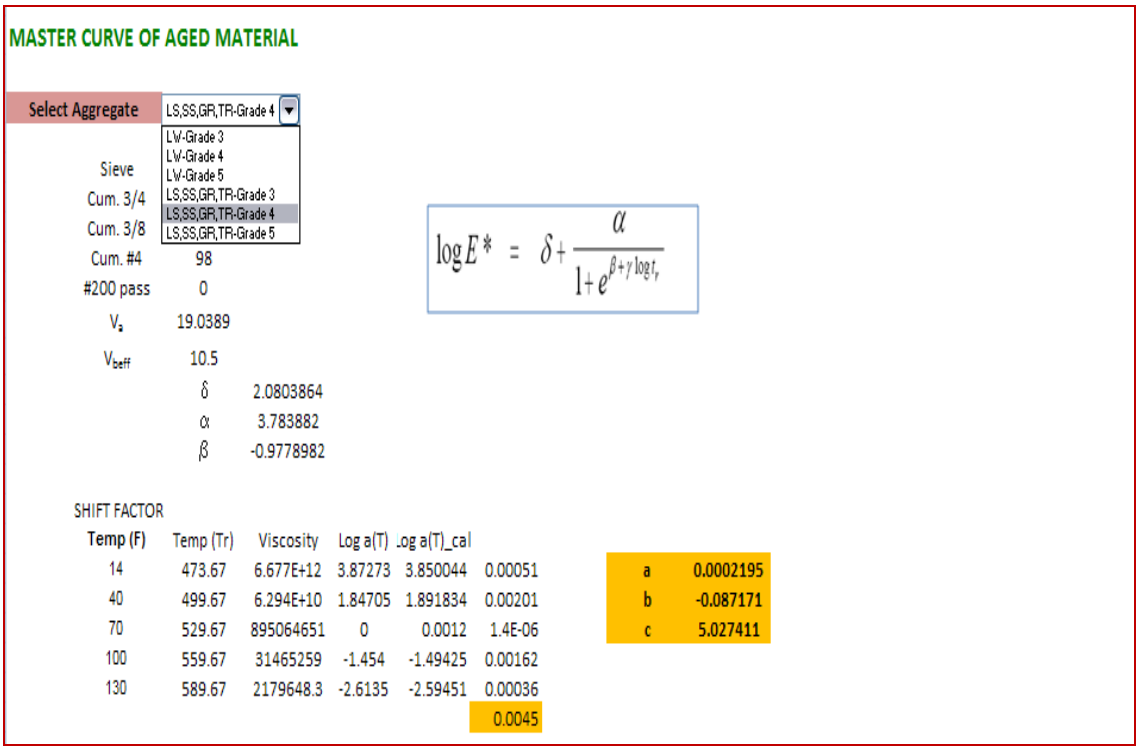

Figure C4. Select Aggregate Gradation.

5) To calculate the total surface energy of mixture, aggregate type needs to be selected. Noted that there are several sources of aggregate under a given material. For example, six different sources of limestone are available in the list. If the user is not able to find a proper source of aggregate for the analysis, engineers need to make an assumption on assigning it.

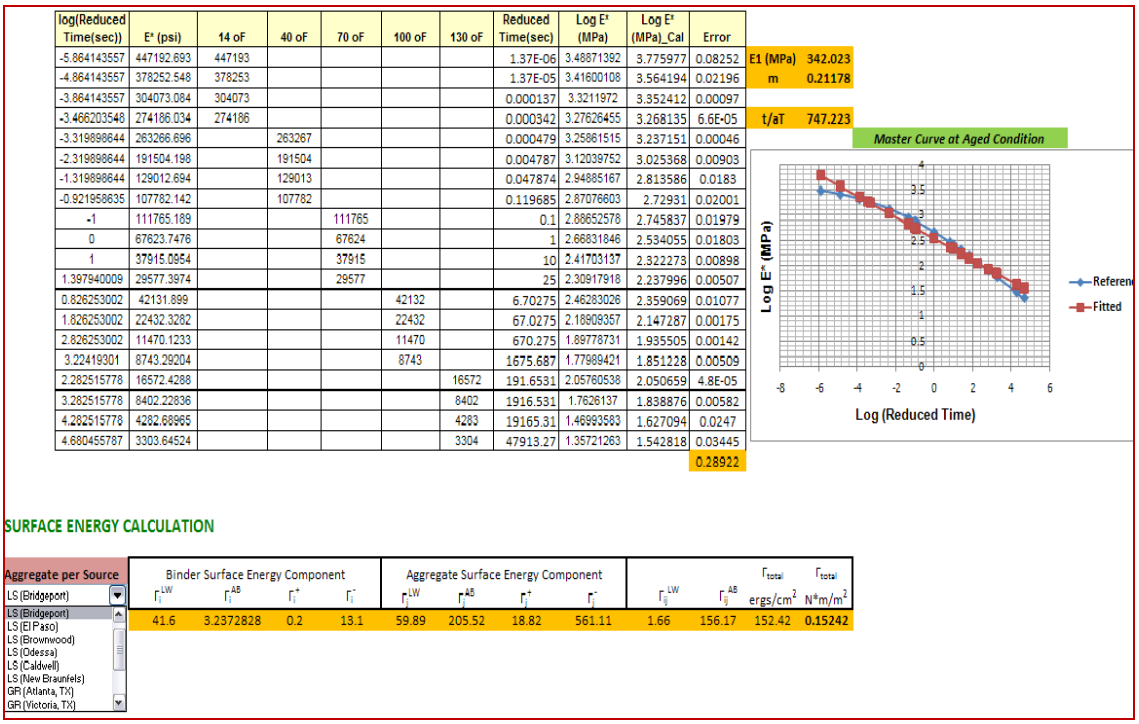

log(Reduced Time(sec))	E* (psi)	14 oF	40 oF	70 oF	100 oF	130 oF	Reduced Time(sec)	Log E* (MPa)	Log E* (MPa)_Cal	Error
-5.864143557	447192.693	447193					1.37E-06	3.48671392	3.775977	0.08252
-4.864143557	378252.548	378253					1.37E-05	3.41600108	3.564194	0.02196
-3.864143557	304073.084	304073					0.000137	3.3211972	3.352412	0.00097
-3.466203548	274186.034	274186					0.000342	3.27626455	3.268135	6.6E-05
-3.319898644	263266.696		263267				0.000479	3.25861515	3.237151	0.00046
-2.319898644	191504.198		191504				0.004787	3.12039752	3.025368	0.00903
-1.319898644	129012.694		129013				0.047874	2.94885167	2.813586	0.0183
-0.921958635	107782.142		107782				0.119685	2.87076603	2.72931	0.02001
-1	111765.189			111765			0.1	2.88652578	2.745837	0.01979
0	67623.7476			67624			1	2.66831846	2.534055	0.01803
1	37915.0854			37915			10	2.41703137	2.322273	0.00898
1.397940009	29577.3974			29577			25	2.30917918	2.237996	0.00507
0.826253002	42131.899				42132		6.70275	2.46283026	2.359069	0.01077
1.826253002	22432.3282				22432		67.0275	2.18909357	2.147287	0.00175
2.826253002	11470.1233				11470		670.275	1.89778731	1.935505	0.00142
3.22419301	8743.29204				8743		1675.687	1.77989421	1.851228	0.00509
2.282515778	16572.4288					16572	191.6531	2.05760538	2.050659	4.8E-05
3.282515778	8402.22636					8402	1916.531	1.7626137	1.838876	0.00582
4.282515778	4282.68965					4283	19165.31	1.46993583	1.627094	0.0247
4.680455787	3303.64524					3304	47913.27	1.35721263	1.542818	0.03445
										0.28922

E1 (MPa) 342.023
m 0.21178
t/aT 747.223

Master Curve at Aged Condition

SURFACE ENERGY CALCULATION

Aggregate per Source	Binder Surface Energy Component				Aggregate Surface Energy Component							
	Γ_j^{LW}	Γ_j^{AB}	Γ_j^+	Γ_j^-	Γ_i^{LW}	Γ_i^{AB}	Γ_i^+	Γ_i^-	Γ_{ij}^{LW}	Γ_{ij}^{AB}	Γ_{total} ergs/cm^2	Γ_{total} N*m/m^2
LS (Bridgeport)	41.6	3.2372828	0.2	13.1	59.89	205.52	18.82	561.11	1.66	156.17	152.42	0.15242

LS (Bridgeport)
LS (El Paso)
LS (Brownwood)
LS (Odessa)
LS (Caldwell)
LS (New Braunfels)
GR (Atlanta, TX)
GR (Victoria, TX)

Figure C5. Select Aggregate Sources for Surface Energy Calculation.

6) Once all inputs entered in Calculate tensile strength worksheet, back to the Calculate Failure Ratio worksheet and click Run Analysis to execute the program. Outputs are fracture pressure, tensile strength, failure ratio, failure (%), damage rate, and reroute.

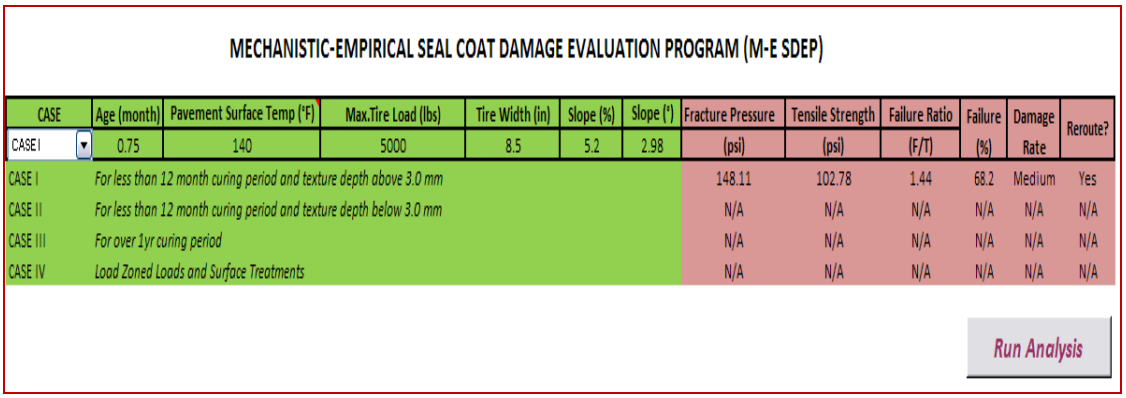

Figure C6. Run Analysis to Calculate Failure Ratio.